
*Safe and Efficient Electrical Vehicle*

7th Framework programme / FP7-2010-ICT-GC /
ICT for the fully electrical vehicle / Grant Agreement Number 258133

# *D130.13 Final Dissemination*

# Authors

| Name | Company |
|---|---|
| GLASER, Sébastien | IFSTTAR |

# Revision chart

| Version | Date | Reason |
|---|---|---|
| 0.1 | 18.09.2013 | Basis document |
| 0.2, 0.3 | 7.10.2013 | Website, brochure, attached papers added |
| 1.0 | 7.10.2013 | Final formatting, released version |

# *Executive Summary*

This deliverable covers the dissemination activities in the frame of the eFuture project. For the scientific dissemination, the project team was very productive:

- More than 25 papers were presented at national and international conferences
- 3 papers were published in technical or scientific journals
- The full project was presented at several workshop and the team will attend at least at ICT 2013 conference and will present the results at a stand promoted by the European Commission.

The dissemination also includes the promotion of the project to a wider audience. A brochure is now available and presents the achievements of the project.

The document will be updated per 30.11.2013 by dissemination activities in November 2013.

# *Table of Content*

# 1 Scientific Dissemination

For the scientific dissemination, the project team was very productive:

- More than 25 papers were presented at national and international conferences
- 3 papers were published in technical or scientific journals
- The full project was presented at several workshop and the team will attend at least at ICT 2013 conference and will present the results at a stand promoted by the European Commission.

In the annex, you will find some articles that present the work of the team.

## 1.3 2013

1. Köhler U.; Decius N.; Masjosthusmann, C.; Büker U. "Development of a scalable multi-controller ECU for a smart, safe and efficient Battery Electric Vehicle " AMAA 2013, Berlin
2. Masjosthusmann, C.; Kohler, U.; Decius, N.; Buker U." Ein Verhaltensmodell und ein Laborprüfstand zur SiL- und HiL-Simulation eines zentralen Steuergeräts für ein intelligent-effizientes Elektrofahrzeug", ASIM Workshop 2013
3. Masjosthusmann, C. ; Buker U.; Kohler, U.; Decius, N., "A Load Balancing Strategy for Increasing Battery Lifetime in Electric Vehicles" SAE Technical Paper 2013-01-0499
4. Rittger, L.; Schmitz, M. "The compatibility of energy efficiency with pleasure of driving" 55th Conference of Experimental Psychologists (TeaP), Vienna, 25.-27.03.2013.
5. Rittger, L.; Schmitz, M. "The compatibility of energy efficiency with pleasure of driving" ICDBT 2013, Helsinki (Finland)
6. Korte M.; Kaiser G.; Holzmann F.; Roth H. " Design of a Robust Adaptive Vehicle Observer Towards Delayed and Missing Vehicle Dynamics Sensor Signals by Usage of Markov Chains" American Control Conference 2013
7. Korte M.; Kaiser G.; Roth H. " Robust Vehicle Observer to Enhance Torque Vectoring in an EV", Autoreg 2013
8. Glaser S.; Orfila O.; Nouveliere L.; Potarusov R.; Akhegaonkar S.; Holzmann F.; Scheuch V. " Smart and Green ACC, adaptation of the ACC strategy for electric vehicle with regenerative capacity", IEEE IV Symposium 2013
9. Glaser S.; Akhegaonkar S.; Orfila O.; Nouveliere L.; Scheuch V.; Holzmann F. "Smart And Green ACC, Safety and efficiency for a longitudinal driving assistance" AMAA 2013, Berlin
10. Glaser S.; Orfila O.; Potarusov R.; Nouveliere L. "Speed profile optimization for electric vehicle with regenerative capacity" FAST zero 2013, Nagoya Japan
11. Schmitz M.; Jagiellowicz M.; Maag C.; Hanig M. "Impact of a combined accelerator–brake pedal solution on efficient driving." IET Intelligent Transport Systems – Special Issue: Human-Centred Design for Intelligent Transport Systems, 7(2), 203 – 209.
12. Rittger, L.; Schmitz, M. "The Compatibility of Energy Efficiency with Pleasure of Driving in a Fully Electric Vehicle." In L. Dorn & M. Sullman (Eds.), Driver Behaviour and TrainingVolume VI (pp. 207-222). Surrey: Ashgate Publishing.
13. Revilloud M.; Gruyer D.; Pollard E. " An improved approach for robust road marking detection and tracking applied to multi-lane estimation.", IEEE IV Symposium 2013

14. FakhFakh N., Gruyer D.; Aubert D. " Weighted V-disparity Approach for Obstacles Localization in Highway Environments", IEEE IV Symposium 2013
15. Scheuch V.; Kaiser G.; Korte M.; Grabs P.; Kreft F.; Holzmann F. "A safe torque vectoring function for an electric vehicle", EVS27 Symposium, Barcelona Spain 2013

## *1.4 2012*

1. Schmitz M.; Jagiellowicz M.; Maag C.; Hanig M. "The impact of different pedal solutions for supporting efficient driving with electric vehicles." In P. V. Mora, J.-F. Pace & L. Mendoza (Hrsg.), Proceedings of European Conference on Human Centered Design for Intelligent Transport Systems (S. 21-28). Valencia: HUMANIST.
2. Schmitz M.; Jagiellowicz M.; Maag C.; Hanig M. "Drivers´ acceptance of limiting vehicle dynamics in electric vehicles." ICTTP 2012, Groningen, 28.08.-31.08.2012.
3. Glaser S.; Orfila, O.; Schmaeche M. "Safety of a torque vectoring LKAS on an in-wheel motor electric vehicle", EEVC 2012, Bruxelles, Belgium
4. Scheuch V.; Kaiser G.; Holzmann F., "Eine innovative Funktionsarchitektur für das Elektrofahrzeug, Ulrich Brill", expert Verlag, Renningen, 2012
5. Jagiellowicz M.; Schmitz M.; Maag C.; Hanig M. "The impact of a combined pedal solution on efficient electric driving and drivers´ acceptance: A driving simulator study". 54. Tagung experimentell arbeitender Psychologen (TeaP), Mannheim, 01.04.-04.04.2012.
6. Schmitz M.; Jagiellowicz M.; Maag C.; Hanig M., "Drivers´ acceptance of limiting vehicle dynamics in electric vehicles." 54. Tagung experimentell arbeitender Psychologen (TeaP), Mannheim, 01.04.-04.04.2012.
7. Masjosthusmann, C.; Kohler, U.; Decius, N.; Buker, U., "A vehicle energy management system for a Battery Electric Vehicle," Vehicle Power and Propulsion Conference (VPPC), 2012 IEEE , vol., no., pp.339,344, 9-12 Oct. 2012
8. Akhegaonkar S.; Nouvelière L.: Potarusov R.; Scheuch V.; Holzmann F.; Glaser S. "Modeling and Simulation of Battery Electric Vehicle to Develop an Energy Optimization Algorithm", AVEC 2012, Seoul, Korea
9. Korte M.; Kaiser G.; Holzmann F.; Scheuch V.; Roth H. "Design of a robust plausibility check for an adaptive vehicle observer in an electric vehicle", 16th International Forum on Advanced Microsystems for Automotive Applications, 30-31 May 2012, Berlin, Germany
10. Scheuch V.; Kaiser G.; Holzmann F.; Glaser S. "Simplified architecture by the use of decision units" 16th International Forum on Advanced Microsystems for Automotive Applications, 30-31 May 2012, Berlin, Germany
11. Scheuch V.; Kaiser G.; Straschill R.; Holzmann F.; " A new functional architecture for the improvement of eCar efficiency and safety", 21st Aachen Colloquium Automobile and Engine Technology 2012

## 1.5 2011

1. Kaiser, G. ; Holzmann, F. ; Chretien, B. ; Korte, M. ; Werner, H. "Torque Vectoring with a feedback and feed forward controller - applied to a through the road hybrid electric vehicle" Intelligent Vehicles Symposium (IV), 2011 IEEE, Publication Year: 2011 , Page(s): 448 - 453
2. Korte M.; Holzmann F.: Scheuch V.; Roth H. "Development of an adaptive vehicle observer for an electric vehicle", EEVC Brussels, Belgium, October 26-28, 2011
3. Scheuch V. "E/E architecture for electric vehicle" ATZ Elektronik, 2011 – 06 (see online www.atzonline.de)

# 2 General presentation

Verdure was selected at the beginning of the project to handle most of the non-scientific dissemination, providing the logo, the website and the final brochure. Partners also promote the full project at several events.

## 2.1 Website and logo

After an internal poll, the logo was selected during the first steering committee. It is presented here.

The website allows a dissemination during the whole project duration, it will be maintained after the project end.

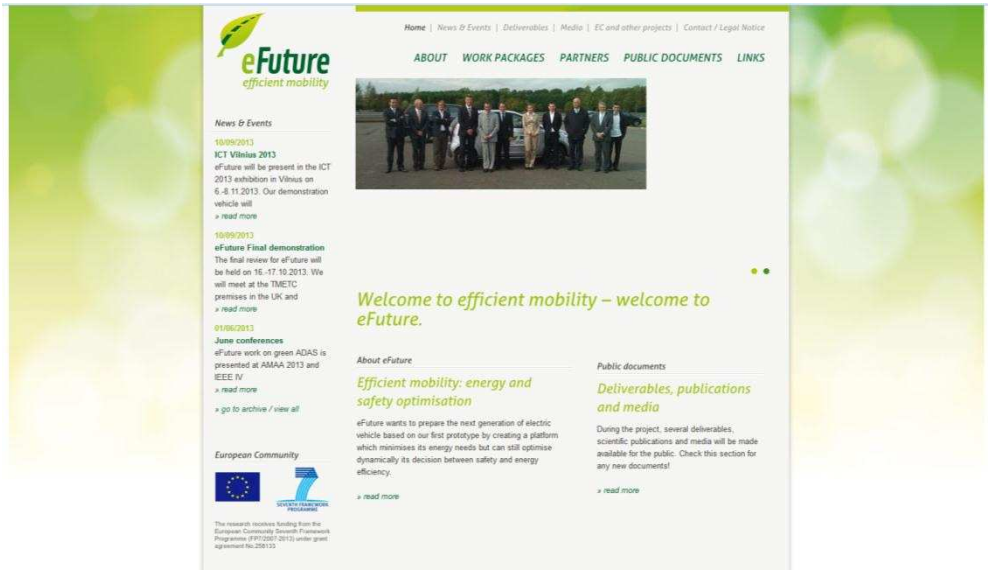

## 2.2 Project presentation

1. June 2011, INTEDIS, "eFuture – General project overview", Third Workshop on Research for the fully electric vehicle, Bruxelles, Belgium
2. June 2011, INTEDIS " eFuture – General project overview" Joint EC / EPoSS / ERTRAC Expert Workshop 2011, Berlin, Germany
3. June 2013, TMETC, WMG Academy trainer
4. November 2013 , All partners, "Efuture - project presentation", ICT 2013, Vilnius, Lituanie

## 2.3 Brochure

The project also chose to publish a brochure explaining for a large audience the work and the improvement realized within the project. The brochure is realized by Verdure and was supported by all partners for the contents.


**Figure 1 Cover page and a middle page**

The topic of the brochure was to define different driving situations, and to explain for each situation what are the technical improvements of the project.

# 3 Appendix

For orientation on the public and scientific articles, we present some selected papers in the appendix of this deliverable:

1. Scheuch V. "E/E architecture for electric vehicle" ATZ Elektronik, 2011 – 06 (see online www.atzonline.de)
2. Glaser S.; Akhegaonkar S.; Orfila O.; Nouveliere L.; Scheuch V.; Holzmann F. "Smart And Green ACC, Safety and efficiency for a longitudinal driving assistance" AMAA 2013, Berlin
3. Revilloud M.; Gruyer D.; Pollard E. " An improved approach for robust road marking detection and tracking applied to multi-lane estimation.", IEEE IV Symposium 2013
4. FakhFakh N., Gruyer D.; Aubert D. " Weighted V-disparity Approach for Obstacles Localization in Highway Environments", IEEE IV Symposium 2013
5. Rittger, L.; Schmitz, M. "The compatibility of energy efficiency with pleasure of driving" 55th Conference of Experimental Psychologists (TeaP), Vienna, 25.-27.03.2013.
6. Schmitz M.; Jagiellowicz M.; Maag C.; Hanig M. "The impact of different pedal solutions for supporting efficient driving with electric vehicles." In P. V. Mora, J.-F. Pace & L. Mendoza (Hrsg.), Proceedings of European Conference on Human Centered Design for Intelligent Transport Systems (S. 21-28). Valencia: HUMANIST.
7. Scheuch V.; Kaiser G.; Korte M.; Grabs P.; Kreft F.; Holzmann F. "A safe torque vectoring function for an electric vehicle", EVS27 Symposium, Barcelona Spain 2013

# E/E-ARCHITEKTUR FÜR BATTERIE-ELEKTRISCHE FAHRZEUGE

In einem europäischen Forschungsprojekt namens eFuture untersucht Intedis gemeinsam mit fünf weiteren Partnern aus vier Ländern neue Funktionen für das Elektromobil, die in eine schlanke E/E-Architektur gebettet sind. Diese soll die zunehmende Komplexität beherrschbar machen und für eine sichere Ansteuerung von Aktuatoren (Motoren, Bremse und Lenkung) sorgen.

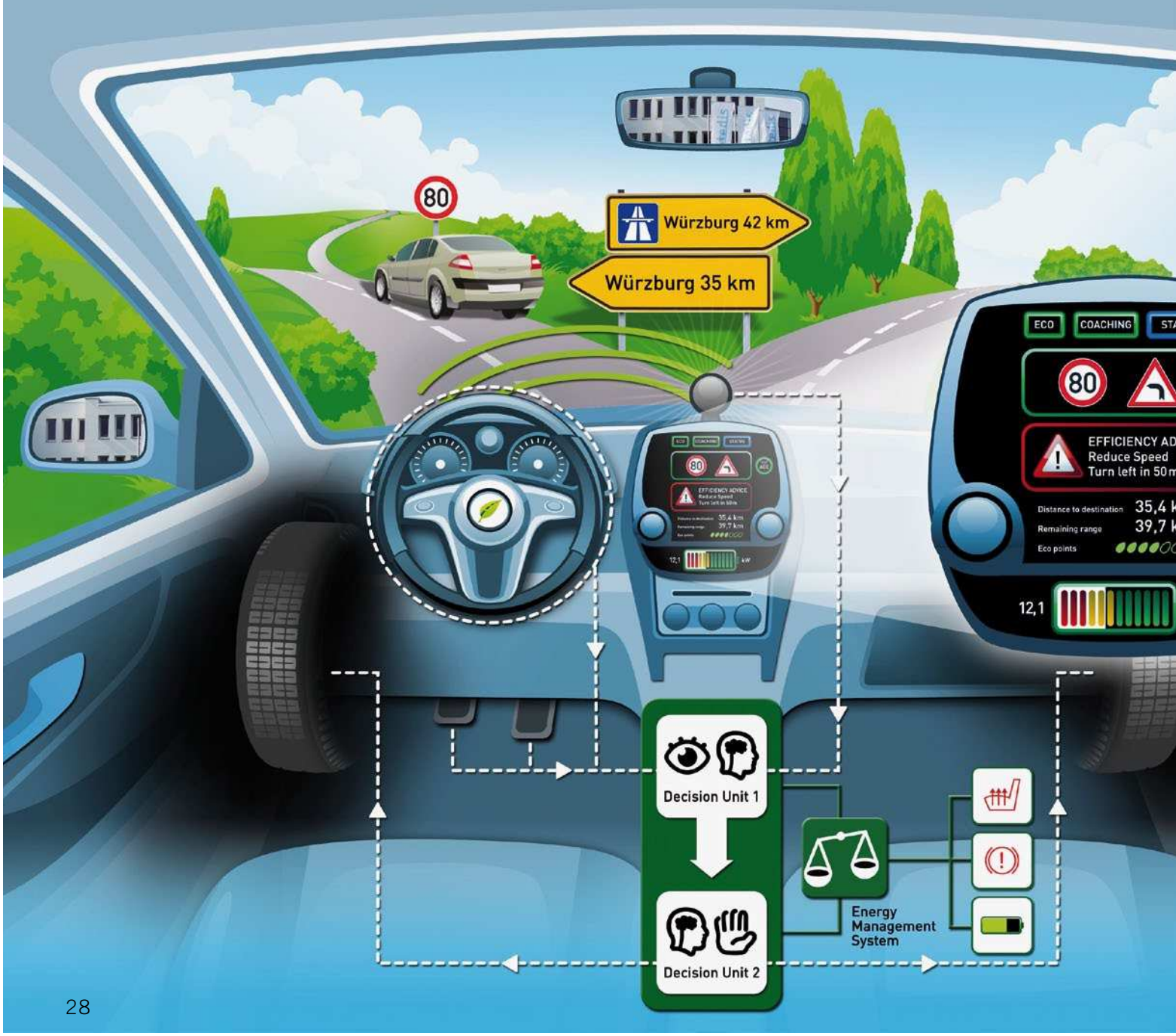


AUTOR

**DR. VOLKER SCHEUCH**
leitet das Projekt eFuture bei der Intedis GmbH & Co. KG in Würzburg.

## ZIELE DES GESAMTPROJEKTS

Das Forschungsprojekt eFuture [1] widmet sich der Reichweitenoptimierung und Fahrsicherheit von Elektrofahrzeugen. Zwei Ansätze verfolgen die fünf Partner der Intedis, Tata, Hella, Miljøbil Grenland, IFSTTAR (Französisches Forschungsinstitut für Transport, Straßenbau und Netze) und WIVW (Würzburger Institut für Verkehrswissenschaften):

- Der Energiehaushalt des Fahrzeugs soll optimiert werden, indem Entscheidungsmodule in einer neu strukturierten E/E-Architektur zwischen den Bereichen Komfort, Sicherheit und Effizienz vermitteln. Zum anderen wird der Fahrer durch Empfehlungen, Hinweise und Assistenzsysteme in die Reichweitenoptimierung einbezogen.
- Die Fahrsicherheit von Elektrofahrzeugen mit mehr als einem Antriebsmotor soll erhöht werden. Um Gefahrensituationen durch nicht-synchrone Radansteuerung zu vermeiden, ist eine Synchronisierung der Steuerungen notwendige, welche ein intelligentes Software- und Sicherheitskonzept erfordert.

Das Konsortium bedient sich dazu der klassischen Werkzeuge Konzeptentwicklung, numerische Simulation und Validierung im Fahrzeugversuch. Nach der ersten Phase der Architekturdefinition, die bereits abgeschlossen ist, werden in der zweiten Phase die Komponenten und das Gesamtfahrzeug aufgebaut. Die dritte Phase beinhaltet die Optimierung und Validierung der Funktionen und Algorithmen im Gesamtfahrzeugversuch.

Dieser Artikel konzentriert sich auf die Reichweitenoptimierung, speziell die E/E-Architektur, die die Basis für mehr Effizienz bildet. Mit Hilfe von zentralen Entscheidungseinheiten (Decision Units), gelingt eine Priorisierung von Anforderungen an den Antriebsstrang, die je nach Fahrzustand den Komfort oder die Effizienz begünstigt, jedoch eine hohe Fahrsicherheit immer gewährleistet.

## E/E-ARCHITEKTUR

Die E/E-Architektur eines Fahrzeugs teilt sich in die Funktionsarchitektur und die physikalische Architektur. Letztere umfasst die Gesamtheit der Steuergeräte, die Netzwerk- und die Kabelbaumtopologie, also die Hardware zur Verteilung von Energie und Signalen. Um diese Netze bedarfsgerecht und schlank zu halten, ist zunächst eine Analyse der gewünschten Fahrzeugfunktionen unerlässlich, denn diese benötigen Sensoren, Aktuatoren, Informationsaustausch mit anderen Funktionen, eine Energieversorgung und ein Steuergerät, auf dem der Algorithmus eingebettet ist. Mit der detaillierten Kenntnis aller Funktionen lässt sich eine Funktionsarchitektur erstellen, die die spezifischen Randbedingungen des Fahrzeugs berücksichtigt. Dies sind im Falle des eFuture-Projekts die maximale Energieeffizienz bei höchster Fahrsicherheit.

Die oberste Ebene der Funktionsarchitektur zeigt ❶. Es wurde ein Lagenmodell gewählt, in dem die klassischen Lagen „Command Layer“ und „Execution Layer“ die Hauptachse für den Fahrbetrieb darstellen. Der „Perception Layer“ vereint alle Umgebungsinformationen über den Fahrer und die Umgebungssensoren inklusive Navigation und eHorizon [2]. Parallel dient der „Energy Layer“ der Steuerung der Energieflüsse und der Zuteilung von Energiereserven an die einzelnen Domänen Fahren, Komfort und Sicherheit. Dies geschieht dynamisch, das heißt in Kenntnis und Abhängigkeit der Fahrsituation und des Fahrerwunsches. Da die Fahrsicherheit

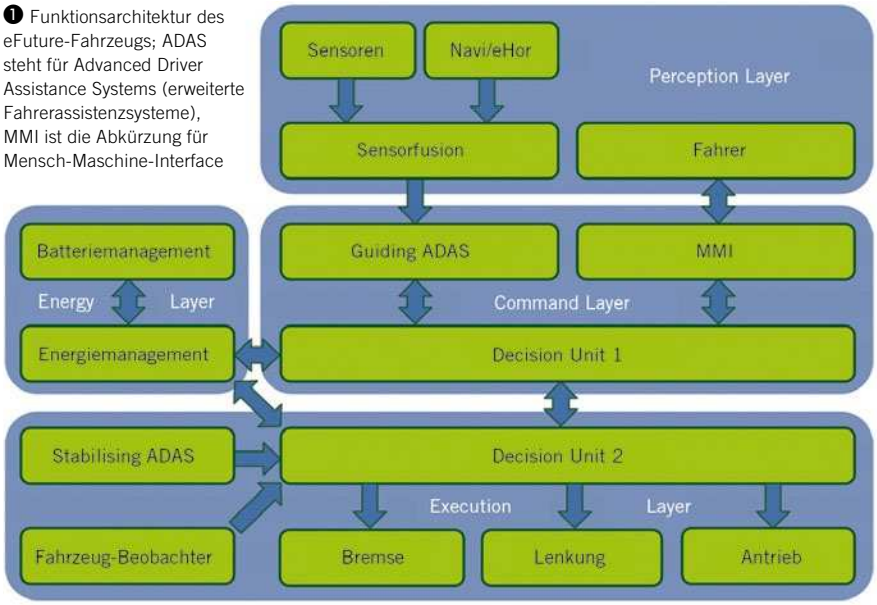


❶ Funktionsarchitektur des eFuture-Fahrzeugs; ADAS steht für Advanced Driver Assistance Systems (erweiterte Fahrerassistenzsysteme), MMI ist die Abkürzung für Mensch-Maschine-Interface

durch Funktionen wie ESC, ABS oder Torque Vectoring realisiert werden, ist eine Kommunikation mit dem „Command Layer“ und dem „Execution Layer“ unerlässlich.

Um die Funktionskomplexität zu beherrschen, verfolgt Intedis das Konzept dezidierter Entscheidungsmodule (Decision Units), die als Zustandsmaschinen (State Machines) ausgeführt sind und gewissermaßen als Zentralintelligenz des Funktionskonzepts dienen. Die Entscheidungsmodule nehmen die Anforderungen oder Randbedingungen der vorgelagerten Funktionen auf und entscheiden aufgrund definierter Kriterien, welche Aktion in dieser Situation durchzuführen ist. Beispielsweise werden während einer Autobahnfahrt verschiedene Anforderungen an das Fahrzeug gestellt: Das adaptive Geschwindigkeitsregelsystem (Adaptive Cruise Control – ACC) möchte aufgrund einer Annäherung an das vorausfahrende Fahrzeug abbremsen, während der Fahrer jedoch durch eine Lenkbewegung zu verstehen gibt, dass er überholen möchte. Falls der Blinker nicht betätigt wurde, würde der Spurhalteassistent (Lane Keeping Assistant – LKAS) mit einem Gegenlenken antworten, das bei gleichzeitigem Bremsen des ACC zu nicht gewünschten Änderungen der Trajektorien oder sogar der Fahrstabilität führen könnte.


❷ Die intelligente Tempomatfunktion hilft durch Kenntnis des Straßenverlaufs, die Geschwindigkeit anzupassen und gleichzeitig sicher und sparsam zu navigieren

Im Falle von einzeln operierenden Funktionen können widersprechende Aktionen nur vermieden werden, indem jede Funktion eine entsprechende Situationsabfrage mit einer Entscheidungslogik beinhaltet. Die Decision Unit stellt dies als Zentralfunktion allen aufrufenden Funktionen zur Verfügung, sodass diese eine schlankere Struktur bekommen können und sich somit auch die Taktzeit reduziert.

Das obige Beispiel lässt noch einen Vorteil des Konzepts erkennen. Der Übergang zwischen verschiedenen Assistenzfunktionen beziehungsweise Fahrzuständen ist durch einfache Regeln möglich. Das Verhalten im Grenzbereich zwischen Lateral- und Longitudinaldynamik kann individuell abgestimmt werden, sodass widersprüchliche und gefährliche Aktionen von verschiedenen Funktionen vermieden werden. Das Gleiche gilt für den Übergang von automatisiertem zu manuellem Fahren, in dem Unstetigkeiten zu unerwünschtem Fahrverhalten führen können.

Die Entscheidung der Decision Unit wird im Normalfall, in dem das Fahrzeug sich in einem stabilen Fahrzustand befindet, im Sinne einer effizienten Fahrweise getroffen. Solange weder der Fahrerwunsch noch die Fahrsicherheit dagegen sprechen, wird immer der für die Reichweiten-Maximierung günstigste Zustand angestrebt („grüne“ Fahrweise). Dieses Prinzip wird durch die Nutzung der zentralen Entscheidung begünstigt, da es keine parallelen Funktionswege gibt.

Um die Komplexität der Decision Unit zu reduzieren, wird diese Zentralfunktion auf den Command Layer und den Execution Layer verteilt. Die Decision Unit 1 im Command Layer ist für die Vermittlung zwischen den spurführenden Fahrerassistenzen (ACC, LKAS, Notbremsassistent), dem Fahrer und den Randbedingungen des Energiemanagement verantwortlich. Die Entscheidung, welcher Trajektorie zu folgen ist, wird der Decision Unit 2 im Execution Layer mitgeteilt. Diese prüft die Anforderung an die Elektromotoren (Beschleunigen versus Rekuperieren), die hydraulischen Bremsen und die Lenkung gegen den aktuellen Fahrzustand und extrapoliert die möglichen Auswirkungen dieses Manövers. Falls es etwa zu einem Übersteuern käme, würde die Decision Unit die Fahrregelung an das ESC übergeben.

Das Konzept unterstützt außerdem die Auslegung der Funktionsarchitektur hinsichtlich der Anforderungen an die Funktionale Sicherheit (ISO 26262). Die sicherheitskritischen Funktionen lassen sich auf die Decision Units beschränken, indem Plausibilitäts- und Sicherheitsprüfungen eingebaut werden, die keine fehlerhaften Funktionsaufrufe zulassen (Safety-Shell-Konzept).

## NEUE FUNKTIONEN UNTERSTÜTZEN EFFIZIENZ UND SICHERHEIT

Die Idee von eFuture ist es, etablierte Funktionen zu nutzen, um neue Funktionalitäten zu erreichen, ohne zusätzliche Hardware zu integrieren. Dabei soll der Begriff „Neu“ eher im Sinne der erstmaligen Anwendung in einem Elektrofahrzeug verstanden werden, da es sich meist um bekannte, aber wenig verbreitete Funktionen handelt. Die Integration neuer Funktionen hat außerdem den Vorteil, dass die Architektur, also die logische und technische Auslegung der Steuergeräte und Netzwerke, auch offen ist für künftige Innovationen. Denn der Anspruch von eFuture ist es, eine zukunftsfähige und erweiterbare Architektur für das Elektrofahrzeug zu schaffen. Neben den bereits beschriebenen „Entscheidungseinheiten“ als Zentralfunktionen umfassen die neuen Funktionen die Themenbereiche:

: Fahrstabilität: Das eFuture-Fahrzeugkonzept sieht einen Doppelmotor-Frontantrieb vor, sodass per se ein elektronisches Differenzial notwendig ist. Die Möglichkeit der unabhängigen Drehmomentverteilung auf die Fronträder wird als Torque-Vectoring-Funktion auch zur Erhöhung der Fahrstabilität auf Fahrbahnen mit lateral unterschiedlicher Reifenhaftung oder in Kurven genutzt.
: Durch eHorizon erhält der Fahrer „vorausschauende“ Informationen, die es ihm ermöglichen, sein Fahrverhalten optimal an die Verkehrssituationen anzupassen. Auch die Assistenzsysteme nutzen diese Informationen für einen effizienten Umgang von Beschleunigen und Rekuperieren. Somit lassen sich kritische beziehungsweise ineffiziente Manöver von vornherein vermeiden [3].
: Reichweitenmanagement: im Sinne eines erweiterten, effizienzsteigernden Energiemanagements mit Hilfe von Assistenzsystemen.

## REICHWEITENMANAGEMENT

Der Begriff Reichweitenmanagement bekommt in Verbindung mit den knappen Energieressourcen (begrenzter Aktionsradius) in einem Elektrofahrzeug eine übergeordnete Bedeutung. Reichweitenmanagement soll den Fahrer dabei unterstützen, den Zielort möglichst energiesparend zu erreichen, oder sich ldurch Fahhinweise eiten zu lassen, um so weit wie möglich mit einer Batterieladung beziehungsweise mit von vorab geplanten Zwischenladungen fahren zu können. Drei Aspekte werden im Reichweitenmanagement genutzt:

: Fahrerassistenz: Die Verschmelzung des Abstandsregeltempomats (ACC) mit der eHorizon-Funktion. Wenn man Daten wie Tempolimits, Steigungen, Kurvenradien, Verzweigungen, Einmündungen für die ACC-Funktion nutzt, lässt sich zur Erhöhung der Fahrsicherheit die Soll-Geschwindigkeit an die Fahrsituation anpassen, ❷. In Verbindung mit einem Eco-Modus lässt sich auch im ACC-Betrieb Energie sparen, indem vorausschauend die Geschwindigkeit redu-

ziert wird oder auf Beschleunigen verzichtet wird, sofern der Straßenverlauf dies nahelegt, ❸.

: Fahrer-Coaching: Im eFuture-Fahrzeug wird der Fahrer in den Regelkreis einbezogen. Er erhält Hinweise zur optimalen Rekuperation oder zum Beschleunigungsverhalten und lernt effizientes Fahren, so fern er die auch abschaltbaren Funktionen nutzt. Schließlich wird dem Fahrer signalisiert, ob sein Fahrtziel mit den vorhandenen Ressourcen und der derzeitigen Effizienz erreichbar ist, ❹.

: Energiemanagement.

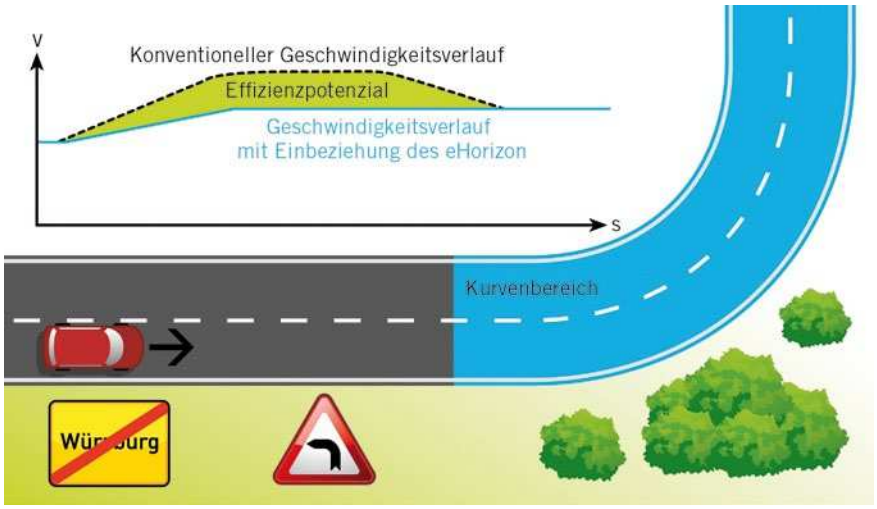


❸ Die neue Funktion des eHorizon erlaubt es, unnötiges Beschleunigen zu vermeiden, falls der Straßenverlauf dies nahelegt

## ENERGIEMANAGEMENT

Ein zentrales und vernetztes Energiemanagementsystem (EMS) sorgt für einen ausgewogenen und bedarfsgerechten Energiefluss zwischen Hochvolt-Batterie und Verbrauchern. Das Projekt eFuture nimmt neueste Erkenntnisse von Batteriemanagementsystemen (BMS) auf, die zur Genüge veröffentlicht worden sind. Neu ist die Integration der beschriebenen Priorisierungen „Sicherheit/Effizienz/Komfort“. Hier kommt zudem das Verhalten des Fahrers ins Spiel, das ebenfalls im Sinne des Energiemanagements vom Fahrer-Coaching beeinflusst werden kann: Eine präzise und detaillierte Ver-


❹ Displaykonzept für Fahrermeldungen zur Energieeffizienz

brauchsberechnung und Reichweitenabschätzung liefert dem Fahrer wertvolle Informationen, um den eigenen Fahrstil zu optimieren und um sein Vertrauen in die Zuverlässigkeit des Elektrofahrzeugs zu steigern. Das EMS ist auch gefragt, falls die Leistungsfähigkeit der Hochvoltbatterie kurzfristig droht, überschritten zu werden. Es kann die Entladeströme dann zu Lasten niedrig priorisierter Verbraucher wie Heizung oder Klimaanlage reduzieren. Durch die Kopplung des EMS mit der eHorizon-Funktion kann es präzisere Aussagen über die Reichweite treffen, da es Informationen über die geplante Strecke, wie zum Beispiel das Höhen- und Geschwindigkeitsprofil, mit einbeziehen kann.

Die beschriebenen Funktionen wurden gemeinsam mit den konventionellen Funktionen in einem numerischen Simulationsmodell dargestellt, sodass Analyse und Optimierung einzeln sowie im Verbund bereits virtuell stattfinden können, bevor im letzten Teil von eFuture die finale Kalibrierung im Realfahrzeug vollzogen wird.

## AUSBLICK

Der nächste Schritt im Projekt ist der Aufbau des Konzepts als fahrfähiger Prototyp. Dazu sind zunächst noch Simulationsstudien notwendig, die das Zusammenspiel der Funktionen in der Fahrer-Fahrzeug-Regelschleife optimieren („Function-in-the-Loop“). Nach der virtuellen Freigabe werden die Steuergeräte mit den Funktionen programmiert und das Fahrzeug kann beweisen, dass die Konzepte im Fahrversuch halten, was sie auf dem Papier versprechen: den Widerspruch zwischen Effizienz, Komfort und Sicherheit aufzulösen helfen. Das eFuture-Konsortium möchte damit einen weiteren Anstoß geben, das Elektrofahrzeug künftig anders zu definieren als konventionelle Fahrzeuge, und so einen Beitrag zur effizienten Elektromobilität leisten.

**LITERATURHINWEISE**

**[1]** www.efuture-eu.org, gefördert durch die Europäische Kommission unter der Fördernummer 258133

**[2]** Ress, C.; Etemad, A.; Kuck, D.; Boerger, M.: Electronic Horizon – Supporting ADAS applications with predictive map data. Cebit Papers 2006

**[3]** Kaiser, G.; Holzmann, F.; Chretien, B.; Korte, M.; Werner, H.: Torque Vectoring with a feedback and feed forward controller – applied to a through the road hybrid electric vehicle. Intelligent Vehicles Symposium (IV), 2011 IEEE, S. 448-453

# Smart And Green ACC, Safety and efficiency for a longitudinal driving assistance

**Sebastien Glaser(1), Sagar Akhegaonkar(2), Olivier Orfila(1), Lydie Nouveliere(1) , Volker Scheuch (2), Frederic Holzmann(2)**

1. LIVIC (Laboratory on Interactions Vehicles-Infrastructure- Drivers), a research unit of IFSTTAR, Batiment 824, 14, Route de la Miniere, 78000 Versailles, France (phone: +33 1 40 43 29 08; e-mail: firstname.lastname@ifsttar.fr).

2. INTEDIS GmbH & Co. KG, Max-Mengeringhausen-Strae 5, 97084 Wuerzburg - Germany (phone: +49 (0) 931 6602-35740; e-mail: firstname.lastname@intedis.com).

**Abstract**

Driving Assistances aim at enhancing the driver safety and the comfort. Nowadays, the consumption is also a major criterion which must be integrated in the driving assistances. Then, we propose to redefine the behavior of an ACC with energy efficiency consideration to perform a Smart and Green ACC. We apply our development to the specific use case of the electric vehicle that allows regenerative braking. The ACC, once activated, operates under two possible modes (speed control and headway spacing control). We define the behavior of the driving assistance under these both possible modes, focusing on the distance control. We present the efficiency of various strategies without trading off safety. We conclude on the efficiency by presenting several use cases that show the SAGA behavior.

## 1 Introduction

Daily traffic congestion or long trip on a highway are issues that the driver must face during his driving experience. However, these tasks may generate anger, stress or drowsiness. In a situation where the driver kept a constant clearance for a long time, and suddenly facing braking, his reaction time is higher and may lead to a collision. Automation, and automated driving seem to be one possible answer to these problems, by delegating partly or totally the driving task. Many projects during the 80's and 90's, have proved the feasibility of automated and autonomous (without driver interaction) driving systems. Eureka Prometheus project in Europe, or the US National Automated Highway System consortium conducted experiments on real road of automated driving or platoon. Even if the concepts were not fully adapted by car manufacturers, current vehicles benefit greatly from these research. Since 10 years, the driving assistances are booming. However these driving assistances present two major drawbacks:

- The optimization process behind the driving assistance aims only at maximizing the safety and/or the comfort of the considered vehicle,
- In order to work, the driving assistance relies only on the perception systems embedded in the vehicle: they are autonomous systems.

In today situation, the energy consumption is one of the major topic for the car users: electric vehicles still have a limited range and for conventional vehicles, the oil price has skyrocketed and the greenhouse gas emissions must be reduced. The consumption criterion must be taken into account in the definition of a driving assistance.

Moreover, communication devices and navigation devices become popular. In a vehicle, we can consider that we have access to these systems to exchange data with other vehicles and with the infrastructure. The driving assistance systems are now cooperative and the driving assistance systems can sense the environment behind the vehicle sensors range.

In the eFuture project, we focus on the shared control between the vehicle automated systems and the driver for electric vehicles. The driving assistance we propose, the Smart and Green ACC (SAGA), derives from a standard ACC (Adaptive Cruise Control). It aims at optimizing the common criteria and also the energy consumption. Moreover, the required variables come from the vehicle sensors and from a digital map which includes information on the upcoming road.

With an Adaptive Cruise Control system, the driver delegates the longitudinal control task. When the system is active, the vehicle speed is controlled automatically either to maintain a given clearance to a forward vehicle, or to maintain the driver desired speed, whichever is lower. Since 1997, car manufacturers propose this system on their high-end cars. However, research is still active. Researchers aim at evaluating the impact of the ACC on traffic, under congested situation [1] or with improved strategies [2]. They also extend the range of possible speeds, driver comfort, safety or road capacity [3], [4]. In 2006, the introduction of a vehicle to vehicle communication (cooperation ACC, C-ACC) allows to decrease drastically the clearance to a forward vehicle [5] and also to create stable vehicle platoon. The evaluation of the C-ACC [6], [7] shows promising results on road capacity and safety. An ISO standard now defines the intended performance of the ACC [8].

In the following, we develop the Smart and Green ACC function. In the next section, we define the function, the notations and the consumption model. Section three explains the two problems: speed control and distance control. This last point, being the main issue, as it means to handle both consumption and safety criteria, will be developed in section four. The section five presents simulation results. In the last section, we conclude on this work.

# 1 Problem definition

## 1.1 Adaptive Cruise Control

When an ACC system operates, the function is either in a speed control or distance control mode (Figure 1). In the first case, there is no vehicle in front of the considered vehicle or in the distance of sensing. The vehicle aims at reaching a driver's desired speed. In the second case, a vehicle is in front of our vehicle. The system aims at maintaining a clearance defined by the driver, as soon as the lead vehicle speed is lower than the driver's desired speed.

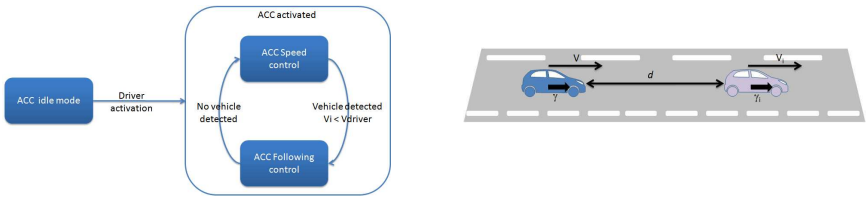


**Fig. 1.** ACC architecture and generic use case

The general variables are represented on the Figure 1, along with the Table 1, for the description and units.

**Table 1.** ACC related variables

| *Variables* | *Description* | *Units* |
|---|---|---|
| $d$ | Clearance to the lead vehicle | m |
| $V, V_d$ | Speed of the ego vehicle, driver desired speed | m/s |
| $\gamma$ | Acceleration of the ego vehicle | m/s² |
| $T, T_d$ | Time Headway ($T = d/V$), driver desired time headway | s |
| $V_i$ | Speed of the lead vehicle | m/s |
| $\gamma_i$ | Acceleration of the lead vehicle | m/s² |
| $\Delta V$ | Relative Speed ($\Delta V = V_i - V$) | m/s |

Moreover, [8] also defines the operating range of the driving assistance. The assistance cannot be activated below a given speed $V_{min}$, which must be higher than 7m/s. The average automatic deceleration of ACC systems shall not exceed 3.5m/s², while the acceleration is limited to 2m/s². the average rate of change of an automatic deceleration (jerk) shall not exceed 2.5m/$s^3$. The ISO standard also defines the minimal performance of the perception system according to the possible value of the speed and of the time gap.
Then, we have to define the behavior of the SAGA function for these two modes: Speed Control and Distance Control.

## 1.2 Consumption and efficiency model

The consumption model that we define here, is based on the evaluation of the torque needed, at each of the two motorized wheel, to overcome resisting forces and generate the desired acceleration. It could be defined as:

$$T = \frac{R_w}{2}\left(\frac{1}{2}\rho S\, C_x V^2 + Mg\, C_{rr} + M\, G \sin\phi_r + M\gamma\right) \quad [1]$$

where $R_w$ is the wheel radius, the air volumetric mass, $SC_x$ the air drag coefficient, V the current vehicle speed, M the vehicle's mass, $C_{rr}$ the rolling resistance coefficient, $\phi_r$ the slope and $\gamma$ the vehicle acceleration. The engine speed, supposing without sliding, is $w_e = V/R_w$. According with the torque definition, we evaluate the kinetic energy and the electric energy that is either consumed or regenerated during a period of time $dt$, depending on the value of the torque, in the table II.

**Table 2.** Energy definition for the consumption model

| *Energy* | *Consumption* | *Regeneration* |
|---|---|---|
| Mechanic | $E_m = 1/\eta_g T_e w_e dt$ | $E_m = \eta_g T_e w_e dt$ |
| Electric | $E_m = 1/\eta_b\, E_m \eta(T_e, w_e)$ | $E_m = \eta_b E_m \eta(T_e, w_e)$ |

where $\eta_g, \eta_b, \eta$ are respectively the efficiency of the transmission, the battery and the motor. This last parameter depends on the torque demand and on the motor speed.

Using previous equations, we can then define the specific regenerative braking area for a given electric motor associated with the regenerated power. A real characteristic of regenerative deceleration is presented on the Figure 2. It is obtained from the first prototype of eFuture project. At low speed, the regenerative braking is not high. The main reasons are technological choices and to avoid that a regenerative braking leads to a blocked wheel. However, at low speed, the energy that could be regenerated is low, because of the low speed of the motor.

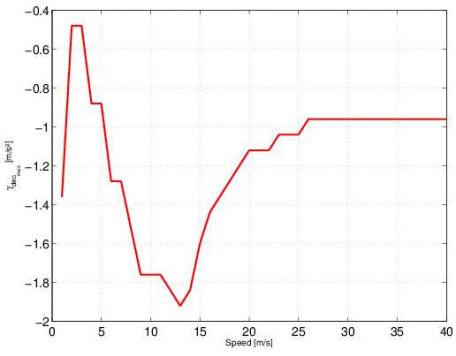


**Fig. 2.** Regenerative braking area for an electric motor

The regenerative braking area could be easily approximated by the following function :

$$\gamma_d(V) = \begin{cases} \gamma_{dec_1} & : \quad V < V_1 \\ \dfrac{A}{V} & : \quad V \geq V_1 \end{cases} \qquad [2]$$

where $A$ is a negative constant, $\gamma_{dec_1}$ is the maximal deceleration below a given speed $V_1$.

# 2 SAGA function

As described in the previous section, our SAGA function must cope with two operating domain. The first one corresponds to the speed control case, where the system must follow a driver's desired speed. The second one deals with the problem of distance control with a lead vehicle. The system must regulate the speed to maintain a constant clearance expressed as a driver desired headway time.

## 2.1 SAGA speed control function

In this operating mode, there is not many safety related issues considering the interaction with the other road users, as, by definition, SAGA system operates in this mode when no vehicle is detected in front of our vehicle.

The main idea is then to supervise the conventional behavior of the ACC by defining a speed profile that includes the regenerative braking limitation and safety issues using a digital map to provide the needed data: legal speed limit if lower, can override the driver desired speed; approaching an intersection, the system automatically decreases the speed limit; using the curvature and slope information, a speed profile is defined to safely pass the curve. In this case, we extend the speed profile computation defined in [9,10] with the deceleration limitation of the regenerative braking described previously.

## 2.2 SAGA distance control function

The distance control function is far more critical as it directly deals with the interaction between vehicles. The objective of the ACC is to regulate the error on the clearance $e_d$ ($e_d = d - T_d V$) around 0. Depending on the sensors used to measure the distance, the algorithm may be more robust by integrating the error on the relative speed $\Delta V$. The resulting acceleration is a function of this two errors, which is limited by the definition of the ACC. However, the regenerative braking is often below this threshold: with only a regenerative braking, we cannot ensure the same safety level of an ACC if we use the same strategy. Figure 3 shows the

safety domain of a conventional ACC and an ACC which uses a regenerative braking. In this figure, we suppose that a front vehicle has a constant speed of 20m/s and that the driver sets the time headway at 2s.

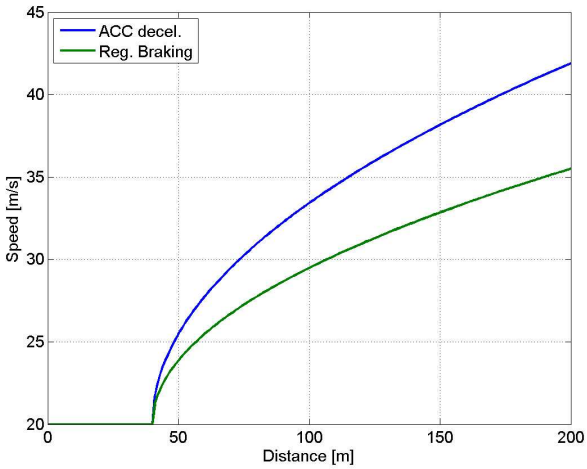


**Fig. 3.** Conventional ACC and regenerative braking safety domain

The objective is then to regulate the acceleration of our vehicle to reach the point $(40m, 20m/s)$. We can define a limit curve as being the points $(d, v)$ which allow to reach this point with a given braking capacity. The points below this curve are in a safe area. As the regenerative braking is lower than the conventional ACC, the safe area is smaller. If we want to keep the performance in term of speed, the sensing range must be greater, at the opposite, if we want to keep the same performance on the sensors, then the maximal speed must be smaller. In the following, we suppose that we keep a constant maximal sensing distance and that we limit the maximal speed.

## 3 SAGA and distance control problem

We must handle two specific situations for distance control:

- We approach a slow vehicle, starting at a given distance and speed in the safe domain
- We follow a vehicle with an error $e_d$ at zero. The lead vehicle start to decelerate with a deceleration that is greater than the possible deceleration.

For the first problem (see Figure 4), we can suppose that the vehicle can either maintain a constant speed until it reaches the limit of the safe area, then decelerate at the regenerative deceleration (red path). Or that the vehicle starts to decelerate early to reach a speed that is slightly higher than the lead vehicle, and then it dece-

lerates slowly (orange path). Between these two extrema, we can tune the SAGA strategy.

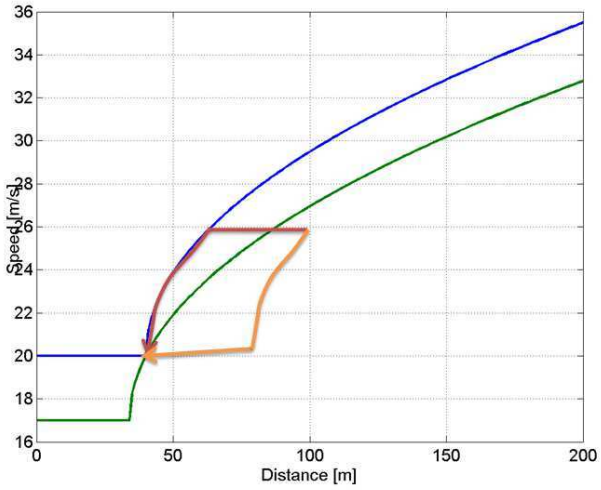


**Fig. 4.** Variation of the safe domain with a deceleration of the lead vehicle

The main drawback of the second strategy is that the gap between the two vehicles diminishes slowly. This situation allows a third vehicle to cut in our lane, leading to possible strong deceleration of our vehicle. If we follow the first strategy, and that the lead vehicle starts to decelerate, we may go out of the safe domain. For instance, if the front vehicle decelerates to 17m/s (green curve in Figure 4), our trajectory may quickly go out of the safe domain, losing the regenerative capacity, while the other strategy allows us to remain in the safe domain. Therefore, we need to define a tradeoff between these two strategies.

For the second problem, we need, at least, to achieve at least the same safety than a conventional ACC. For instance, we consider the following use case: a lead vehicle that drives at 30m/s, our vehicle is at the same speed and the time headway is set at 2s. The lead vehicle decelerates with a given deceleration $\gamma_i$ up to a speed of 7 m/s. The ACC system can achieve the deceleration without any collision for a large variation of the lead vehicle deceleration, even if the time headway drops to very low value (0.6 s for a considered deceleration of -8 m/s²). Figure 5 represents the clearance when the vehicle reaches the same speed than the lead vehicle. Even for a very strong deceleration, the vehicle does not collide.

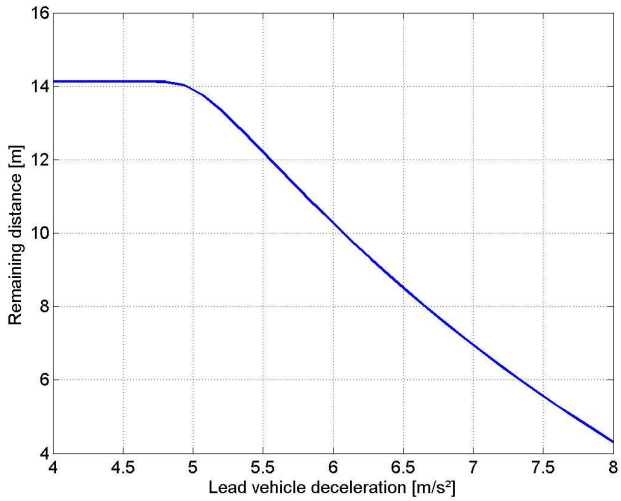


**Fig. 5.** Final clearance as a function of the deceleration of the lead vehicle

Using the regenerative deceleration only, it is not possible to obtain the same safety level than a conventional ACC with the same use case (initial time headway of 2 s, speed of 30 m/s and final speed of the lead vehicle of 7 m/s). The possible solutions are:

- To increase the minimal time headway that is defined by the driver. However, to obtain the same safety, we need to increase the minimal time headway up to 5s. The resulting distance is hardly achievable as the sensor range is limited and other road user may cut in the space between vehicles.
- To switch to conventional braking if the time headway drops below a given threshold. For instance, we can maintain a collision free system, as for a conventional ACC, with an initial time headway of 3.7s and an activation of a stronger braking at a threshold on the time headway of 1.5s
- To switch to an emergency braking if the deceleration of the lead vehicle and the distance drops below given thresholds. If the emergency braking can generate a deceleration of -6m/s² when the time to collision (difference of distance divided by the difference of speed) is below 2s, we can set the minimal time headway at 3s.

As we want to use only the ACC system, then we choose the second option. However, we do not evaluate the acceptability by the user of the resulting clearance.

# 4 Simulation results

In the following, we develop two different use cases to present the efficiency of the system. In a first scenario, our vehicle drives at the driver desired speed and it approaches a slow vehicle. The second scenario shows the reaction on a cut in situation. The new target first decelerates slowly to increase the clearance with the previous lead vehicle, then accelerates to reach the traffic flow speed.

In the following, the ACC aims to regulate the distance at an headway of 2s, the SAGA parameter is at 3.5s. For SAGA, we use the conventional ACC if the headway drops below 1.2s, and we start to control the vehicle with a 20% longer distance.

## 4.1 Approaching a slow vehicle

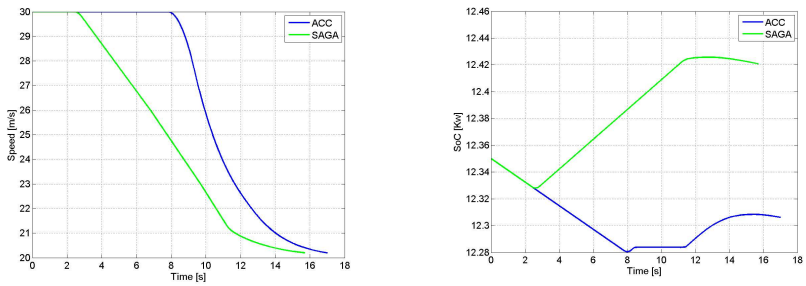


**Fig. 6.** Approaching a vehicle, comparison of SAGA and ACC outputs on speed and state of charge

In this scenario (see Figure 6), we suppose that the lead vehicle is at 150m in front of our vehicle. The lead vehicle's speed is constant and equal to 20m/s. SAGA takes into account this front vehicle very early and decelerates slowly to reach the same speed and the correct clearance. The clearance decreases slowly and the complete maneuver takes more than 12s. For the ACC, the same result is achieved in 8s. During this maneuver, the State of Charge (SoC) increases of 0.07kw for the SAGA, while it decreases of 0.05kw for the ACC.

## 4.2 Vehicle cut in

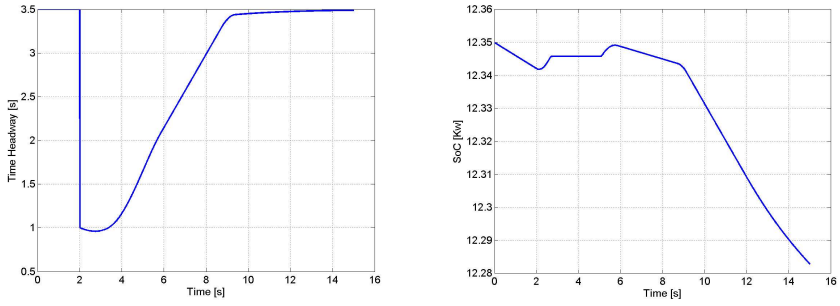


**Fig. 7.** Evolution of the time headway and the SoC during a cut in use case

In this use case (see Figure 7), we suppose that our vehicle follows a lead vehicle at a speed of 20m/s with a time headway of 3.5s. At t=1s, a vehicle inserts at a distance of 20m in front of our vehicle. Its speed is 20m/s and it decreases slowly to 18m/s in order to increase its gap with the lead vehicle. At t=1s, our vehicle starts to decelerate, first with a regenerative deceleration, but as the new lead vehicle may be dangerous, the system shift to a conventional ACC, without regenerative capacity. During this deceleration, the vehicle's speed drops to 12.7m/s. In the last phase the vehicle has to accelerate to reach the lead vehicle speed and the driver desired time headway. The system manages this dangerous situation without any collision.

## 5 Conclusion

In this article, we have presented the Smart and Green ACC, namely SAGA. This application enhances the conventional ACC for electric vehicle with regenerative capacity. The main aim of the application is to deliver, at least, the same level of safety than a conventional ACC, and to integrate a consumption criteria. Given the motor specification, and the possible deceleration, the tradeoff is to increase the clearance and to replace the regenerative deceleration with a conventional braking if the clearance drops below a low value. Moreover, the deceleration has to start early to allow a regenerative braking when the vehicle approach a slower vehicle. This behavior could maintain a large clearance for a long time, allowing a third vehicle to cut in the gap. On daily situation, the driving assistance shows to be efficient, increasing or at least maintaining the state of charge of the battery. We demonstrate the efficiency and the safety of our application on two use cases.

However, the behavior of the driving assistance has a huge impact on the acceptability: increased clearance, long deceleration and resulting smaller time headway, which need to be evaluated under the user point of view.

# 6 References


[1] Marsden G., McDonald M., Brackstone M., Marsden G., Towards an understanding of adaptive cruise control, Transportation Research Part C 9 (2001) 33-51

[2] Kesting A., Trieber M., Schonhof M., Helbing D., Extending adaptive cruise control to adaptive driving strategies, Transportation Research Record: Journal of the transportation research board, N2000, 2007, pp 16-24

[3] Vahidi A., Eskandarian A., Research advances in intelligent collision avoidance and adaptive cruise control, IEEE Transactions on Intelligent Transportation Systems, 4(3), 143-153.

[4] Moon S., Moon I., Yi K., Design, tuning,and evaluation of a full-range adaptive cruise control system with collision avoidance, Control Engineering Practice (2009)442-455

[5] Naus G., Vugts R., Ploeg J., van de Molengraft R., Steinbuch M., Cooperative Adaptive Cruise Control, IEEE Automotive Engineering Symposium Eindhoven, The Netherlands, April 6, 2009

[6] Van Arem B., Van Driel C.J.G. and Visser R., The impact of cooperative adaptive cruise control on traffic flow characteristics, IEEE Transactions on Intelligent Transportation Systems, Vol. 7, No. 4, pp. 429-436, Dec. 2006

[7] Nowakowski C, Shladover S.E., Cody D. et al., Cooperative Adaptive Cruise Control: Testing Drivers Choices of Following Distances, UCB-ITS-PRR-2010-39

[8] ISO 15622:2010, Intelligent transport system, Adaptive Cruise Conrol system, performance requirements and test procedures

[9] Glaser S., Aguilera V., Vehicle Infrastructure Driver Speed Profile : Towards the next Generation of Curve Warning Systems, In Proc. of the 10th ITS World Congress, Madrid, Spain, nov. 2003.

[10] Aguilera V., Glaser S., Von Arnim A., An advanced Driver Speed Assistance in Curves : risk function, cooperation modes, system architecture and experimental Validation. In Proc. of the IEEE Intelligent Vehicle Symposium, Las Vegas, 2005.

## 7 Full Author information

Sebastien GLASER
LIVIC, 14 route de la minière
Bat 824
78000 Versailles
France
E-mail: Sebastien.glaser@ifsttar.fr

Sagar Akhegaonkar
INTEDIS GmbH & Co. KG, Max-Mengeringhausen-Strae 5
97084 Wuerzburg
Germany
E-mail: Sagar.Akhegaonkar@intedis.com

Olivier Orfila
LIVIC, 14 route de la minière
Bat 824
78000 Versailles
France
E-mail: olivier.orfila@ifsttar.fr

Lydie Nouveliere
LIVIC, 14 route de la minière
Bat 824
78000 Versailles
France
E-mail: lydie.nouveliere@ifsttar.fr

Frederic Holzmann
INTEDIS GmbH & Co. KG, Max-Mengeringhausen-Strae 5
97084 Wuerzburg
Germany
E-mail: Frederic.Holzmann@intedis.com

Volker Scheuch
INTEDIS GmbH & Co. KG, Max-Mengeringhausen-Strae 5
97084 Wuerzburg
Germany
E-mail: volker.scheuch@intedis.com

## 8 Keywords

Driving assistance, longitudinal control, energy efficiency

2013 IEEE Intelligent Vehicles Symposium (IV)
June 23-26, 2013, Gold Coast, Australia

# An improved approach for robust road marking detection and tracking applied to multi-lane estimation.

Marc Revilloud, Dominique Gruyer IEEE Member, Evangeline Pollard

*Abstract*— **In this paper, an original and innovative algorithm for multi-lane detection and estimation is proposed. Based on a three-step process, (1) road primitives extraction, (2) road markings detection and tracking, (3) lanes shape estimation. This algorithm combines several advantages at each processing level and is quite robust to the extraction method and more specifically to the choice of the extraction threshold. The detection step is so efficient, by using robust poly-fitting based on the point intensity of extracted points, that correction step is almost not necessary anymore. This approach has been used in several project in real condition and its performances have been evaluated with the sensor data generated from SiVIC platform. This validation stage has been done with a sequence of 2500 simulated images. Results are very encouraging : more than 95% of marking lines are detected for less than 2% of false alarm, with 3 cm accuracy at a range of 60 m.**

## I. INTRODUCTION

For at least two decades, the development of transportation systems have led to the developement of embedded applications allowing to improve the driving comfort and to minimize the risk level of hazardous areas. More specificaly, the researches in intelligent and Advance Driving Assistance Systems have provided a great number of devices on many types of automatic vehicle guidance and security systems such as obstacle detection and tracking [1], road visibility measurement [2], pedestrian detection, road departure warning systems.... However, one of the first embedded system that was studied is probably the lane detection system. This application is usually based on road marking detection algorithms. [3]. This system is also one of the most important source of information in order to build a local perception map of an environment surrounding an ego-vehicle. Indeed, this information provides relative vehicle location information to all other perception systems (obstacles, road signs, ...) that need to know the road and lanes attributes. For this reason the system must be as robust as possible. Moreover, for several year, it appears evident the automation of the driving task is probably a solution in the reduction of the road injuries. But for automated or partially automated driving task, the road marking and lane localization are very important and provide a critical information. This information needs to be really accurate, certain, reliable in order to achieve some manoeuvers like lane changes or generate safe path planing (co-pilot) [4].

M. Revilloud and D. Gruyer are with the LIVIC research laboratory, IFSTTAR, 14 route de la Miniére, bat 824, 78000 Versailles, France

E. Pollard is with the INRIA Paris-Rocquencourt research laboratory, in the project-team IMARA evangelinepollard@gmail.com

The research and the study proposed in this paper are directly dedicated to this important topic of road markings detection and tracking , and lanes estimation for automated and/or partialy automated driving applications. Our objective is to provide an assessment of the road surface attributes (road markings attributes, type of road marking, number of lane and characteristic of lanes). This method is based on use of one or several embedded cameras.

Most of the algorithms are basically based on a three-step scheme summarized as follows. First, images are processed in order to extract road marking features. Second, extracted primitives are analyzed in order to extract point distributions corresponding to a road marking. And finally in a third step, extracted and validated points are used to extract lane shape. In some previous work [5], the first extraction part has been studied, tested, and evaluated in order to determine the best way to extract road marking primitives. In this paper, a double extraction strategy is proposed to achieve the discimination of the points for marking points and non-marking points. To guaranty the robustness of our approach, we proposed in addition a performance evaluation protocol for the first road primitives extraction stage based on the use of the SiVIC platform, which is presented in [6]. This protocol provides an accuracy measurement of the clustering and robustness relatively to a clustering threshold $T_g$.

In this paper, we present several significant improvements of the original method proposed by S. S. Ieng and D. Gruyer in [7]. The global scheme is the same one but some enhancements have been done in each part. For instance, the combination strategy of several extractors, the management of the primitives in the detection stage, and the lane and markings estimation in the lane estimation part has been modified. In addition, instead of imposing a very discriminative threshold into the extraction part, we propose the use of the intensity of the extracted point into both the detection and the estimation parts. Lane marking detection, originally based on the study of an histogram containing projected points, is now made by using the same type of histogram but where the projected point are weighted in function of their uncertainty. Moreover, the poly-fitting mechanism has been replaced by a a weighted poly-fitting, for the same reason. Higher is the extracted intensity points, more strongly weighted are these points in the estimation process. To robustify our approach and avoid false alarms, distribution points which are not satisfying very discriminative criteria for peak clustering are submitted to a robust weighted poly-fitting. In this way, point distributions containing outliers (as it could happen in the case of sidewalks or guardrail which

978-1-4673-2754-1/13/$31.00 ©2013 IEEE

produce false alarms), are still validated as road markings. Finally, comparatively to the initial version of this algorithm, the proposed improvements lead to better results. These changes in the different part of this method allow to affirm that the use of the filtering step is not important anymore.

The Fig. 1 gives an global overview of the proposed road marking detection and tracking and lane estimation architecture. The paper is organized as follows. In Sec. II, the

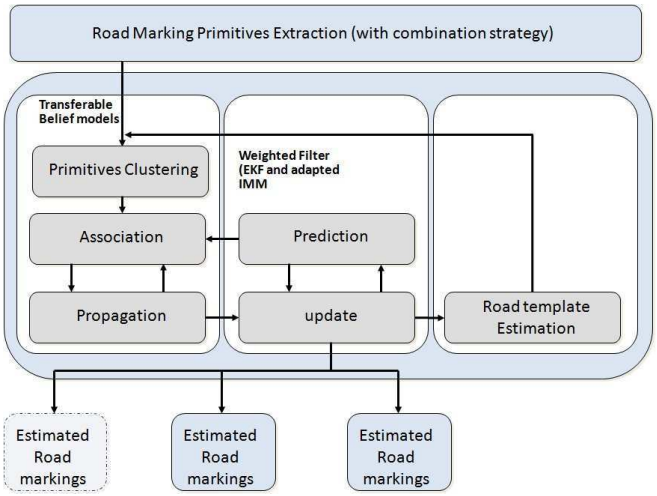


Fig. 1. The entire process for road marking detection

SiVIC platform used for the evaluation of marking detection is presented. In Sec. III, the three main parts of this approach are detailed. Sec. IV described the evaluation protocol used for road marking detection algorithm. Sec. V presents a set of results with differents road conditions and levels of quality for the road markings.

## II. The SiVIC platform

SiVIC is a virtual sensor simulation platform for ADAS prototyping. It simulates different embedded sensors (camera, telemeters, GPS, radar, communication devices, INS, odometer ...) and the dynamic vehicle behaviour of vehicle as described in [6]. In order to prototype and to test ADAS, a realistic 3D reproduction of the real Satory's test track was produced by LIVIC. Fig. 2 shows the similarity of this simulation in comparison with the same perspective on the real track. In this figure, the first line provides virtual renderings and the second line gives the real pictures from the same point of view. This simulation takes into account a great number of detail such as as the road shape, guard rails, buildings, road sign elements, trees, etc. The images generated by the SiVIC platform can be considered relatively close to the images which could be provided by a real camera Fig. 2. The quality of this virtual platform is mainly due to:

- The high accuracy of both the shapes of the Satory's track (build from a centimetric GPS-RTK) and the additional element of the environment (buiding, guardrail, sidewalk, trees, road signes, differents fences, ...)
- Natural images of bitumen used as road textures

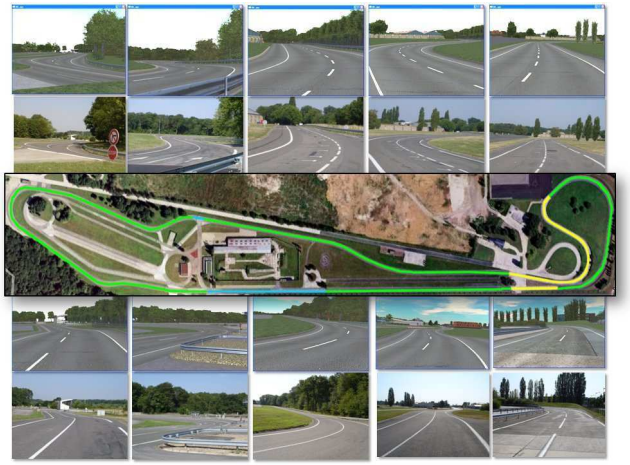

Fig. 2. Comparison of SIVIC and natural images

- The realistic model of the vehicle dynamics
- An accurate modeling of the optical sensor as describe in [8]
- The capabilities of SiVIC to provide both camera images and the associated ground truth.

## III. Road marking detection and estimation

On the same principle as [7], a three step process for lane marking detection and estimation is proposed. The main purpose is to obtain the number of lane markers $N_k$, their position and their shape. For each validated lane marker $m$, the goal is also to provide an estimation of the road shape as a second degree polynomial in the vehicle coordinate system

$$x = a_0^m + a_1^m \cdot y + a_2^m \cdot y^2 \quad (1)$$

As illustrated in Fig. 1, the first step consists in extracting road marking primitives. The second step is dedicated to the association stage. In fact from a set of extracted primitives, the objective is to detect the number of road markings and to associate them with the last ones (the road marking tracks). In a third step, given a set of labeled primitives, the goal is to provide, for each frame $k$, an estimation of the real state $A_{m,k}$ of any road marking $m$:

$$A_{m,k} = \left[a_{k,0}^m, a_{k,1}^m, a_{k,2}^m\right]^T \quad (2)$$

corresponding to eq. (1), where $(\cdot)^T$ denotes the transpose transformation. With this information, an associated uncertainty matrix $P_{m,k}$ is also estimated.

### A. Lane marker feature extraction

The first step consists also in establishing which input image points belong to a lane marker. Most of the time, lane marker forms bright region (white or yellow paint) on a dark background (asphalt), having a limited width. Extraction purpose is also to detect regions with a gradient intensity higher than a certain threshold $T_g$ and bounded by the interval $[S_m, S_M]$. It has been shown in [9], that local thresholding methods provide the best results. In some previous work [10], a protocol was proposed for the evaluation of road marking

extraction algorithms, based on synthesized images coming from simulator Sivic. After a study about performances of four extraction algorithms based on local thresholding, we proposed a new lane feature extraction algorithm based on a double extraction scheme. However, experimental results show that the assumption that better are the extraction step (using the procole used in [5]), more accurate is the road state estimation is uncorrect. Results presented in Sec. V prove that with the improvement of detection part, if double extraction scheme does not degrade performances, it does not improve it and necessarily increases time processing. Extraction step is also limited to SLT (Symmetric Local Threshold) in order to provide a set of extracted points $E$ and their corresponding intensity.

Finally, to enable the processing of extracted point, each extracted point of each cameras are projected in the vehicle coordinate system. This projection stage uses intrinsic and extrinsic parameters of the camera which are known. The position is fixed, perpendicularly to the car frame. The origin of the camera coordinate system $\mathcal{R}_{cam} = (O_{cam}, \vec{X}_{cam}, \vec{Y}_{cam}, \vec{Z}_{cam})$ is also established at coordinates $(0, 0, h)$ in the vehicle coordinate system, denoted $\mathcal{R}_v = (O_v, \vec{X}_v, \vec{Y}_v, \vec{Z}_v)$, as illustrated in Fig. 3, with $h$ the height of the camera knowing the car reference. This coordinate system is centered on the car referential, perpendicularly to the road surface, assumed to be plane.

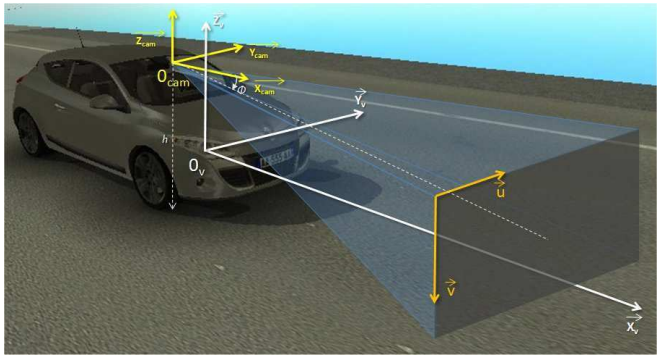


Fig. 3. Observation and coordinate system

## B. Lane marker detection

*1) Point projection:* Knowing the set of extracted points $E$ (*cf.* Fig. 4-(a)), the goal is now to detect marking lines and label extracted points according to detected lines. Their associated intensity is used in addition in order to take into account their uncertainty. Even if Hough transformation, traditionally used to detect straight lines can be extended to curves [11], the proposed approach is based on an analysis of the spatial distribution of extracted points on the $X_v$ axis. $X_v$ space is first cut into constant space intervals between $X_v^{min}$ and $X_v^{max}$. Contrary to [3], where points are projected along the $Y_v$ axis, our 2D-detected points are projected along the road shape on the $X_v$ axis. They are projected between 1 and 255 times depending on the value of their intensity. Shape of the road is established by using best available estimation states. More details are given to define what is a good estimation in Sec. III-F. According to its projection state $x_i^p$, each point $i$ ($\forall i \in \{1, \ldots, n\}$) given by primitive extraction step illustrated in Fig. 4-(a) and projected to vehicle coordinate system, can be associated to a $x$-interval corresponding to a dynamic projection template, illustrated in Fig. 4-(b). A point density histogram is then constructed. To distinguish marking lines to false alarms and to precisely establish peak coordinates, the histogram is convoluted with a Normal distribution $\mathcal{N}(\cdot, (\sigma_i^c)^2)$ with a variance $(\sigma_i^c)^2$ corresponding to the width of two histogram intervals, as shown in Fig. 4-(c). Histogram peaks correspond to marking lines. The next step consists in precisely and reliably detect histogram peaks.

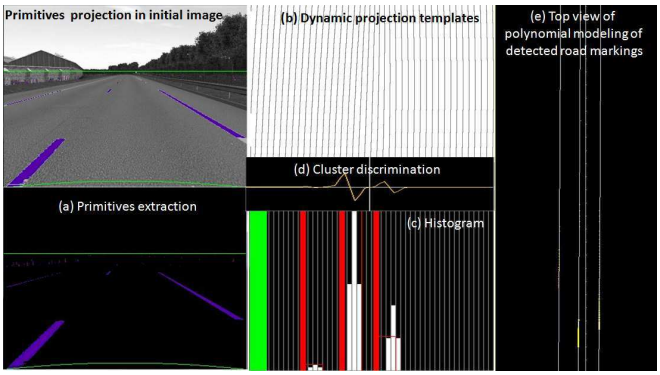


Fig. 4. Marking line detection

It has been shown in [12], that a non-Gaussian model is more adapted to describe perturbations on the observation of lane markers. Ieng *et al.* also propose to model noise measurements as a Smooth Exponential Family (SEF) distribution defined according parameters $\alpha$ and $\zeta$. The approach consists in detecting error minima by calculating zero crossing of the following third derivative (illustrated in Fig. 4-(d)) of the error function $\phi_\alpha$:

$$\frac{\partial^3 \phi_\alpha}{\partial t^3} = \frac{4t}{\zeta^4}\left(1 + \frac{t^2}{\zeta^2}\right)^{(\alpha-3)}(\alpha - 1)\left(3 + \frac{t^2}{\zeta^2}(2\alpha - 1)\right) \quad (3)$$

Zero crossing corresponds to the projected position $X_m^p$ of potential marking lines.

*2) Peak validation:* Peaks are first filtered according to the number of points: the number of points forming the peak must be higher than the minimum number of points $N_{min}$.

Sets of labeled points (labeled according to the peak label) are written under a matrix form as:

$$X_{m,k} = \begin{bmatrix} 1 & x_1 & x_1^2 \\ \vdots & \vdots & \vdots \\ 1 & x_{N_m} & x_{N_m}^2 \end{bmatrix}, Y_{m,k} = \begin{bmatrix} y_1 \\ \vdots \\ y_{N_m} \end{bmatrix} \quad (4)$$

The polynomial fit of $A_{m,k}$, denoted $\tilde{A}_{m,k}$ is obtained by using a weighted least squares estimation as follows:

$$\tilde{A}_{m,k} = (X_{m,k}^T W_{m,k} X_{m,k})^{-1} X_{m,k}^T W_{m,k} Y_{m,k} \quad (5)$$

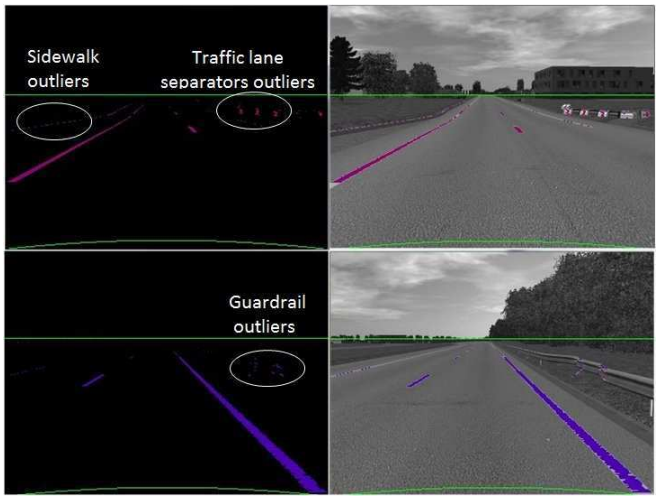


Fig. 5. Outliers due to a sidewalk

where $W_{m,k}$ is a diagonal matrix containing weight dedicated to each point. Here, the weight is calculated as the intensity point. Several criteria are here tested. The associated variance must be smaller than the maximum variance $\sigma_{max}$. The average intensity point must be higher than a threshold $\gamma_{min}$. The curvature ($a^m_{k,2}$) must be smaller than the maximum road curvature coming from the route code $\theta_{max}$. The $y$-intercept ($a^m_{k,0}$) must be smaller than a given distance $d^0$ (lane markings which are too far away from the vehicle cannot be detected).

Due to the inversion of a $N_m \times N_m$ matrix, poly-fitting step can be time consuming. However, following [13], this computation is largely optimized to respect real-time constraints.

If the associated variance is higher than the maximum variance $\sigma_{max}$, then a robust poly-fitting estimation is tested in order to discriminate cases where a lot of outliers occur. It can happen for example if there is a sidewalk along the road or a traffic barrier on the highway as illustrated on Fig. 5.

Due to its robustness to a high number of outliers, Ransac method is currently used for robust poly-fitting [14]. However, there is no upper bound in processing time and in the case presented in Fig. 5, it could converge toward the bad solution. On the observation that, the right point set is closer to the camera than the one generated by the sidewalk or the traffic barrier, we suppose that the number of points in the right set is higher. Assuming that the lane marking distribution points are distributed according to a Gaussian distribution, we simply proposed, from the first estimate, to calculate the association probability for each point, according to the standard deviation $\sigma^r$. Points with a probability lower than a given threshold $\gamma$ (this threshold is obtained from the inverse $\chi^2$) are eliminated. In this way, unlikely points are mainly eliminated and a second more precise estimate is then calculated.

Finally, according to this robust poly-fitting, the corresponding variance must be smaller than the maximum variance $\sigma^r_{max}$.

As an output, a set of detected marking lines $\tilde{A}_m$ ($\forall m < M_k$) is obtained, with $M_k$ the number of detected marking lines at the current iteration $k$ as illustrated in Fig. 4-(e)).

### C. Lane marker association

Now, an association step is necessary in order to establish relationship between the set of detected marking lines $\tilde{A}_m$ and the set of estimated marking lines $\hat{A}_{m,k-1}$ $\forall(m < N_{k-1})$ known from the previous iteration $k-1$. The proposed approach uses the Transferable Belief Model (TBM) framework [15]. This formalism, instead of manipulating probability distribution, manipulates belief mass distribution, also called basic belief assignment (bba). The belief mass is defined as the mass of elementary probability on an assumption $A$:

$$\begin{array}{rccc} m^\Omega: & 2^\Omega & \rightarrow & [0,1] \\ & A & \rightarrow & m^\Omega(A) \end{array} \quad (6)$$

This mass is calculated for each proposition $A$ of the referential defined as $2^\Omega = \{A|A \subseteq \Omega\}$ called the power-set. The power-set contains all singleton hypothesis, but also the union of hypotheses. The union of all hypotheses constitutes the doubt or the absence of knowledge. The data association is made following the Gruyer's and Royere's approach initially proposed in [16] and extended in [17]. The idea is to first calculate a prior bba for each peak-to-line association, based on a similarity measure. Then, prior bbas are combined to calculate each association hypothesis belief. This operation is carried out twice in an extended open world: a fist time for the peak-to-line association allowing to manage the road marking appearance, and a second time for the line-to-peak association in order to detect the line disappearance.

The distance function used to quantified the similarity between a new detected road marking (histogram peak) and a road marking track (previous road marking) has been initially proposed by Gruyer [18] in order to calculate a similarity distance between two clusters taking into account their uncertainties (both the variance and co-variance of each cluster). This distance function is the same one used in the original algorithm [7], it is based on the computation of the outer clusters distances normalized by the sum of the inner distances.

### D. Lane marker certainty propagation

As for obstacle tracking, it is important to ensure a temporal continuity in the association. The management of this temporal continuity is essential to estimate the dynamics of an object and to predict its future state. Furthermore, in order to quantify its relevance and temporal coherence, a certainty value called $c$ is assigned to each object. The way to update and propagate this certainty is illustrated in Fig. 6. At the previous iteration $k-1$, an estimated marking line $\hat{A}_{m,k-1}$ has a current certainty denoted $c(\hat{A}_{m,k-1})$ (case 1). The certainty is then projected on the propagation function (case 2 on the blue line), in order to obtain a normalized corresponding number of iterations (case 3). In case 4.1,

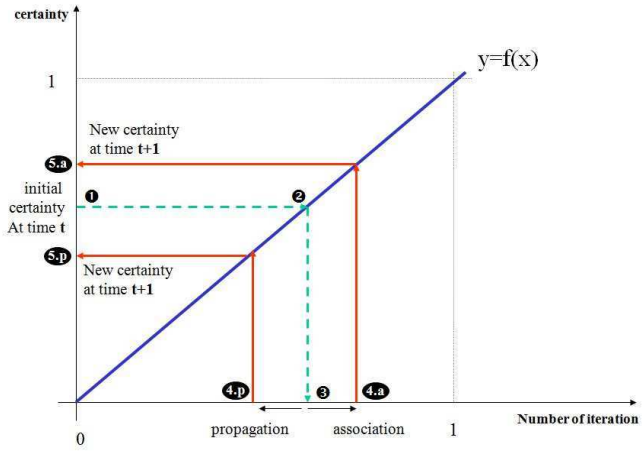


Fig. 6. Certainty with $n'$ the normalized number of iterations

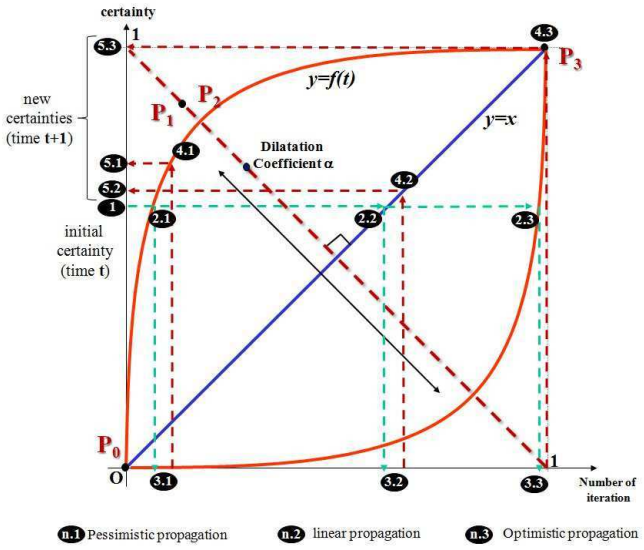


Fig. 7. Certainty propagation

the estimated object $\hat{A}_{m,k-1}$ is associated to a detected object $\tilde{A}_{m'}$. In this case, the corresponding relative number of iterations increases relatively to both the belief into this association $m^{\Omega^\star_{M_k}}_{1\ldots M_k}\left\{\hat{A}_{m,k-1}\right\}\left(\tilde{A}_{m'}\right)$ and the quality of the road marking detection. This corresponding normalized number is yet reprojected following the same propagation function to obtain the new increased certainty $c(\hat{A}_{m,k})$ at iteration $k$ (case 5.1). In the case where the estimated line marking is not associated, then the corresponding normalized number of iterations decreases by 1 (case 4.1) and the corresponding certainty $c(\hat{A}_{m,k})$ also decreases. Each detected object is initialized with a certainty $c_0$. In the current method, this value is fixed to 0.5 but it will be clever to initialize this value in function of the quality of the current road marking detection.

In the Fig. 6, the certainty propagation is made with a linear fonction (with a slope of 1). However, in a more generic approach,this function is chosen depending on a coefficient $\alpha$ which is fixed relatively to the data reliability and confidence. The ability to choose a specific function, in order to propagate a certainty, is done to model both the optimistic and pessimistic behaviors of the certainty propagation as shown in Fig. 7. In the optimist case, the certainty increases quicker than in the pessimist case. The propagation function must be chosen symmetrical, continuously increasing and derivable. In this application, the used propagation function is a Bezier curve as proposed in [16].

When the certainty $c(\hat{A}_{m,k})$ decreases until 0, the object is deleted.

### *E. Lane marker estimation*

Assuming that each road marking (lane marker) $m$ is now detected with a certainty $c(\hat{A}_{m,k})$ and a set of labeled points $\{x_i, y_i\}_{\forall i\in\{1,\ldots,N_m\}}$ converted into the vehicle coordinate system, the goal is to provide an estimation $\hat{A}_{m,k}$ of the road marking shape as a second degree polynomial function as described in eq. 2.

Lane markers are not strictly constant over time and across successive images. They can be simply estimated using a linear Kalman filter, whom assumptions are now described. However, they change relatively slowly assuming a constant vehicle speed and under flat road assumption (required assumption for the point conversion into the vehicle coordinate) following the state equation:

$$A_{m,k+1} = F_k \cdot A_{m,k} + \nu_{m,k} \tag{7}$$

where $F_k$ designates the evolution matrix, $A_{k,m}$ the real road marking state at iteration $k$ and $\nu_{m,k}$ the model noise representing the uncertainty in the road marking evolution over time. If some authors like [19] uses elaborated and complex evolution matrix, we assume that the change between two successive image is negligible (matrix $F_k$ is equal to the identity matrix) and can be modeled thanks to the model noise, which must be adequately chosen. The model noise $\nu_{m,k}$ can be estimated by studying the maxium evolution of parameters of a road marking between iteration $k$ and $k+1$.

Measurement-to-state equation can be simply written as:

$$X_{k,m} \cdot A_{k,m} = Y_{k,m} + w_{k,m} \tag{8}$$

where $w_{k,m}$ represents the measurement noise estimated at each iteration as the error of one pixel shift in the vehicle coordinate system.

Assuming that extracted features cannot be modeled as Gaussian distribution, Ieng *et al.* estimates lane marker states by using a Robust Kalman Filter [1]. We propose as an alternative to use a gating computation [2] and to re-estimate road marking shape $\tilde{A}_{m,k}$. A gate is also designed around the predicted position at iteration $k$ of road marking $\hat{A}_{k|k-1,m}$, based on the maximum acceptable measurement error according to the prediction error magnitude. Only points that are within the track gate are considered for update the lane marker at iteration $k$. As shown in Fig. 8, false points are filtered and selected points can be modeled as a Gaussian distribution.

At this stage, $\tilde{A}_{m,k}$ are so close to the reality that a corrective step is unnecessary and $\hat{A}_{m,k} = \tilde{A}_{m,k}$ .

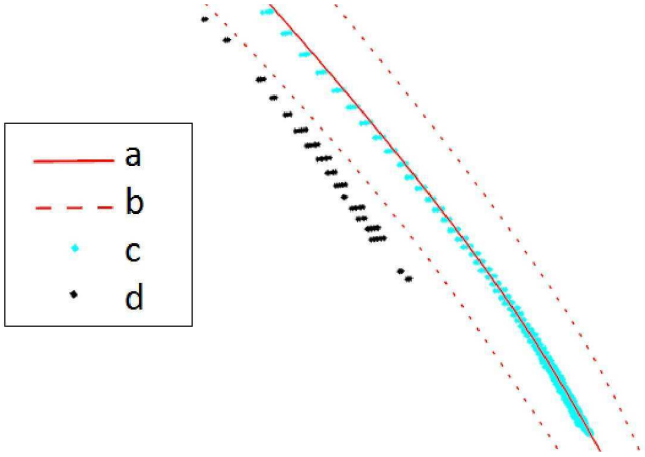


Fig. 8. Gating process illustration

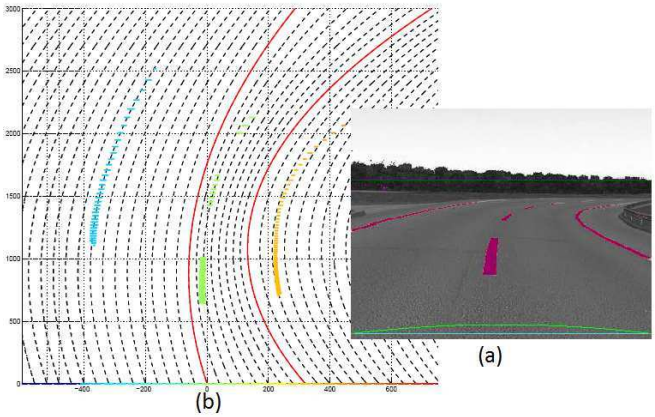


Fig. 9. Road shape interpolation in case of high curvature. (a) original images and its extracted points. (b) Interpolated road shape for each interval (red lines: previous road shape estimates, dotted lines: interpolated road shape). Points are colored accordingly to their interval.

### F. Road shape update

As explained in Sec. III-B, extracted points are projected according to the global road shape. One solution consists in selecting the best road marking estimation (best to the point of view of varying criteria such as the number of extracted points, and the smallest error estimation) in order to project the points (road marking primitives) for the next iteration. However, in case of strong curvatures, we can note that the inside road markings have a stronger curvature than the outside ones as illustrated in Fig. 9-(a). The proposed solution consists in selecting several lane markers as road shape reference. Road markings are selected if they satisfy strict criteria (more strict than detection criteria) on:

- the number of points forming the peak must be higher than the minimum number of points $N^p_{min}$ ($N^p_{min} > N_{min}$),
- the variance of the peak must be smaller than the maximum variance $\sigma^p_{max}$ ($\sigma^p_{max} < \sigma_{max}$).

If several road marking estimates are selected as road shape reference, they are first tested to detect cross road markings (cross lane markers). In fact, they are not supposed to cross each other. If road marking crossing is detected, only the lane marker with the minimum variance is selected. They are then used to interpolate a second degree polynomial function for each interval as illustrated in Fig.9-(b).

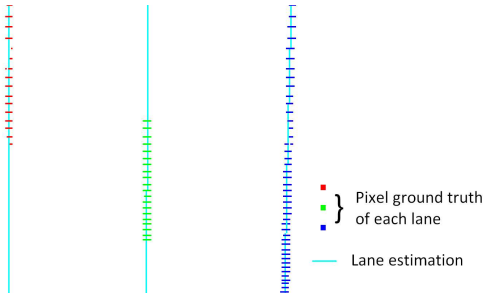


Fig. 10. Evaluation protocol

## IV. Evaluation Protocol

To evaluate the quality of this algorithm and the impact of each parameter, an evaluation tool and a protocol have been developed. The evaluation protocol uses the estimates from the lane detection algorithm and ground truth images provided by SiVIC as illustrated in Fig.10. This protocol is based on four criteria:

- Detection rate: Rate of good detection estimated according to the ground truth for one lane. This rate corresponds to the line ratio where distance between the estimate and the ground truth is below a given threshold $d_{min}$. For the l line of our image, this distance $e_{m,k,l}$ between the estimate $\hat{A}_{m,k,l}$ and the the average points of the line $\overline{T_{m,k,l}}$ is calculated as an Euclidian distance:

$$e_{m,k,l} = d(\hat{A}_{m,k,l}, \overline{T_{m,k,l}}) \quad (9)$$

  where $d(.,.)$ the euclidian distance. This threshold $d_{min}$ was chosen after empirical testing of different ADAS system.
- Precision: Accuracy in the case of correct detection for one lane. This accuracy is calculated as the mean of each $d(l)$ for each line of the ground truth image.
- False alarm rate: Ratio between the number of false detections and the real number of lanes.
- Global detection rate: Ratio between the number of correct detections and the real number of lanes.

## V. Results

In this section, some results are presented according to the dedicated performance protocol developped with the SiVIC platform. This evaluation has been done on a Sivic sequence of images combining several situation: straight line, strong curvature, guardrails, sidewalks, fences, trees, different conditions of shadows.... Detection rate (DR) and false alarm rate (FAR) quantify the quality of the detection. Detection rates per lane marking and their associated error measure the quality of the estimation.

Numerous parameters are used in this multi-lane detection method, which is determined before this evaluation step

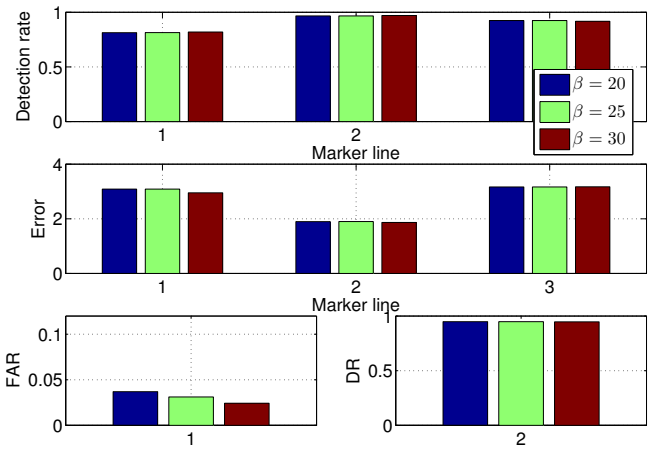


Fig. 11. Influence of the threshold on the average point intensity

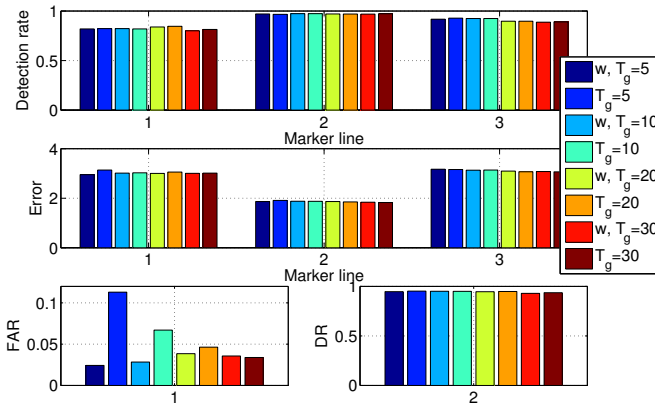


Fig. 12. Influence of extraction threshold $T_g$ by using intensity of extracted points or not (in legend, w means that weighted projection is used for histogram build)

using real and simulated image sequences. Except the minimum number of points for a peak to be validated (which depends on the image size), a great part of these parameters are independent of the road conditions. The minimum number of points $N_{min}$ is fixed equal to 100. Concerning the peak validation, the average point intensity threshold $\beta_{min}$ has been tested in Fig. 11. The best results are obtained with $\beta_{min} = 30$ and the threshold only influence FAR.

The maximum road curvature comes from the French regulations of road infrastructure as $\theta_{max} = 1.6e^{-4}$ and we limit detection to a distance $d^0 = 8$ m.

Coefficients for the Smooth Exponential Family (SEF) distribution are defined as $\alpha = 0.01$ and $\zeta = 0.1$.

Poly-fitting parameters have been established as: $\sigma_{max} = 50$, $\sigma^r_{max} = 100$ and $\sigma^r = 400$.

Extraction parameters such as minimum and maximum width for lane marking are set to $[S_m, S_M] = [10, 50]$ pixels. We use as an extraction threshold $T_g = 5$ to limit time computation. Influence of this threshold is studied in Fig. 12. In this experiment, influence of the threshold is conjointly studied to the influence of the histogram with weighted points or not. We observe that with the weighted histogram, results are quite stable, whatever the value of the threshold, while with the unweighted histogram, threshold highly influences the quantity of false alarm.

As an estimation method, different model noises have been tested for a Kalman filter, but due to the high detection quality, best results are obtained without correction step and the impact of the Kalman filtering is not significant in the tested scenario. An extended evaluation will be necessary in order to confirm the uselessness of Kalman filter.

A robust weighted poly-fitting has been proposed in Sec. III-B.2. Different way to calculate the weight matrix $W_{k,m}$ have been tested: point intensity, distance to the vehicle and residual. 13 shows that best results are obtained with the intensity point.

In Fig. 14, several methods for the road update stage are tested: Several road marking estimates satisfying restrictive

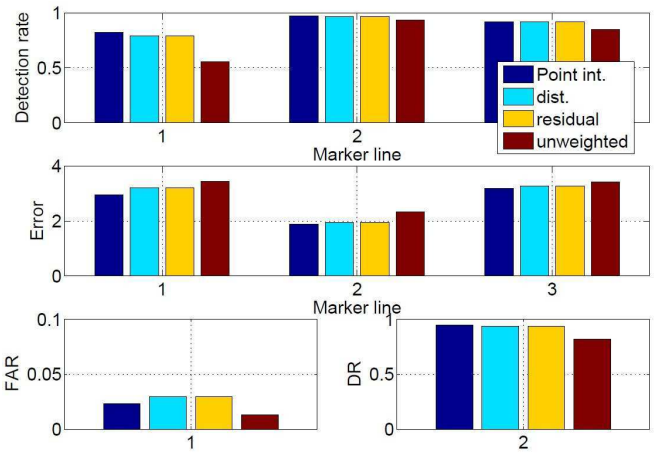


Fig. 13. Influence of robust weighted poly-fitting

constraint and best road marking estimate in terms of number of points or minimal variance. Best results are obtained when several road marking estimates are used, specially in case of strong curve.

## VI. Conclusion

In this paper, an original algorithm for multi-lane detection and estimation is proposed based on a three-step process, (1) extraction - (2) detection - (3) estimation. The algorithm is quite robust to the extraction method and more specifically to the choice of the extraction threshold. The detection step is so efficient, by using robust poly-fitting, that no estimation step is really necessary. Consequently, this algorithm respects the real-time constraint and produces very encouraging results: more than 95% of lane markers are detected for less than 2% of false alarm. Road shape estimate is close to the reality because the average error is less than 3m for a range of 60m.

A new evaluation protocol also has been proposed. This protocol is based on synthesized images coming from the SIVIC simulator. It is the first time such a protocol is

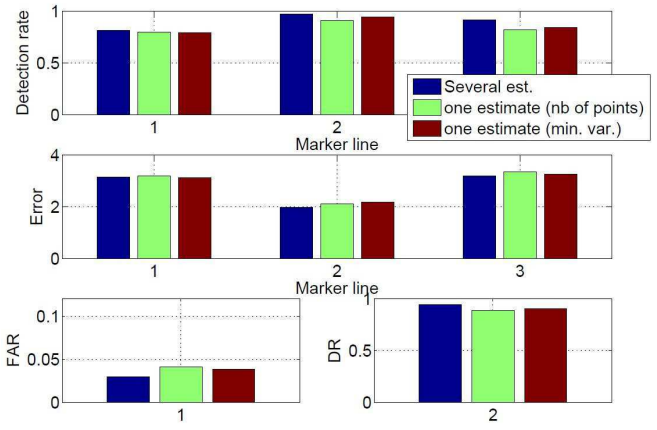


Fig. 14. Result with different road shape update

implemented with virtual data in order to validate a road marking detection method. The images provided by this platform are quite enough realistic to effectively validate an image processing application [8]. The evaluation protocol is based on three criteria: the detection rate of road markings (lane markers), the precision of their estimation and a false alarm rate. Numerous tests on a set of parameters prove the robustness of this approach. Finally, the proposed system has been tested with success on several hours of data collected on the real Satory's test tracks under varying lighting and curvature conditions. The real images recorded during these trials correspond to the same one generated with the SiVIC platform. The main goal was to obtain similar results and the same behavior in both the real and the simulated scenarios for autonomous driving applications. Unfortunatly, some difficulties can appear in the road marking detection when the vehicle is accelerating (due to the pitch) or when the flat road assumption is not respected, but this should be solved by integrating information on the pitch into the data conversion stage (image space toward 1D space).

To improve the performances of this innovative approach, numerous perspectives are possible. First, other evaluation tests must be done to quantify the influence of moving objects on the road. To filter primitives corresponding to these objects, it is proposed to combine our approach with obstacle detection algorithm (ie. from stereovision, laser, or radar processing). Furthermore, to compensate vehicle pitch, a new estimator will be added to apply a real time correction in the projection module. Finally, this approach was originally made to identify the road lanes by using of a multi-camera fusion architecture. It is therefore appropriate to continue this multi-cameras study to quantitatively determine the gain provided by the use of other cameras. In addition it will be interesting to study the intrinsic and extrinsic best configuration for this network of embedded optical sensor.

## ACKNOWLEDGEMENT

This work is part of e-future, a 3-year European FP7 research project (project number: 258133) for electric car automation and of CooPerCom, a 3-year international research project (Canada-France). The authors would like to thank the European committee, the National Science and Engineering Research Council (NSERC) of Canada and the National Agency for Research (ANR) of France for supporting these projects.

## REFERENCES

[1] J.-P. Tarel, S.-S. Ieng, and P. Charbonnier, "Using Robust Estimation Algorithms for Tracking Explicit Curves," in *ECCV 2002*, ser. Lecture Notes in Computer Science, A. Heyden, G. Sparr, M. Nielsen, and P. Johansen, Eds. Springer Berlin / Heidelberg, 2002, vol. 2350, pp. 492–507, 10.1007 3-540-47969-4 33. [Online]. Available: http://dx.doi.org/10.1007/3-540-47969-4 33

[2] R. Sittler, "An optimal data association problem in surveillance theory," *IEEE transactions on military electronics*, vol. 8, no. 2, pp. 125–139, 1964.

[3] M. Bertozzi and A. Broggi, "Gold: a parallel real-time stereo vision system for generic obstacle and lane detection," *IEEE Transactions on Image Processing*, vol. 7, no. 1, pp. 62 –81, Jan. 1998.

[4] B. Vanholme, D. Gruyer, S. Glaser, and S. Mammar, "A legal safety concept for highly automated driving on highways," in *Intelligent Vehicles Symposium (IV), 2011 IEEE*. IEEE, 2011, pp. 563–570.

[5] E. Pollard, D. Gruyer, J. Tarel, S. Ieng, and A. Cord, "Lane marking extraction with combination strategy and comparative evaluation on synthetic and camera images," in *Intelligent Transportation Systems (ITSC), 2011 14th International IEEE Conference on*. IEEE, 2011, pp. 1741–1746.

[6] D. Gruyer, S. Glaser, and B. Monnier, "Sivic, a virtual platform for adas and padas prototyping, test and evaluation," in *FISITA 2010 World Automotive Congress, Budapest, Hungary*, 2010.

[7] S. Ieng, J. Vrignon, D. Gruyer, and D. Aubert, "A new multi-lanes detection using multi-camera for robust vehicle location," in *Proc. on thee IEEE Intelligent Vehicles Symposium*. IEEE, 2005, pp. 700–705.

[8] D. Gruyer, M. Grapinet, and P. De Souza, "Modeling and validation of a new generic virtual optical sensor for adas prototyping," in *Intelligent Vehicles Symposium (IV), 2012 IEEE*. IEEE, 2012, pp. 969–974.

[9] T. Veit, J. Tarel, P. Nicolle, and P. Charbonnier, "Evaluation of road marking feature extraction," in *IEEE 11th International Conference on Intelligent Transportation Systems*. IEEE, 2008, pp. 174–181.

[10] E. Pollard, D. Gruyer, J.-P. Tarel, S.-S. Ieng, and A. Cord, "Lane marking extraction with combination strategy and comparative evaluation on synthetic and camera images," in *Intelligence Transportation System Conference*, 2011.

[11] B. Yu and A. Jain, "Lane boundary detection using a multiresolution hough transform," in *Proceedings of the International Conference on Image Processing*, vol. 2. IEEE, 1997, pp. 748–751.

[12] S. Ieng, J. Tarel, and P. Charbonnier, "Modeling non-gaussian noise for robust image analysis," in *Proceedings of International Conference on Computer Vision Theory and Applications*. Citeseer, 2007, pp. 175–182.

[13] B. Flannery, W. Press, S. Teukolsky, and W. Vetterling, "Numerical recipes in c," *Press Syndicate of the University of Cambridge, New York*, 1992.

[14] Z. Kim, "Robust lane detection and tracking in challenging scenarios," *IEEE Transactions on Intelligent Transportation Systems*, vol. 9, no. 1, pp. 16 –26, march 2008.

[15] P. Smets, "The combination of evidence in the transferable belief model," *IEEE Transactions on Pattern Analysis and Machine Intelligence*, vol. 12, no. 5, pp. 447–458, 1990.

[16] D. Gruyer, "Etude du traitement de données imparfaites pour le suivi multi-objets: Application aux situations routières," Ph.D. dissertation, 1999.

[17] C. Royère, D. Gruyer, and V. Cherfaoui, "Data association with believe theory," in *International Conference on Information Fusion*, vol. 1, 2000, pp. 2–3.

[18] D. Gruyer, C. Royere, and V. Cherfaoui, "Heterogeneous multi-criteria combination with partial or full information," *Fusion03 {29}*, p. 1, 2003.

[19] B. Southall and C. Taylor, "Stochastic road shape estimation," in *Computer Vision, 2001. ICCV 2001. Proceedings. Eighth IEEE International Conference on*, vol. 1, 2001, pp. 205 –212 vol.1.

2013 IEEE Intelligent Vehicles Symposium (IV)
June 23-26, 2013, Gold Coast, Australia

# Weighted V-disparity Approach for Obstacles Localization in Highway Environments

Nizar Fakhfakh[1], Dominique Gruyer[1] and Didier Aubert[2]

*Abstract*— **The employment of embedded passive sensors in order to perceive environment for reducing the accident risk level is a tendency of intelligent vehicles research. From such sensors, one can extract useful informations which can assist the driver to identify hazardous situations. While safety improvement is a substantial requirement for driving assistance, localizing and tracking obstacles in complex road environment became an important task. One promising approach is to use the V-disparity based on the stereovision technique. It is a cumulative space estimated from the disparity image. We propose a sound framework and a complete system based on a real-time stereovision for detection, 3D localization and tracking of dynamic obstacles in highway environment. The main contribution we propose is the improvement of the V-disparity approach by extending the basic approach by merging it with a confidence term. This consists on weighting each pixel in the V-disparity space according to a confidence value which measures the probability of associating a pair of pixels. Furthermore, we propose a tracking system which is based on the belief theory. The tracking task is done on the image space which takes into account uncertainties, handles conflicts, and automatically dealt with targets appearance and disappearce as well as their spatial and temporal propogation. Extensive experiments on simulated and real dataset demonstrate the effectiveness and the robustness of the weighted V-disparity approach.**

## I. INTRODUCTION

Establishing vehicle-infrastructure-driver interactions depends on the effectiveness of the perception task in a specific road scenario. The outstanding development of hardware have significantly improved the capabilities of embedded algorithms for accidents avoidance and drivers' safety improvement. One of the early researche works introducing stereovision for road obstacles detection and road-line markings extraction is the one that is proposed in [1]. Unfortunately, this previous work has proposed a sparse disparity map and the detection of obstacles is not performed in real time. The use of binocular stereopsis principle for collision avoidance or mitigation has been first successfully demonstrated by JPL's planetary robotic vehicle [2] which presents a trade-off between the computational time and the density of the disparity map. The authors in [3] uses vision-based detectors for estimating of the road profile. This is done by detecting road-line markings and all of obstacles not lying on the road plane are discarded. In [4] the authors have proposed an approach for the construction of occupancy grids using stereo camera pair for obstacles detection implemented on a GPU. Their method considers the geometrical visibility of the different regions of the image and can deal with partially-occluded objects. In [5] the regions so that a fixed-size volume contains a sufficient number of points are considered as potential obstacles.

In this paper, we propose a real-time video-based obstacles localization and tracking system at daytime which makes extensive use of stereovision principle. The proposed system allows detecting, localizing and tracking obstacles in highway environments in daytime. After a digitalization and a pre-processing stage, a stereo algorithm based on a local approach is then performed for dense disparity map generation from which the U- and V-disparity maps are built. The proposed work fits into earlier work initiated in [6] which exploits the cumulative spaces termed U- and V-disparity. The main contribution of this paper is in the improvement of the V-disparity approach by extending the basic approach by merging it with a confidence approach. This consists on weighting each pixel in the V-disparity space according to a confidence value which measures the probability of associating a pair of pixels. The two maps, U and V-disparity, are useful for estimating the 2D bounding box for each potential obstacle. A set of targets is therefore obtained with a state vector for each target. Each state vector contains the lateral and longitudinal position, the bounding box parameters and the uncertainty information. We have introduced a tracking filter with an association step based on belief theory and a filtering step using a linear Kalman filter. The association step allows to provide a link between a target and a track. The filter provide an update of the track state vector given the target data. This allows decreasing false positive rate and avoiding missed detections. The tracking task is done on the image space and allows taking into account uncertainties, handles conflicts, and automatically dealt with the appearance and the disappearing of targets as well as their spatial and temporal propogation. Then, the objects which are not lying in the road plane and hence non-potential obstacles are removed. The remaining potential obstacles are kept and are subject for further treatment.

Section II provides a brief overview of the proposed system. Section III gives the first contribution of this work with the presentation of an improved dense disparity map building with confidence approach applied to each pixel. This confidence approach is used to improve the V-disparity approach. Section IV explains the second contribution dedicated to the tracking stage using probabilistic approach and

[1]N. Fakhfakh and D. Gruyer are with French Institute of Science and Technology for Transport, Development and Networks, LIVIC unit. 14, route de la Minière, Bât 824. -78000 Versailles - Satory. {nizar.fakhfakh, dominique.gruyer}@ifsttar.fr

[2]D. Aubert is with French Institute of Science and Technology for Transport, Development and Networks, LEPSIS unit. 58, boulevard Lefebvre, 75732 Paris Cedex 15. didier.aubert@ifsttar.fr

978-1-4673-2754-1/13/$31.00 ©2013 IEEE

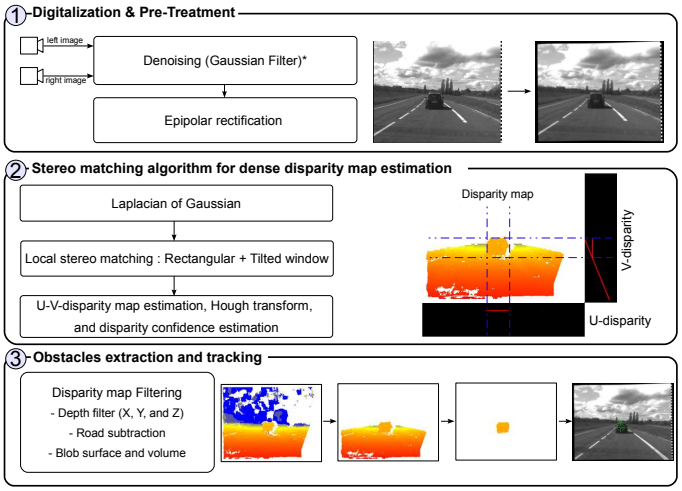


Fig. 1. Obstacles localization system.

the belief theory. Section V describes the implementation both in simulated and real scenarios, displays results, and evaluated the quality of this method with specifics scenarios related to the intelligent vehicle application. This evaluation part provides a third contribution with the use of automatic ground truth generation with the SiVIC virtual environment. Finally, section VI concludes and discusses future work.

## II. PROPOSED OBSTACLES LOCALIZATION SYSTEM

Figure 1 illustrates the global block diagram of our obstacles localization system based on stereovision principle. The first step consists of the digitalization task and some pre-processing applied on both the left and the right images. The second and third sub blocks allows detecting and localizing obstacles by means of a robust stereo matching algorithm. All of the blocks are described in detail in the following sub sections.

### A. Likelihood function for disparity map estimation

Estimating the real position of each point depends only on one unknown parameter which is the disparity measurement obtained usually by applying a stereo matching algorithm. The stereovision problem, also known as stereopsis problem, consists in determining the depth of all the objects in the image from the viewer, according to two images coming from two cameras. The depth of any pixel is inversely proportional to its disparity, namely how much a pixel in the right image is shifted to obtain the corresponding pixel in the left image.

In order to reduce the complexity of such a stereo algorithm, one can exploit prior knowledge of the observed scene and cameras configuration, which allows promptly achieving an optimal solution to the matching task. Actually, known camera geometry with respect to the locally planar road is used to localize objects which are not lying in the road plane and hence can be considered as potential obstacles. An important step is the calibration process of the stereo cameras enables estimating the intrinsic and extrinsic parameters which will be useful for reducing the huge range of the disparity space search for each pixel. By means of a mechanical and soft calibration process, the stereo camera is then rectified in such a way that epipolar line appears horizontal in both images. Actually, the search for similarity between the two images can be reduced in this way to horizontal scanlines in the images. Currently, a correlation window is shifted for each pixel along a horizontal scanline and computes likelihood measurement between the left and the right images. Each pair of pixels having an optimal score is considered and then a disparity measure is computed.

The local stereo matching we propose is a two steps patch matching process. For each pixel to be matched, two scores are obtained by applying once a rectangular window and once using a tilted window. This choice is motivated by considering the following observations:

– For a pixel which belongs to a vertical fronto-parallel plane, the score obtained with a rectangular window is less than the one obtained with a tilted window.

– For a pixel lying on the road plane, the score obtained with a tilted window is less than the one obtained with a rectangular window.

Local methods are known to rapidly achieve the stereo matching problem in reasonable processing time but are subject to many matching error. The estimation of disparities according to global approaches such as graphical model is known to be NP-hard, or computationally intractable problem. Another way for reducing the complexity of such a stereo algorithm is in exploiting prior knowledge of the observed scene and cameras configurations.

### B. Confidence Approach for Disparity Characterization:

Each pair of matched pixels is evaluated by referring to the idea initiallty described in our recent work [7]. Once a likelihood function is applied to initialize the disparity map, for each matched pair of pixels a confidence measure is computed. It is termed $\psi(p_l^{u,v}, p_r^{u',v})$ which represents the level of certainty considering a label $l$, i.e. disparity, as the best label for pixel $p$. We will start from an example given by figure 2 which shows a pixel which corresponds to a point of interest to be matched. The homologous of this pixel in the other image is unique and is well distinguished from all other candidate pixels. The proposed disparity confidence function gives a value scaled within the [0, 1] range. The closest to zero, the less confidence is it. This function depends on several local parameters and is given by Equation 1:

$$\psi(p_l^{u,v}, p_r^{u',v}) = P(p_r^{u',v}/p_l^{u,v}, \rho, min, \sigma, \omega) \qquad (1)$$

In order to well understand the parameters detailed later, figure 3 illustrates the scores obtained by applying the likelihood function on the pixel to be matched of figure 2. Each score obtained with a candidate qualifies the correlation degree with the pixel to be matched in the reference image. The right-hand curve of the figure 3 represents the scores obtained with the likelihood function. Their scores are ordered and are shown in the left-hand curve of the figure 3.

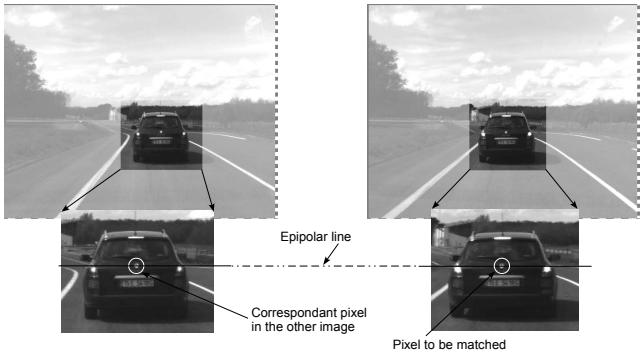


Fig. 2. An example of a point of interest to be matched from the right image which visibilly have one well identified correspondant in the left image.

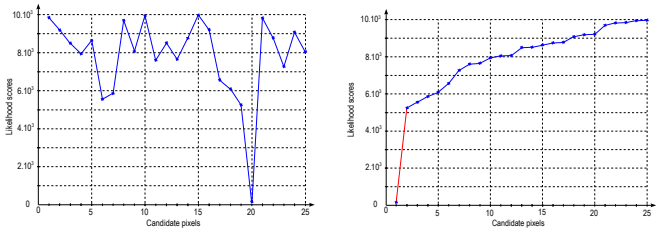


(a) (b)

Fig. 3. Likelihood scores of the pixel of figure 2 obtained for each candidate pixels (a) non-ordered scores (b) ordered scores.

The confidence measurement function is given by Equation 2:

$$\psi(p_l^{u,v}, p_r^{u',v}) = \left(1 - \frac{min}{\omega}\right)^{\tau^2 log(\sigma)} \tag{2}$$

Where *min* is the Best Correlation Score, $\tau$ is the number of potential candidate pixels among all of the candidates, $\sigma$ is the standard deviation of the disparity of the $\tau$ pixels, $\omega$ is the Gap between the $\tau^{th}$ and $(\tau+1)^{th}$ scores.

– *Best Correlation Score (min):* The output of the likelihood function is a measure of the degree of similarity between two pixels. Then, the candidate pixels are ranked in increasing order according to their corresponding scores. The couple of pixels that has the minimum score is considered as the best-matched pixels. The lower the score, the better the matching. The nearer the minimum score to zero, the greater the chance of the candidate pixel to be the actual correspondent.

– *Number of Potential Candidate Pixels ($\tau$):* This parameter represents the number of potential candidate pixels having similar scores. $\tau$ has a big influence because it reflects the behavior of the likelihood function. A high value of $\tau$ means that the first candidate pixel is located either in a uniform region or in a repetitive pattern of the image. The lower the value of $\tau$, the fewer the candidate pixels. If there are few candidates, the chosen candidate pixel has a greater chance of being the actual correspondent. Indeed, the pixel to be matched belongs to a region with high variation of gray component. A very small value of $\tau$ and a *min* score close to zero, means that the pixel to be matched probably belongs to a region of high gray variations.

– *Disparity variation of the $\tau$ pixels ($\sigma$):* A disparity value is obtained for each candidate pixel. For the $\tau$ potential candidate pixels, we compute the standard deviation $\sigma$ of the $\tau$ disparity values. A small $\sigma$ means that the $\tau$ candidate pixels are spatially neighbors. In this case, the true candidate pixel should belong to a particular region of the frame, such as an edge or a transition point. Therefore, it increases the confidence measure. A large $\sigma$ means that the $\tau$ candidate pixels taken into account are situated in a uniform gray region.

– *Gap value ($\omega$):* This parameter represents the difference between the $\tau^{th}$ and $(\tau+1)^{th}$ scores given with the dissimilarity function used. It is introduced to adjust the impact of the minimum score.

For numerical purpose and to ensure that the function $\psi$ has a value between 0 and 1, a few constraints are introduced. The *min* parameter have not to be higher than $\omega$. If so, parameter $\omega$ is forced to $min+1$. Moreover, the $log(\sigma)$ term is used instead of $\sigma$, so as to reduce the impact of high value of $\sigma$ and obtain coherent confidence measures.

In the following, the way of estimating the parameter $\tau$ is detailed. The number $\tau$ of potential candidate pixels is deduced from all scores obtained with the local likelihood function. The main idea is to detect major differences between successive scores. These major differences are called main gaps. Let $\phi$ denote a discrete function which represents all the scores given by the dissimilarity function in increasing order. We introduced a second function denoted $\eta$, which represents the average growth rate of the $\phi$ function. $\eta$ can be seen as the ratio of the difference between a given score and the first score, and the difference between their ranks. This function is defined in Equation 3:

$$\eta(\phi^{u',v}) = \frac{\phi^{u',v}(z_m) - \phi^{u',v}(z_1)}{z_m - z_1} \qquad m \in \mathscr{L} \tag{3}$$

where $\mathscr{L}$ is the number of all candidates and $\phi^{u',v}(z_m)$ is the $m^{th}$ dissimilarity cost among all scores obtained for the pair of matched pixels $(p^{u,v}, p^{u',v})$. $z_m$ is the rank of the $m^{th}$ score. $\eta(\phi^{u',v})$ is a discrete function that allows to highlight the large gaps between scores. It is materialized using Equation 4:

$$\xi(\phi^{u',v}) = \begin{cases} \frac{\nabla\eta^{u',v}}{m^2} & \text{if } \nabla\eta^{u',v} \geqslant 0 \\ -1 & \text{otherwise} \end{cases} \tag{4}$$

The previous function (Equation 4) is used to characterize the major scores and is applied only in the case where the gradient $\nabla\eta^{u',v}$ has a positive sign. We have introduced parameter $m^2$ in order to penalize the candidate pixels according to their rank. The number of candidate pixels is given by Equation 5:

$$\tau = \arg\max_m \xi(\phi^{u',v}) \tag{5}$$

Figure 4 illustrates an example of estimating the number of potential candidate pixels $\tau$ by applying the $\xi$ function on the scores showed in figure 3. In this example there is only one pixel which has a distinguished score among all scores. This is visibly highlighted in figure 4 so that the $\tau$ parameter corresponds to the rang of the higher value.

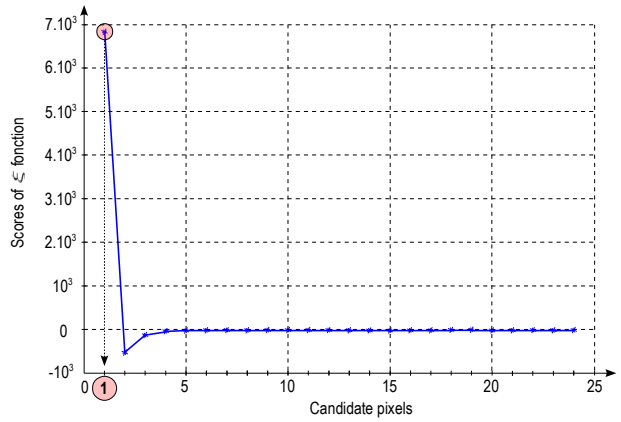


Fig. 4. The number of potential candidate pixels $\tau$ is given as the rank of the highest number obtained with the $\xi$ function.

### C. Weighted U- and V-disparity :

As detailed in section *A*, the likelihood function used for estimating the disparity map is a two steps procedure. For each step, a confidence map is obtained by applying the confidence function, detailed in section *B*, in each matched pixel. These confidence maps are termed the *Obstacles Confidence Map (OCM)* and the *Road Confidence Map (RCM)*. Recall that the basic version of the so called V-disparity map is basically obtained by cumulating all of disparity values along lines and columns of the dense disparity map. Each point in the V-disparity space corresponds to the sum of all disparities along the same $v$ image line. Figure 5 illustrates the two cumulating spaces.

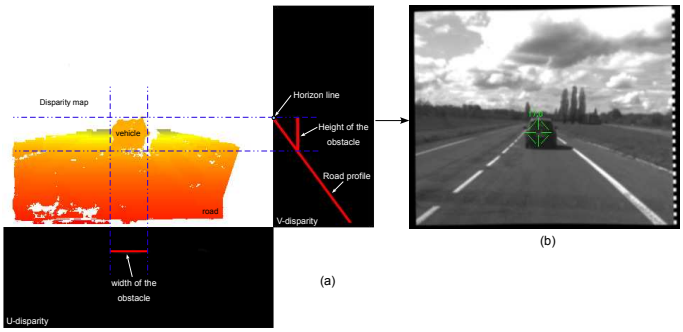


Fig. 5. (a) U- and V-disparity estimation from filtered dense disparity map (b) bounding box of an obstacle in the right image.

According to our knowledge, there is no improvement of the V-disparity method since its inception. In our approach, we propose a more general method which we term *WV-disparity*. It is obtained starting from the dense disparity map, the OCM and the RCM maps. Unlike the standard form of the V-disparity, each pixel in the dense disparity map is weighted by two confidence values as follow $\alpha \times C_o + \beta \times C_r$. The parameters $C_o$ and $C_r$ correspond to the confidence values given by the *OCM* and the *RCM* maps. In our approach, a powerful tool is introduced in the formulation of the V-disparity map by re-weighting the confidences values with a non normalized parameters, $\alpha$ and $\beta$. Depending on the application, one can give more importance to the obstacles detection component or the road plane subtraction. For obstacles detection, $C_o$ is more weighted than $C_r$ by assigning a hight value to $\alpha$ while a small one for $\beta$. This allows highlighting frontal obstacles and ignore the road plane. For road plane extraction, one can simply inverse the weighting of $\alpha$ and $\beta$.

Empirically, the obtained weighted cumulative space, i.e. *WC-disparity*, is more accurate than the original V-disparity. The use of the *WV-disparity* and *WU-disparity* maps allows to highlight obstacles lying on the road and best discriminating the most of unlikely obstacles more precisely than using the standard version of the *V-disparity* method. However, the localization of obstacles is done by exploiting the dense disparity map and the cumulative spaces named Weignted U- and V-disparity map. The pixels are clustered into two classes, road and obstacles, after applying a Hough transform on *WV-disparity* and *WU-disparity* in order to highlight each principal line. The presence of vertical line means the presence of a potential obstacle and the presence of a sloped line illustrate the road profile. The $v$ coordinate of the intersection between the road profile and the v-axis gives the horizon line. After the clustering step, the mean weight obtained for all pixels representing each obstacle is computed. This additional information is very useful for the tracking module because of the attribution of an uncertainty measure to each obstacle to be tracked. Figure 6 shows the obtained *WV-disparity* map compared to the standard *V-disparity* map.

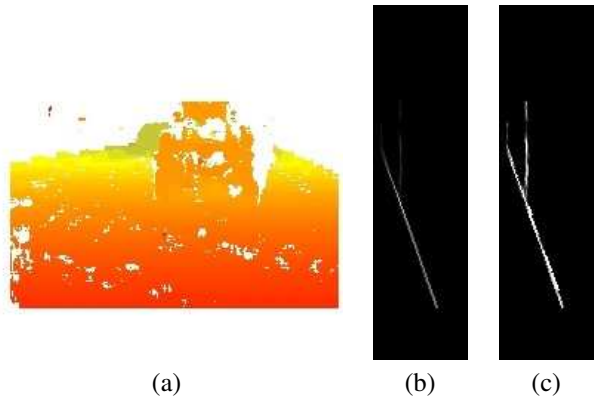


Fig. 6. The basic *V-disparity* maps vs. the *WV-disparity* map. (a) dense disparity map (b) *V-disparity* map (c) *WV-disparity* map.

In order to identify the most of false alarms, we have defined same filters such as the allowed volume depending on the location of each obstacle. Each filter corresponds to a condition which must be fulfilled and leading to eliminate,

if possible, all of erroneous disparities and all of ambiguities regions. A list of obstacles, i.e. target, is therefore obtained on which a tracking procedure is applied.

## III. TRACKING ALGORITHM

Once obstacles have been extracted from the two stereo images, a multi-objects association algorithm is needed to estimate the dynamic state of the targets and to monitor appearances and disappearances of tracks. The position of previously perceived objects is predicted at the current time using Kalman Filtering. These predicted objects are already known objects and will be denoted in what follows by $Y_j$. Perceived objects at the current time will be denoted by $X_i$. In a general framework, the problem consists in identifying an object designated by a generic variable $X$ among a set of hypotheses $Y_i$. One of these hypotheses is supposed to be the solution. The current problem consists in associating perceived objects $X_i$ to known objects $Y_j$. Belief theory allows assessing the veracity of $P_i$ propositions representing the matching of the different objects.

A basic belief allowing the characterization of a proposition must be defined. This basic belief (mass $m_\Theta(.)$) is defined in a [0,1] interval. This mass is very close to the one used in probabilistic approach, except that it is distributed on all the propositions of the referential of definition $2^\Omega = \{A/A \subseteq \Omega\} = \{\varnothing, \{Y_1\}, \{Y_2\}, ..., \{Y_n\}, \{Y_1Y_2\}, ..., \{\Omega\}\}$. This referential is the power set of $\Omega = \{Y_1, Y_2, ..., Y_n\}$ which includes all the admissible hypotheses. These hypotheses must also be exclusive ($Y_i \cap Y_j = \varnothing, \forall i \neq j$). The masses thus defined are called *basic belief assignment* and verify:

$$\sum_{A \subseteq \Omega} m^\Omega(A) = 1 \qquad A \in 2^\Omega, \;\; A \neq \varnothing \tag{6}$$

The sum of these masses is equal to 1 and the mass corresponding to the impossible case $m^\Omega_{1..n}\{X_i\}(\varnothing)$ must be equal to 0. In order to succeed in generalizing the Dempster combination rule and thus reducing its combinatorial complexity, the reference frame of definition is limited with the constraint that a perceived object can be connected with one and only one known object. For example, for a detected object, in order to associate among three known objects, the frame of discernment is $\Omega = \{Y_1, Y_2, Y_3, Y_*\}$ where $Y_i$ means that *$X$ and $Y_i$ are supposed to be the same object*. In order to ensure that the frame of discernment is really exhaustive, a last hypothesis noted $Y_*$ is added. This one can be interpreted as *a target has no association with any of the tracks*. In fact each $Y_j$ represents a local view of the world and the $Y_*$ represents the rest of the world. In this context, $Y_*$ means that *an object is associated with nothing in the local knowledge set*. The tracking module is designed to be a tool allowing a temporal filtering of the set of detected targets. This allows a spatial and temporal filtering of each obstacle. This tracking stage also allows reducing both the false detections rate and the missed detection rate. Previously, this approach has been used in order to track obstacles with telemetric sensors in a cartesian referential [8]. In this work, this approach has been adapted to the image space.

## IV. EVALUATION AND RESULTS

In this section we describe the quantitative and qualitative results of our proposed stereovision-based system for detection and 3D localization of any kind of obstacles in road environment in daytime. This evaluation stage has been also done in both simulated and real environments. We begin at the first time by evaluating the performances of our algorithms by referring to a simulated dataset in which all of disparity maps and obstacles ground truth are available [9]. Figure 7 illustrates the Satory's closed loop tracks used for building images database on which the proposed algorithm is evaluated. A lap around the Satory's track is 3.4 km with various geometrical configurations such as straight segments, slight and sharp bends, and a nonconstant road plane, i.e. with different slopes. The track is also equipped with some guardrail. The guardrails are considered as static obstacles are ignored for the detection process. We considered only dynamic obstacles belonging to the road plane. For qualitative evaluation purposes, we need a ground truth at any time in order to get information about the depth of any real point and the set of obstacles. For experiments, the following parameters have been fixed: the baseline, i.e. the distance between the two optical axis of cameras, is 0.5 meter. The size of the optical sensor is of 5.12×3.84 cm which corresponds to an image of size 640×480. For reducing processing time, only the quarter of the image is processed. For the research of corresponding pairs of pixels, the window size is fixed to 8×8. Knowing that the sensors are positioned at 1.4 meter from the road plane, the set of possible disparities values is up to 60. In the following, the ability of the proposed system for detecting obstacles in simulated and real database is demonstrated.

Fig. 7. Satory's track used for evaluationg our algorithm on real environment. A lap around the track is 3.4 km with different geometrical configurations.

### A. Evaluation on simulated database

The performance of our algorithm is assessed by comparing the obtained detection results with a ground truth generated by means of the *SiVIC* platform developed in the LIVIC laboratory. This simulator allows modeling any complex environment, sensors, and vehicles with realistic rendering. However, it offers diverse and useful functionalities such as adding gaussian or arbitrary noise or even rain or fog on simulated images. The database we have generated is obtained by simulating two cameras which gives left and right images with their corresponding ground truth depth maps and obstacles mask. Figure 8 illustrate a right image with its corresponding disparity map and an image on which real obstacles are identified.

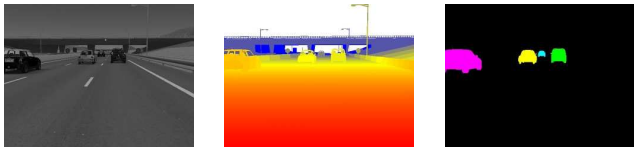

(a) (b) (c)

Fig. 8. Images obtained with SIVIC simulator. (a) image acquired from right camera (b) disparity map ground truth (c) list of obstacles.

To better evaluate the localization accuracy, we opted for testing our algorithms with different image sequences and various obstacle configurations. Three simulated sequences had been generated on the virtuel Satory's track. Each one of these dataset contains 5 vehicles with only one moving in front and in the same lane than the ego-vehicle. In the third sequence, the front vehicle dynamically changes its longitudinal position. In the first sequence the frontal obstacle, e.g. a car, is at 10 meters while for the second one is at 23 meters. Note that each sequence has around four thousand frames. For the moment, the accuracy of the 3D localization processes is first performed only on the frontal car. Errors of lateral and longitudinal positions of the frontal obstacle for all database are given in table I.

| **Frontal obstacle location** | **10 m** | **23 m** | **various distances** |
|---|---|---|---|
| **Lateral errors** | 0.11 (m) | 0.17 (m) | 0.18 (m) |
| **Longitudinal errors** | 0.34 (m) | 0.59 (m) | 1.06 (m) |

TABLE I

LATERAL AND LONGITUDINAL ERROR POSITIONS (METERS) OF THE FRONTAL OBSTACLE FOR ALL SEQUENCES.

The errors in lateral and longitudinal positions given in Table I are obtained by measuring the Euclidean distance between the centre of mass of both the ground truth and the frontal obstacle. The nearer is the obstacle, the lower is the error. By considering only frontal obstacles, the rate of correct detections for the first two sequences, (i.e. scenarios with constant interdistance: 10 and 23 meters), is 99.52 %. For the last sequence, the rate of correct detections is 95.39 %. The false detections rate is 0 % for all tested sequences. Note that considering all of obstacles in each frame, the correct detection rate are 89.6 %, 94.75 % and 91.2 % for the three evaluated sequences, and the false detection rate is 11.93 %, 12.4 % and 23.31 % respectively. This is can be explained by the fact that by considering all obstacles, the whole of image is processed and therefore the number of obstacles not belonging to the road increases. We illustrate in Figures 9 and 10 the errors of lateral and longitudinal positions respectively, given for each frame.

The uncertainty on lateral positions grows significantly either in the case of a turn so that the lateral positions of each obstacle varies substantially, or in the case of partial occlusions due to lane changing of some obstacles.

Another evaluation criterion is expressed by the *Recall* $R$ and *Precision* $P$ parameters which describe the way the obstacles image matches the corresponding ground truth. We remind that the *Recall* measures the ability of an algorithm to well detect obstacles, while the *Precision* is an intrinsic criterion which gives a clue to the accuracy of the detection. Instead of presenting these measures separately, we propose to use a correlated measurement defined by $F_\beta - measure$.

$$F_\beta = \frac{(\beta^2+1)PR}{\beta^2 P + R} \qquad (0 \leq \beta \leq \infty) \tag{7}$$

$\beta$ is a parameter that controls a balance between $P$ and $R$. When $\beta = 1$, $F_1$ comes to be equivalent to the harmonic mean of $P$ and $R$ which equally weighs precision and recall. If $\beta > 1$, $F_\beta$ becomes more recall-oriented and if $\beta < 1$, it becomes more precision-oriented, e.g., $F_0 = P$.

Figures 11 and 12 shows the ROC curves which express the $F_\beta - measure$ by varying the $\beta$ parameter for only frontal obstacles and all of obstacles in the observed scene, recpectively. By fixing the $\beta$ parameter to 1, both of $R$ and $P$ measures are weighted equally. The weight put on $R$ and $P$ critera can be change in order to highlight one of them.

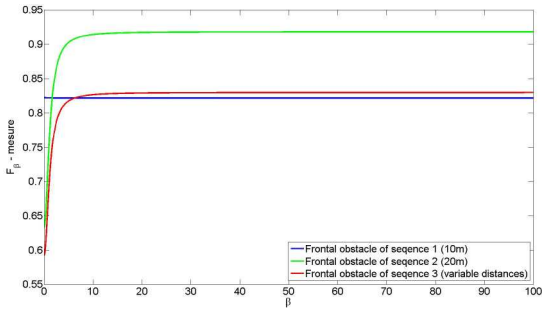


Fig. 11. Evolution of $F_\beta - measure$ by varying the $\beta$ parameter which attributes less or more weight for *recall* and *precision* measures, for only frontal obstacles of the three sequences.

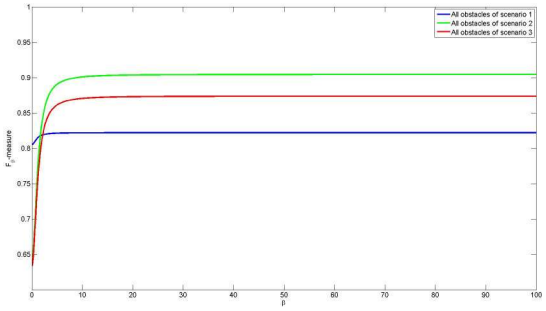

Fig. 12. Evolution of $F_\beta - measure$ by varying the $\beta$ parameter which attributes less or more weight for *recall* and *precision* measures, for all obstacles of the three sequences.

## B. Evaluation on real database

An intensive evaluation is made on real sequences acquired in normal and degraded weather conditions such as the case of dazzle by the sun and cloudy time. The vehicle used for experiments is shown in Figure 13 on which we have mounted a pair of stereo cameras with the same geometrical

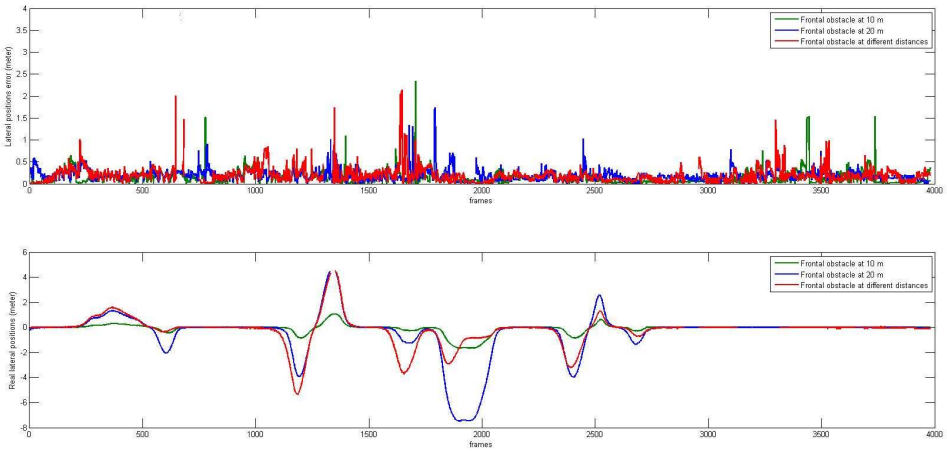


Fig. 9. The error of lateral positions (meter) for frontal obstacles: At 10m (green), 23m (blue) and variable distances (red).

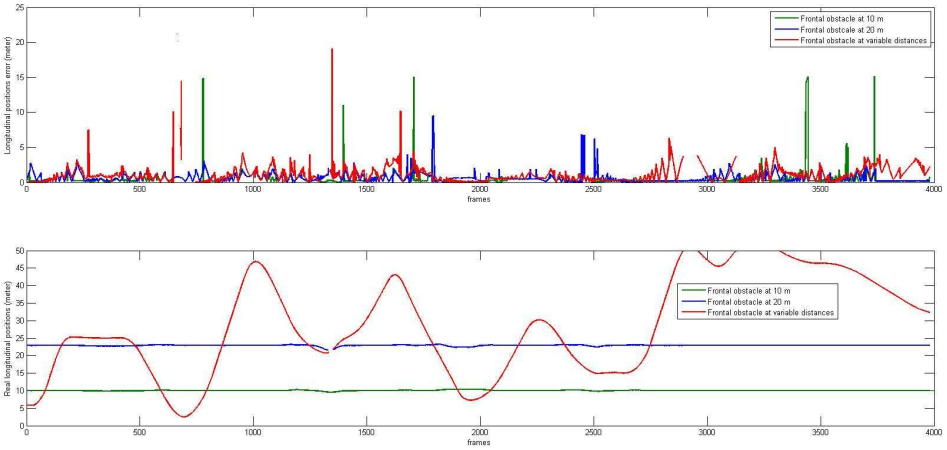


Fig. 10. The error of longitudinal positions (meter) for frontal obstacles: At 10m (green), 20m (blue) and variable distances (red).

(a) (b)

Fig. 13. Overview of the proposed system (a) instrumented vehicle (b) stereovision configuration.

configuration described in the previous section. Some dozen of sequences with four thousand images for each are used for the evaluation.

In the database, the number of obstacles is limited to three vehicles. We estimate that the number of obstacles considered for the experiment is quite enough because the road is only a two-line. Despite the use of only three obstacles, several and various scenario are build to perform the evaluation. The evaluated sequences are manually labeled while considering the correct detections, the missed detection, and the false positives rates as a criterion for the evaluation. For each frame, an obstacle is considered as *well detected* if it is highlighted by the stereovision algorithm relatively to the ground truth. The detection range is limited to 5 m for the nearest obstacle and to 55 m for the farthest one. By considering 30000 frames which are processed, the results in terms of correct detections, missed detections, and false detections are given in the following tables:

| | Correct detections | Missed detections | Fp |
|---|---|---|---|
| **without tracking** | 96.49% | 3.51% | 2.74% |
| **with tracking** | 99.04% | 0.96% | 0.85% |

TABLE II
RATE OF CORRECT DETECTIONS, MISSED DETECTIONS AND FALSE POSITIVES COMPUTED FOR ALL OBSTACLES.

Table II shows that the correct detections rate obtained for the real dataset is more important that the one obtained for simulated dataset. This can be explained by the fact that we do not consider as obstacle both all of obstacles which are partially overlapped by another ones and those which

overtake the ego-vehicle on the left and on the right. Figure 14 shows some screenshots of the output of the stereovision detection and tracking algorithm. The Z component of each obstacle, i.e. how far is an obstacle from the ego-vehicle, is displayed over each bounding box shown in green.

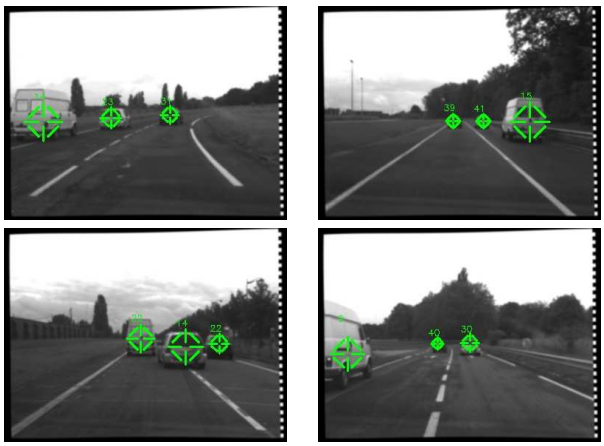

Fig. 14. Screenshot of some detection results obtained from real sequence.

### C. Performances analysis

The proposed system has demonstrated the ability to provide a set of relevant obstacles in daytime environment. To be useful and in referring to the main requirement that such a system must be embedded in a vehicle, any system must reach the real-time performances. It is the case with our proposed system which is first evaluated, in term of processing time, on an Intel(R) Xeon 2.00 GHz quadruple core processor. From all the 20 real and simulated videos we have processed, the processing time varied between 30 and 40 ms. This time processing is lower than the sensor sampling time (40 ms).

## V. CONCLUSION

We presented comprehensive an efficient obstacle detections, 3D localization and tracking system based on stereovision principle. Results demonstrate the effectiveness of our system in road environment. First, a dense disparity map is estimated starting from two images. A confidence approach is then applied for measuring the matching quality of each pair of matched pixels. Second, a *WU-* and *WV-disparity* maps are built which allows estimating the 2D bounding box for each obstacle. A set of targets is then obtained from which a tracking algorithm is applied. We note that the main contribution of this paper is the extention and the generalization of the *V-disparity* approach by weighting each pixel in the dense disparity map for the estimation of the *WV-disparity* map. Unlike the standard method, the ours offers the possibility of highlighting either the obstacles or the road plane. After the segmentation step, a confidence value is attributed to each obstacle. This additional infomation is very useful for the tracking module which makes it more robust.

The evaluation stage shows a high rate of correct detections whereas a low rate of false detections and missed detections. We have shown that most of false detections are due mainly to the guardrail in front of the ego-vehicle in case of sharp turn which is considered as a potential obstacle. Missed detections mainly occurs in the case that the nearest obstacle from the ego-vehicle is very far away (about 50m). In this situation, the correlation window must be adapted in order to be efficient and to allows a good enough stereo matching. Another cause of failure in detection occurs also in the case that two or more obstacles are at the same distance from the ego-vehicle and are in different traffic lanes. This leads to fuse these obstacles and the algorithm is unable to discriminate objects really present in the disparity map. In order to dealt with this failing, one can make dynamically change the window size/shape for the stereo matching task. However, the proposed approach can be applied to detect other kind of obstacles such as pedestrian in urban scenes. To do this, some parameters for the WU- and WV-disparity must be adjusted.

In future work and in order to improve the current algorithm, a cooperative fusion stage will be added in order to enhance the accuracy of the obstacles localization. Reducing false negative rate and filtering out false positives can effectively be done by merging the proposed system with a lane markings detection module which allows identifying all of real obstacles lying on the road. Currently, the integration of this algorithm in a dedicated hardware architecture is in progress.

## ACKNOWLEDGMENT

The authors would like to thank the eFuture project for funding this work. eFuture is an European IP project of the Seventh Framework Programme (FP7).

## REFERENCES

[1] D. Koller, T. Luong and J. Malik, Binocular stereopsis and lane marker flow for vehicle navigation Lateral and longitudinal control, Technical Report UCB/CSD 94-804, University of California at Berkeley, Computer Science Division, 1994.

[2] L. Matthies, *Stereo vision for planetary rovers : Stochastic modeling to near real time implementation*, In International Journal of Computer Vision, Vol. 8, pp. 71–91, 1992.

[3] R. Wang, Y. Xu and Y. Zhao, *A vision-based road edge detection algorithm*, In Proceedings of the IEEE Intelligent Vehicles Symposium, Versailles, France, 2002.

[4] M. Perrolaz, J.D. Yoder, A. Negre, A. Spalanzani and C. Laugier, *A visibility-based approach for occupacy grid computation in disparity space*, In IEEE Trans. on Intelligent Transportation Systems, 2012.

[5] K. Huh, J. Park and D. Hong, *A stereo vision-based obstacle detection system in vehicles*, In Optics and Lasers in Engineering, Vol. 26, No. 2, 2008.

[6] R. Labayrade and D. Aubert, *Robust and fast stereovision based road obstacles detection for driving safety assistance*, In MVA, Nara, Japan, 2002.

[7] N. Fakhfakh, L. Khoudour, J.L. Bruyelle and E. El-Koursi, *Intelligent Surveillance System Based on Stereo Vision for Level Crossings Safety Applications*, In Chapter of book 'Recent Developments in Video Surveillance'. ISBN 978-953-51-0468-1, pp. 75-100, 2012.

[8] D. Gruyer and V. Berge-Cherfaoui, *Matching and decision for Vehicle tracking in road situation*, In IEEE/RSJ International Conference on Intelligent Robots and Systems, IROS99, Kyongju, Core, 17-21 octobre 1999.

[9] D. Gruyer, S. Glaser and B. Monnier, *SiVIC, a virtual platform for ADAS and PADAS prototyping, test and evaluation*, In proceeding of FISITA10, Budapest, Hungary, 30 may-4 june 2010.

# The Compatibility of Energy Efficiency with Pleasure of Driving in a Fully Electric Vehicle

Lena Rittger[1] and Marcus Schmitz[2]

[1]*University of Wuerzburg, Germany;* [2]*Wuerzburg Institute for Traffic Sciences (WIVW), Germany*

## Introduction

Over the past two decades there has been an increased effort in the development of environmentally friendly mobility (Åhman, 2001; Chan, 2002; Chan & Chau, 1997; Kamal, Mukai, Murata, & Kawabe, 2010; Neumann, Cocron, Franke, & Krems, 2010). Despite the clear advantages of electric vehicles (e.g., higher efficiency through regenerative braking, no emissions, more dynamic driving behaviour), the process of introducing electric vehicles to a broad range of drivers is so far missing.

Pleasure in driving is a critical factor for the acceptance of, and attitude towards, vehicles. The driver's decision regarding the type of vehicle driven depends upon a number of factors, including the positive experience and pleasure while driving (Engelbrecht, Engeln, & Arndt, 2009). The development of larger, faster, more dynamic and more comfortable vehicles for everyday driving and to suit a broad range of buyers, supports this assumption (Dick, 2002).

The main focus of the present study was to expand research on environmentally friendly driving and electric vehicles by applying the additional dimension of driving pleasure. The goal was to identify driving behaviour which is energy efficient (i.e., consumes a low amounts of energy) while at the same time is pleasant for the driver. A driver centred approach was chosen, in which the focus of the driver as an *energy optimiser* who tries to improve his energy efficiency was changed towards a view of the driver looking for pleasure and fun when driving.

Researchers have already tried to combine energy efficiency with driver acceptance (Schmitz, Jagiellowicz, Maag, & Hanig, 2012), energy efficiency with safe driving (Fairchild et al., 2009), and safe driving with pleasure in driving (Wedlin, Tillback, & Bane, 1992). However, this was one of the first approaches to consider the compatibility of energy efficiency and pleasure in driving.

**Pleasure of driving**

The concept of pleasure of driving has been defined in various ways in scientific and public communication. For example, the positive emotions drivers experience when interacting with a vehicle have, been described as *physio-pleasure and psycho-pleasure* (Tischler & Renner, 2007). The former described the pleasure mediated through the sensory experience with the vehicle, which might be comparable to a comfort component. The latter describes the pleasure arising from the interaction with the machine and the driving action. On this background, Tischler and Renner (2007) defined pleasure of driving as the "*positive emotional state of a person, caused by active action and determined by an actual sensory experience of the interaction of human, vehicle, and environment"* (p. 109). Using this definition, the dynamic features of the vehicle become a crucial aspect in the examination of driving pleasure, since the dynamic operations the driver intends to achieve directly depend on the dynamic conversion the vehicle is able to. This means that behaviour can only be realised in between the borders of the according dynamic values (e.g. acceleration) by which the vehicle is characterised. The vehicle *offers the sense of mastering the power and speed of the car* (Hagman, 2010, p. 25), which releases the experience of dynamic properties from the actual car.

Adding to the distinction of comfort and pleasure in driving, Engeln, Engelbrecht, and Kieninger (2008) defined their model of joy and convenience in activities. Their framework was

based on the two axis of hedonic tone and intensity of action (i.e., arousal). Pleasant situations can be reached when convenience and joy are high. Convenience refers to extrinsically motivated actions and is improved by reducing the number of extrinsic acts. On the other hand, joy is high, when an optimal level of intrinsically motivated activities is reached.

The present study focused on the pleasure of the driving experience as a result of the experience of vehicle dynamics in longitudinal and lateral direction. As a research method, direct questioning of non-professional drivers was chosen. This is because, in terms of the evaluation of subjective feelings when engaged in driving a vehicle, every driver can be seen as an expert regarding his or her own experience (Krüger, Neukum, & Schuller, 1999; Tischler & Renner, 2007).

**Driving styles**

In order to increase the range of dynamic experiences participants had with the electric vehicle model, driving behaviour was defined according to different driving styles. Drivers have different preferences, needs, motivations and safety estimations for everyday driving (Ayres, Li, Schleuning, & Young, 2001; Hoedemaeker & Brookhuis, 1998), which result in different starts and strengths of the dynamic reactions in various traffic situations. For example, different drivers start decelerating in order to stop at a red traffic light at different points in time and with different strengths of deceleration, which in consequence results in different speed profiles. Driving style has been distinguished from driving skill. The former concerns the ability of the driver to control the vehicle, the latter reflects the habitual mode of operating the vehicle (West, French, Kemp, & Elander, 1993). For the classification of driving styles, various classification parameters have been investigated, such as speed (e.g., Ebersbach, 2006), acceleration (e.g., Canale, Malan, & Murdocco, 2002), deceleration (Tomaszewski, 2011), lateral accelerations (e.g., Neumerkel,

Rammelt, Reichardt, Stolzmann, & Vogler, 2002) and distance to the lead vehicle (Doshi & Trivedi, 2010). These styles have been classified as part of a continuum (e.g., Ehrenpfordt, 2009) and as distinct styles (De Vlieger, 1997). Amongst others, König, Weiß and Mayser (2002; cited in Ebersbach, 2006) reported that the distinction of the three driving styles (i.e., sporty, normal and relaxed) was most appropriate for the evaluation of driver assistance systems.

In the present approach, an efficient driving style was developed as an anchor for the two driving styles of relaxed and sporty driving. It was assumed that stronger dynamic reactions (e.g., stronger deceleration and stronger acceleration) were associated with sporty driving behaviour, whereas less strong dynamic reactions were associated with relaxed driving. The efficient driving style contained components of both styles.

## Method

### *Design*

The experiment had a 3 (driving style) x 4 (driving situation) within-subject design. Every participant experienced the three different driving styles of efficient, relaxed and sporty driving when driving three different times on the same test track. The test track consisted of a number of different combinations of the four main driving situations: (1) deceleration towards a lower speed limit, (2) acceleration towards a higher speed limit, (3) curve driving and (4) car following. The dependent variables were the energy efficiency and the pleasure drivers experienced in each driving situation.

### *Apparatus*

A driving simulator with a motion system based on a Steward platform with six degrees of freedom was used in this research (Figure 1).

**[insert Figure 1 here]**

A vehicle and consumption model for a fully electric vehicle was implemented in the existing simulation environment. The vehicle was equipped with an intelligent adaptive cruise control (ACC) system. The system was able to conduct full longitudinal control, since it detects and reacts to traffic signs, place-name signs, traffic lights, sharp corners and lead vehicles. This ensured a consistent representation of vehicle dynamics for all participants.

*Test track*

The test track consisted of rural and urban areas and one inner city section. Overall the track was 24,760 metres long and included various speed changes of different velocities. The corners on which the ACC regulated speed were always approached at a speed of 100 km/h. The two car following situations were operated with a lead vehicle fluctuating between 60 to 80 km/h on a rural road. Figure 2 depicts the speed profile of the track with the highlighted areas representing inner city sections.

**[insert Figure 2 here]**

*Parameterisation*

For the realisation of dynamic behaviour, the ACC system was programmed with three sets of parameters, representing the three different driving styles of efficient, relaxed and sporty driving. The parameter combination of the efficient style was based on pre-tests. In the pre-tests, the energy efficient driving style was defined according to the four types of driving situations: deceleration, acceleration, lateral accelerations for cornering and distance to the lead vehicle. After completing the definition of efficient driving, adaptations of the parameter combinations in the four situations were made to simulate either a sporty or a relaxed driving style. The criteria used were based on data from the literature and adjusted by trial and error. The final parameter combinations for each simulated mode of driving are shown in Table 1. As can be seen, the objective was to keep two of the three versions equal in the definition of the parameters for one

specific situation. Because of its high complexity and the interaction between the variables, this goal could not be achieved in the car following situation, where the weighting factors for approaching distance and the speed of the lead vehicle (*kd* and *kv;* for a more detailed explanation see Ludmann & Weilkes, 1999), and the distance to the lead vehicle (*TdistTarget)* differed between all three systems.

**[insert Table 1 here]**

*Participants*

Twenty four participants (50% female) from took part in the study. Their mean age was 36.58 years old (SD = 11.843) and they ranged in age from 25 to 59 years old. All drivers had previously been trained for driving in the simulator, but they were not familiar with the new electric vehicle model.

*Procedure*

After arriving in the laboratory, drivers completed a data privacy statement and received an overview of the experimental structure. The ACC system and the instrument panel were explained to the participants. After a test drive, in which participants familiarised themselves with the dynamics of the electric vehicle and the handling of the ACC system, the simulated ACC drives were conducted with all three driving styles in randomised order. Drivers were not aware of the underlying parameter combinations, but were only instructed to evaluate three versions of dynamic driving behaviour. During the drives, participants were asked two questions in all of the relevant situations:

*How strong was the driving behaviour (e.g., the deceleration)?*

*How pleasant was the driving behaviour (e.g., the deceleration)?*

They replied on a scale from 0 (Not at all) to 15 (Very strong) and the experimenter recorded their verbal evaluations. Drivers also had the chance to have a rest between each ACC trial. After

all the trials were completed, participants were thanked and received a compensation for expenses.

## Results

The results were analysed according to the objective energy efficiency of the drive as well as the subjective pleasure experienced by the drivers. The ANOVAs were conducted in a repeated measures design, and subsequent Bonferroni post-hoc tests for paired samples were reported with adjusted alpha-levels. For the analyses, the start and the end of each single dynamic manoeuvre were defined by the start and the end of the least dynamic system (i.e. the relaxed ACC) for all three trials. This guaranteed that the length of the relevant sections (in which e.g. a specific deceleration manoeuvre takes place) was the same for all systems, which is especially crucial for the comparison of the energy efficiency.

*Deceleration*

In terms of energy efficiency, the three systems differ significantly ($F(2,766) = 245.10$, $p = .000$). The relaxed system consumed less energy than both other ACC systems (relaxed vs. efficient, $p = .000$; relaxed vs. sporty, $p = .000$), and the sporty ACC consumed less energy than the efficient ACC ($p = .000$). Furthermore, the energy recuperation (i.e., the sum of all regained energy) also differed significantly ($F(2,766) = 80.793$, $p = .000$), with all systems differing from each other (efficient vs. relaxed, $p = .000$; efficient vs. sporty, $p = .000$; relaxed vs. sporty, $p = .000$; Figure 3). This was the case, even though as intended, the efficient and the sporty versions decelerated more strongly than the relaxed ACC ($F(2,766) = 8269{,}1$, $p = .000$; efficient vs. relaxed, $p = .000$; efficient vs. sporty, $p = .000$; relaxed vs. sporty, $p = .000$; Figure 3).

**[insert Figure 3 here]**

A closer examination of the data revealed the reason for the unexpected better energy consumption of the relaxed ACC, in comparison to the efficient system. As can be seen in Figure 4, the efficient ACC drives with a constant high speed for a longer period of time than is the case for the relaxed ACC. Therefore, in the efficient ACC energy recuperation starts later and lasts a shorter period of time than in the relaxed ACC. Hence, the longer recuperation period of the relaxed ACC compensates for the fact that the maximum recuperation was not as strong compared to the efficient ACC.

**[insert Figure 4 here]**

The pleasure drivers experienced in the deceleration situations differed most clearly between the efficient and the relaxed ACC modes ($F(2, 752) = 10.935$, $p = .000$; efficient vs. relaxed, $p = .000$; efficient vs. sporty, $p = .021$; relaxed vs. sporty, $p = .022$). Additionally, Figure 5 shows that in general greater dynamic behaviour was associated with less pleasure (supported by a significant negative correlation of $r = -.349$).

**[insert Figure 5 here]**

*Acceleration*

As intended, the sporty ACC version accelerated more strongly than the relaxed ($p = .000$) and the efficient versions ($p = .000$; $F(2,334) = 29554$, $p = .000$; Figure 6). As a consequence, the sporty ACC consumed significantly more energy than the efficient ($p = .000$) and the relaxed ACC versions ($p = .000$; $F(2,334) = 387.18$, $p = .000$). However, when only considering the amount of energy consumed in the acceleration manoeuvre itself, the sporty ACC consumed significantly less energy than the other two versions ($F(2,334) = 32.558$, $p = .000$; sporty vs. efficient, $p = .000$; sporty vs. relaxed, $p = .000$). One of the factors influencing the higher energy consumption in the sporty version was reaching the maximum speed earlier in each situation, and with that, a higher overall mean speed in each driving scenario. This means that in particular start

and relative speed combinations, the shorter duration of the manoeuvre compensates for the stronger acceleration (i.e., the shorter time period leads to less energy consumption).

**[insert Figure 6 here]**

In the acceleration situations, no differences in pleasure were found, even though the difference in the strength of acceleration were correctly identified by the drivers ($F(2,332 = 555.05$, $p = .000$). The sporty version of the ACC was reported to accelerate more strongly than the efficient ($p = .000$) and the relaxed ACC modes ($p = .000$) (see Figure 7).

[**insert Figure 7 here**]

*Cornering*

Cornering was investigated as a composition of the deceleration when approaching the corner, constant speed when driving through the corner and subsequent acceleration when exiting the corner. The three ACC systems differ significantly in their dynamic behaviour in all three parts of the corner (maximum deceleration $F(2,190) = 867817$, $p = .000$; minimum speed while cornering $F(2,190) = 270232$, $p = .000$; maximum acceleration $F(2,190) = 110378$, $p = .000$; Figure 7).

**[insert Figure 8 here]**

The different approaches to cornering resulted in an overall energy consumption that differed significantly between the ACC versions ($F(2,190) = 429.17$, $p = .000$). The efficient ACC consumed more energy than the relaxed ($p = .000$) and the sporty versions ($p = .001$), while the relaxed mode consumed less energy than the sporty version of the ACC ($p = .000$). Therefore, even during cornering the relaxed ACC had the best overall energy balance of all three ACC modes.

Figure 8 shows the decomposed energy consumption for the three parts of a single right hand corner. When decelerating in the approach phase of the corner, the relaxed version

regenerated more energy than the efficient ($p$ = .000) and the sporty versions of ACC ($p$ = .000; $F$(2,46) = 16003, $p$ = .000), which confirms the observations made during the deceleration phase (longer deceleration compensated for the more gentle deceleration). In the steady driving phase, higher speeds lead to higher energy consumption ($F$(2,46) = 11680, $p$ = .000), meaning that the relaxed ACC consumed less energy than the efficient ($p$ = .000) and the sporty ACC ($p$ = .000). Finally, when exiting the corner the systems accelerate back to 100 km/h. Here, the relaxed system consumed more energy than either the efficient ($p$ = .000) or the sporty versions ($p$ = .000; $F$(2,46) = 124898, $p$ = .000). Additionally, the sporty mode consumed more energy than the efficient ACC ($p$ = .000), which demonstrates that at certain relative speeds lower strength of acceleration (and with that a longer acceleration period) is still more beneficial for energy efficiency, compared to shorter, but stronger acceleration..

**[insert Figure 9 here]**

Figure 9 shows the drivers' reported pleasure while decelerating when approaching a corner and passing through it. The drivers' evaluations of pleasure differed significantly between the ACC systems ($F$(1,184) = 28.540, $p$ = .000; efficient vs. relaxed, $p$ = .000; relaxed vs. sporty, $p$ = .000; Figure 9).

**[insert Figure 10 here]**

*Car following*

The investigation of the dynamic driving behaviour in car following situations showed that the intended maximum accelerations and decelerations were achieved. However, the distances to the lead vehicle were not achieved as intended and there appeared to be inconsistencies between the two car following situations.

The relaxed version consumed less energy than the efficient ($p$ = .000) and the sporty versions ($p$ = .000), and the efficient version consumes less energy than the sporty ACC ($p$ =

.000; $F(2,94) = 1070.0$, $p = .000$). In terms of energy recuperation, the lowest recuperation was found in the efficient version, followed by the sporty ($p = .000$) and the relaxed ACC ($p = .000$; $F(2, 94) = 975.74$, $p = .000$; Figure 10).

Even though drivers experienced the differences in dynamic behaviour (the relaxed version was evaluated as decelerating and accelerating more gently than the efficient ($p = .000$) and the sporty versions ($p = .000$), $F(2,94) = 9.449$, $p = .000$), but no differences in pleasure was found. In general, many drivers expressed their preference for overtaking in this section of the drive, where the speed limit was actually 100 km/h. Additionally, as the lead car fluctuated between 60 and 80 km/h closely following the speed profile of the lead vehicle was experienced as unpleasant for drivers in all ACC versions, which was mentioned in the free comments of drivers after the drive.

**[insert Figure 11 here]**

## Discussion

Firstly, it can be concluded that with the described method of using an intelligent ACC system, the goal of realising consistent driving behaviour between drivers was achieved. All drivers experienced decelerations, accelerations and cornering in the exact same way. Additionally, the manoeuvres were all operationalised as intended. This was important in order to guarantee a controlled dynamic experience for drivers and to make the energy consumption values comparable. The method of using the ACC system as a research tool was also found to be useful, except in the car following situation, where the large number of parameters made the interactions difficult to predict.

Secondly, the differences in the dynamic behaviour of the ACC systems were noticed by the participants. For the large variety of dynamic experiences, drivers were able to perceive even

small differences between and within the systems. Additionally, the participants identified the direction in which the differences had occurred. This was particularly important for the investigation of pleasure, in that only when drivers notice differences in dynamic behaviour can differences in pleasure can be interpreted in a meaningful way.

Thirdly, in terms of energy efficiency the hypotheses were only partially confirmed. The relaxed ACC mode showed the most efficient driving behaviour and outperformed the efficient and the sporty version of the ACC in terms of its energy consumption. One reason for this can be seen in the approach of defining efficient driving behaviour on a manoeuvre level as in the pilot research, the deceleration and acceleration manoeuvres were considered separately. However, the sequence of manoeuvres has a major influence on efficiency. Various combinations of dynamic behaviour and especially the consequences of present dynamic reactions for the immediately following driving (e.g., stronger acceleration leads to reaching the target speed earlier and driving for longer at a high speed) need to be considered in order to assure the most energy efficient way of solving each particular situation. Also confirming this, the main reason for the lower energy consumption in the relaxed mode was the lower mean speed the system chose in comparison to the efficient and the sporty systems, which was caused by earlier speed reductions and reaching the maximum speed later in each situation. Hence, the mean speed (which was not systematically varied between systems in the present research) is one of the most important influences on energy consumption.

Fourthly, lower vehicle dynamics resulted in higher ratings of pleasure evaluations, which resulted in the driving behaviour of the relaxed ACC system being evaluated as the most pleasant. In general, the pleasure evaluations were quite high, which leads to the conclusion that none of the ACC modes were was dramatically lowering pleasure. However, differences were

observed which can be seen in relation to the differences in the experience of the vehicle dynamics.

One factor influencing the high level of pleasure reported in the relaxed driving mode might be the passive experience drivers had with the ACC systems. More dynamic behaviour (as shown by the sporty and efficient system) might result in higher pleasure evaluations when longitudinal control is actively chosen by the drivers. Regarding the definition of driving pleasure (Tischler & Renner, 2007) the criterion of a sensory experience was reached using this research method, whereas the criterion of applying active action did not apply for longitudinal control. As an alternative approach, future research could try to instruct concrete driving behaviour in order to achieve more active driving while still ensuring the comparability of the dynamic experiences.

Finally, from the investigation of energy efficient driving and the pleasure evaluations, driving behaviours could be identified which increased energy efficiency and driving pleasure (Table 2). It can be concluded that energy efficiency and pleasure in driving are not contradictory goals, but can both be achieved using the same dynamic behaviour.

**[insert Table 2]**

## References

Åhman, M. (2001). Primary energy efficiency of alternative powertrains in vehicles. *Energy, 26*(11), 973-989.

Ayres, T., Li, L., Schleuning, D., & Young, D. (2001, August 25-29). *Preferred time-headway of highway drivers.* Paper presented at the IEEE Intelligent Transportation Systems., Oakland (CA) USA.

Canale, M., Malan, S., & Murdocco, V. (2002). *Personalization of ACC Stop and Go task based on human driver behaviour analysis*. Paper presented at the 15th Triennial World Congress, Barcelona, Spain.

Chan, C. (2002). The state of the art of electric and hybrid vehicles. *Proceedings of the IEEE, 90*(2), 247-275.

Chan, C., & Chau, K. (1997). An overview of power electronics in electric vehicles. *Industrial Electronics, IEEE Transactions on, 44*(1), 3-13.

De Vlieger, I. (1997). On board emission and fuel consumption measurement campaign on petrol-driven passenger cars. *Atmospheric Environment, 31*(22), 3753-3761.

Dick, M. (2002). Auf den Spuren der Motive, Auto zu fahren - Die Perspektive der Fahrenden [Searching for the motifs of driving - the driver's perspective]. *Verkehrszeichen, 18*(4), 9-16.

Doshi, A., & Trivedi, M. M. (2010). *Examining the impact of driving style on the predictability and responsiveness of the driver: Real-world and simulator analysis*. Paper presented at the Intelligent vehicle symposium (IV), IEEE.

Ebersbach, D. (2006). *Entwurfstechnische Grundlagen für ein Fahrerassistenzsystem zur Unterstützung des Fahrers bei der Wahl seiner Geschwindigkeit [Technical basis for a driver assistance system to assist the driver in choosing the speed]*. Doktorarbeit, Technische Universität Dresden, 2006.

Ehrenpfordt, I. (2009). *Zur belastungsoptimierten Routengenerierung im Straßenverkehr [Work load optimised route generation in road traffic]*: Dt. Zentrum für Luft-und Raumfahrt.

Engelbrecht, A., Engeln, A., & Arndt, S. (2009). *Unterstützung von Fahrkomfort und Fahrspaß durch Fahrerassistenzsysteme [Support for driving comfort and driving pleasure with advanced driver assistance systems]*. Paper presented at the Beiträge 8. Berliner Werkstatt MMS, TU Berlin.

Engeln, A., Engelbrecht, A., & Kieninger, C. (2008). *Joy and convenience of driving.* Paper presented at the 4th International Congress of Traffic and Transport Psychology (ICTTP), Washington D.C.

Fairchild, R., Brake, J., Thorpe, N., Birrell, S., Young, M., Feldstead, T., & Fowkes, M. (2009). *Using on-board driver feedback systems to encourage safe, ecological and efficient driving:The Foot-LITE Project*. Paper presented at the AISB 2009 Convention: Adaptive and Emergent Behaviour and Complex Systems, Aberdeen, Scotland.

Hagman, O. (2010). Driving Pleasure: A Key Concept in Swedish Car Culture. *Mobilities, 5*(1), 25-39.

Hoedemaeker, M., & Brookhuis, K. (1998). Behavioural adaptation to driving with an adaptive cruise control (ACC). *Transportation Research Part F: Traffic Psychology and Behaviour, 1*(2), 95-106.

Kamal, M., Mukai, M., Murata, J., & Kawabe, T. (2010). Ecological driver assistance system using model-based anticipation of vehicle-road-traffic information. *Intelligent Transport Systems, IET, 4*(4), 244-251.

Krüger, H.P., Neukum, A., & Schuller, J. (1999). *Bewertung von Fahrzeugeigenschaften – vom Fahrgefühl zum Fahrergefühl [Assessment of vehicle characteristics - from the driving experience to the drivers' experience]*. VDI Bericht, 22.

Ludmann, J., & Weilkes, M. (1999). Fahrermodelle als Hilfsmittel fuer die Entwicklung von ACC-Systemen [Driver models as a tool for the development of ACC systems]. ATZ. *Automobiltechnische Zeitschrift, 101*(5).

Neumann, I., Cocron, P., Franke, T., & Krems, J. F. (2010). *Electric vehicles as a solution for green driving in the future? A field study examining the user acceptance of electric vehicles*.

Paper presented at the European Conference on Human Interface Design for Intelligent Transport Systems, Berlin, Germany.

Neumerkel, D., Rammelt, P., Reichardt, D., Stolzmann, W., & Vogler, A. (2002). Fahrermodelle - Ein Schluessel fuer unfallfreies Fahren? [Driver models – A key for accident-free driving?] *KI, 16*(3), 34-36.

Schmitz, M., Jagiellowicz, M., Maag, C., & Hanig, M. (2012). *Drivers´ acceptance of limiting vehicle dynamics in electric vehicles.* 5th International Conference on Traffic and Transport Psychology (ICTTP), Groningen, The Netherlands.

Tischler, M. A., & Renner, G. (2007). Ansatz zur Messung von positivem Fahrerleben - Die Messung von Fahrspaß und Ableitungen für die Fahrzeuggestaltung [Approach for measuring positive driving experience - The measurement of driving pleasure and outlets for the vehicle design]. *VDI Bericht Nr. 2015*, 105-117.

Tomaszewski, M. (2011). *Identifikation und Vorhersage des Fahrstils über Geschwindigkeits- und Beschleunigungsverhalten des Fahrers [Identification and prediction of the driving style regarding speed and acceleration behaviour of the driver]*. Report. Julius-Maximilians-Universität Würzburg. Würzburg.

Wedlin, J., Tillback, L. R., & Bane, O. (1992). *Combining properties for driving pleasure and driving safety: a challenge for the chassis engineer*: Society of Automotive Engineers, 400 Commonwealth Dr, Warrendale, PA, 15096, USA.

West, R., French, D., Kemp, R., & Elander, J. (1993). Direct observation of driving, self reports of driver behaviour, and accident involvement. *Ergonomics, 36*(5), 557-567.

**Figure 1. Driving simulator with motion system**

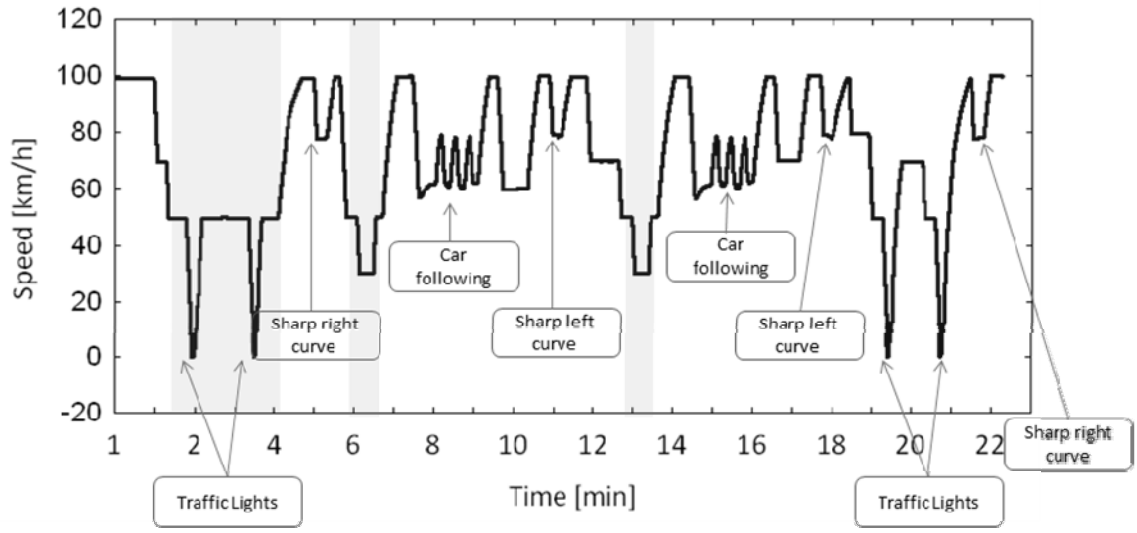


**Figure 2. Speed profile of the test track.**

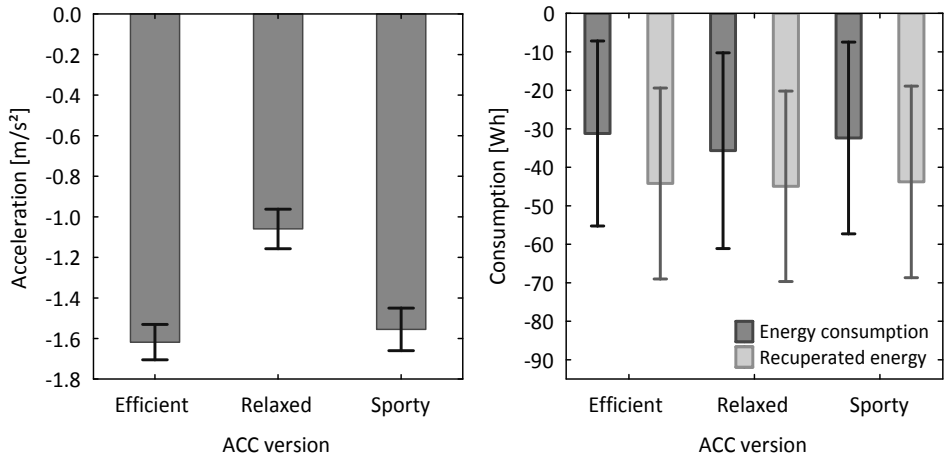


**Figure 3. Means (SD) of maximum deceleration (left) and energy consumption and energy recuperation (right) in deceleration situations by ACC versions [n=24]**

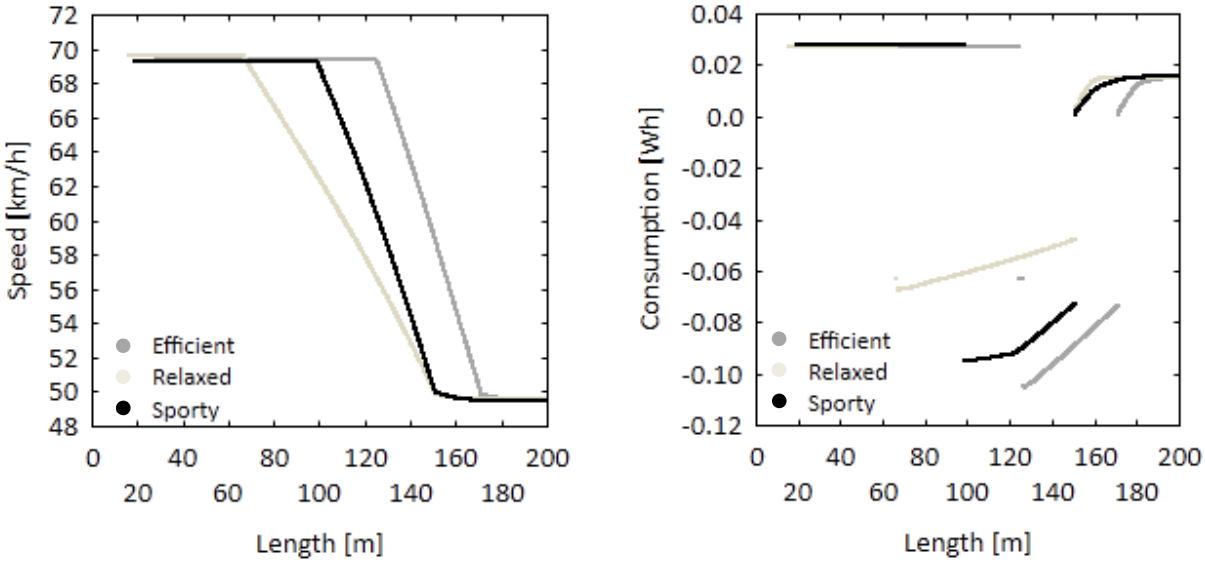


**Figure 4. Scatterplots for speed and energy consumption while decelerating from 70 to 50 km/h for the three ACC versions [n=1]**

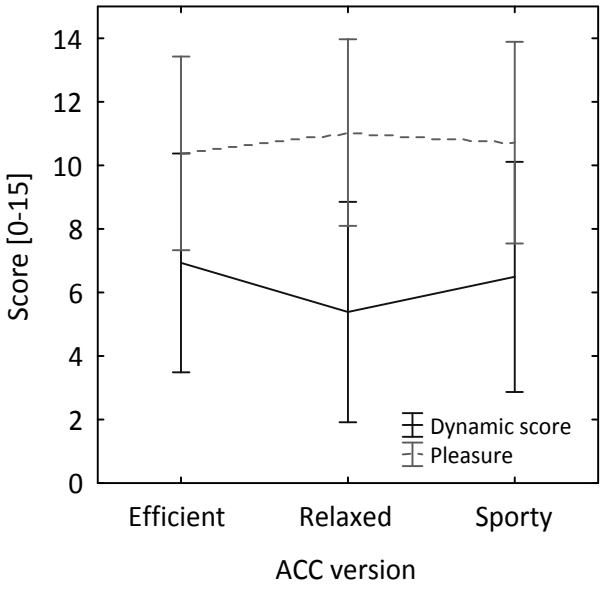


**Figure 5. Means (SD) of scores for strength of the vehicle movements and pleasure in all deceleration situations for the three ACC versions [n=24]**

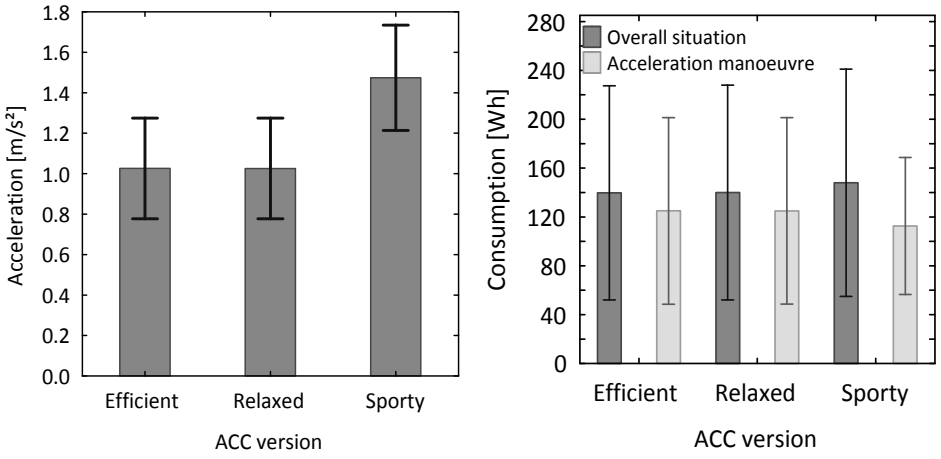


**Figure 6. Means (SD) for maximum acceleration (left), overall energy consumption and in the acceleration process (right) for the three ACC versions [n=24]**

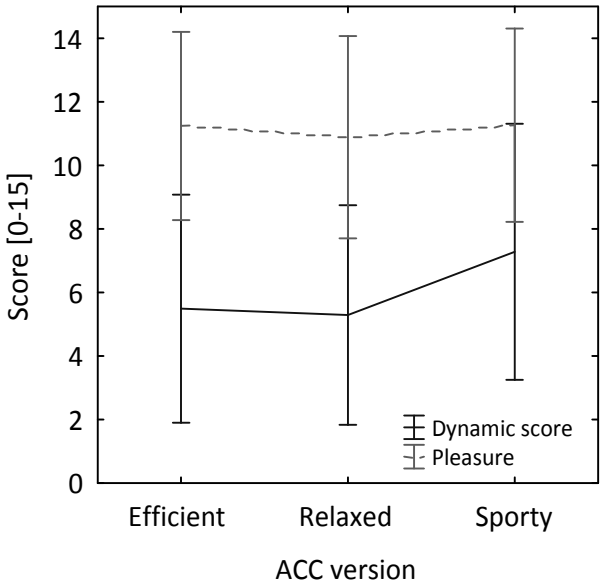


**Figure 7. Means (SD) strength of the vehicle movements and pleasure evaluations in all acceleration situations for the three ACC versions [n=24].**

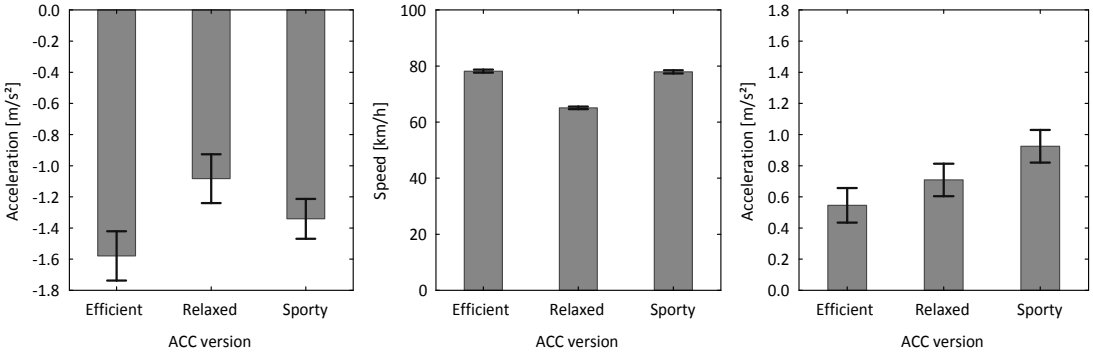


**Figure 8. Means (SD) for maximum deceleration when approaching a corner (left), minimum speed when cornering (middle) and maximum acceleration when exiting the corner (right) for the three ACC versions [n=24]**

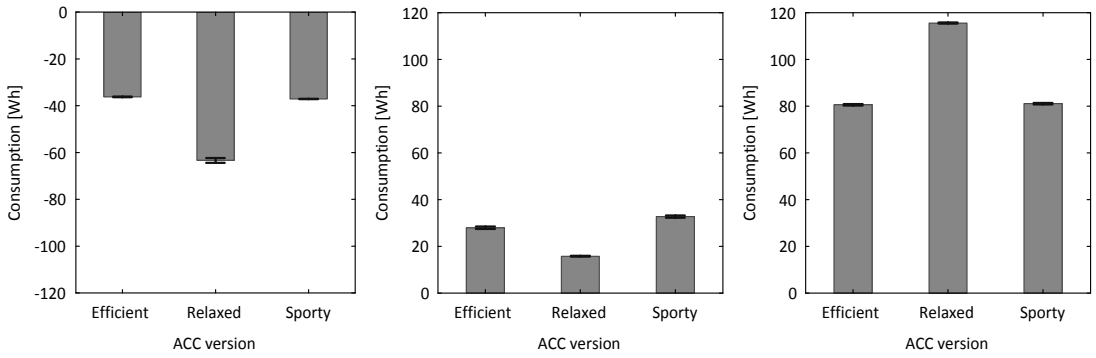


**Figure 9. Means (SD) of fuel consumption for approaching the corner (left), cornering (middle) and leaving the corner (right) for the second sharp right corner [n=24]**

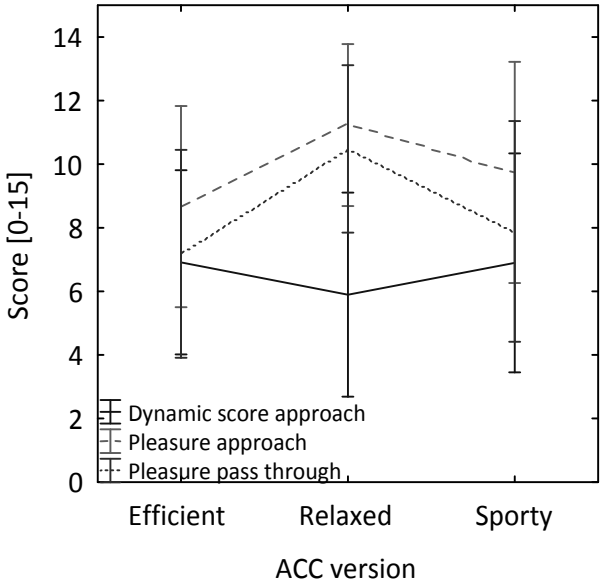


**Figure 10. Means (SD) for the strength of the deceleration and pleasure when approaching the four corners and cornering in the three ACC versions [n=24]**

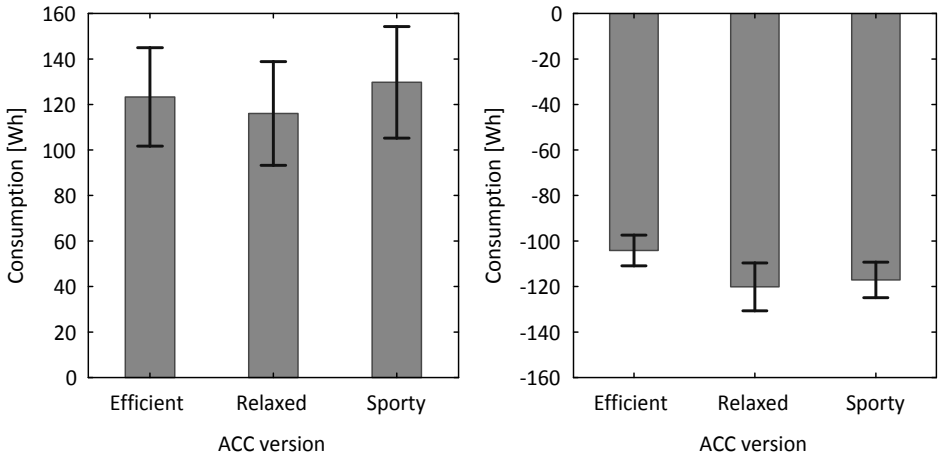


**Figure 11. Means (SD) for overall energy consumption (left) and energy recuperation (right) in the car following situations for the three ACC versions [n=24]**

**Table 1. Parameters for the three ACC versions in the four different driving situations**

| Situation | Parameter | Efficient ACC | Relaxed ACC | Sporty ACC |
|---|---|---|---|---|
| Deceleration | Max. torque limit | 1550 Nm | 200 Nm | 1550 Nm |
| | Max. power limit | 25 kW | 10 kW | 25 kW |
| Acceleration | Max. torque limit | 700 Nm | 700 Nm | 1550 Nm |
| | Max. power limit | 12.5 kW | 12.5 kW | 25 kW |
| Curves | Max. lateral acceleration | 3.2 m/s² | 2.2 m/s² | 3.2 m/s² |
| Car following | kd | 0.1 | 0.5 | 2.0 |
| | kv | 0.1 | 0.1 | 0.8 |
| | TdistTarget | 2.0 s | 3.0 s | 1.3 s |

**Table 2. Factors increasing energy efficiency and driving pleasure in the present electric vehicle**

| Situation | Increasing energy efficiency | Increasing pleasure |
|---|---|---|
| Deceleration | Earlier deceleration and longer recuperation times to compensate for more gentle deceleration | More gentle and early decelerations |
| Acceleration | Lower acceleration and subsequently shorter times spent with high speed positively influence energy consumption. | Pleasure is not decreased by more gentle acceleration. |
| Curves | More gentle and longer deceleration when approaching corners, lower speeds when cornering (but only if subsequent acceleration time is not substantially increased), more gentle acceleration when leaving the corner. | More gentle deceleration when approaching corners, lower speeds when cornering. |
| Car following | More gentle acceleration and decelerations when adapting speed. | Possibility of overtaking; if not possible, longer following distances that do not closely imitate lead vehicle's behaviour. |

# The impact of different pedal solutions for supporting efficient driving with electric vehicles

Marcus Schmitz, Monika Jagiellowicz, Christian Maag, Michael Hanig

Wuerzburg Institute for Traffic Sciences (WIVW)

Raiffeisenstraße 17, 97209 Veitshoechheim, Germany

schmitz@wivw.de

**ABSTRACT**:

The functionality of an electric vehicle enables to regenerate energy into the battery by using the electric motors for electric braking. By integrating this electric brake into the accelerator pedal, drivers are expected to use more often the electric brake and less often the hydraulic brake. However, the pedal system of a car is a crucial connection between driver and car. Any modification of this part can lead to decreasing acceptance. A driving simulator study was conducted to investigate the impact of this combined pedal solution (CPS) on acceptance and energy consumption. 24 participants performed test drives in rural and urban environment with both, the CPS and a conventional pedal solution. With the CPS, drivers used less often the hydraulic brake. This behaviour led to less energy consumption. Additionally, using the CPS resulted in higher subjective ratings due to the comfort of managing most traffic situations with only one pedal.

## 1 Introduction

One key feature of an electric vehicle is the partitioning between the electric and the hydraulic brake force. This fact makes it possible to combine accelerating and electric braking on the accelerator pedal (combined pedal solution (CPS)). Another more conventional solution is to implement the electric brake into the hydraulic brake pedal and thus split up braking completely from the accelerator (split pedal solution (SPS)). The CPS can be understood as an “augmentation of existing in-car interfaces” [1], because drivers can use it without the necessity of further changes of the pedal system. The idea behind this solution is simple: by integrating the electric brake into the accelerator pedal, drivers can use the regenerative brake force to decelerate the car similar to the drag torque of a conventional combustion engine. As regenerative brake forces can even be higher than the drag

torque, drivers are expected to manage most deceleration manoeuvres with regenerative braking. Former research showed that such consequent usage of the regenerative braking has a significant positive impact on the overall energy consumption [2]. Thus, the CPS supports the driver in avoiding energy losses by braking hydraulically. However, the pedal system of a car is a crucial and safety-critical connection between driver and car. Any modification of this part could negatively influence the driving performance in terms of safety and usability. This paper describes a study that determined the impact of the CPS in comparison to the SPS on both the driver's acceptance and the energy consumption. In addition, frequency and duration of hydraulic brake pedal usage were recorded and examined.

# 2 Method

## *2.1 Pedal configurations*

Figure 1 illustrates the pedal configurations of the CPS (left) and the SPS (right). The braking pedal of the CPS remains reserved for the hydraulic brake only. The electric brake is set on the first 20 % of the accelerator pedal way; accelerating starts at 30 %. The sailing area (i.e. neither acceleration nor braking) lies between electric braking and acceleration (i.e. between 20-30 % of pedal way). The vehicle brakes with maximum electric brake forces when neither the accelerator pedal nor the brake pedal is pressed.

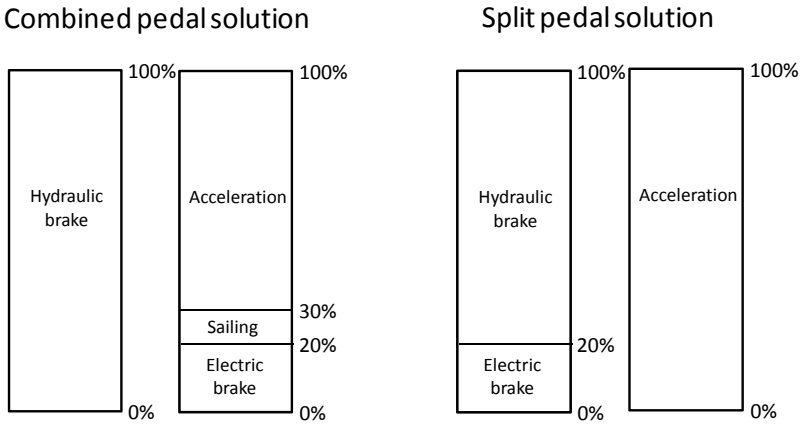


**Figure 1. Configuration of brake pressure and accelerator pedal way for CPS (left) and SPS (right)**

The SPS integrates the electric brake into the first 20 % of the brake pedal pressure and the hydraulic brake between 80-100 %. The accelerator pedal

remains for acceleration only. The vehicle is in the sailing mode when neither the accelerator pedal nor the brake pedal is pressed.

## *2.2 Driving simulation*

The simulator that is used for the study is a driving simulator with motion system based on a Stewart platform with six degrees of freedom (Figure 2).

**Figure 2. Driving simulator (left) and an exemplary track section (right)**

For the study's purpose, a vehicle and consumption model of a fully electric vehicle was implemented into the simulation including the two different pedal solutions. The maximum regenerative brake force of the vehicle model realises maximum deceleration values of about -1.6 m/s². This is much higher than simply using the drag torque with typical deceleration values for routine driving situations of -0.5 m/s² [3], and also higher than average deceleration values of -1.0 m/s² reported for normal driving in urban environments [4].

A particular instrument cluster was integrated in the vehicle including a power gauge that shows positive values (in kW) when energy is spent while accelerating and negative values if energy is recuperated into the battery while braking electrically. During sailing the gauge shows zero power.

## *2.3 Test procedure*

The test track consists of a rural and an urban area (see Figure 2). It includes different speed sections, variations in slope, and typical traffic situations like passing intersections. The track has a total length of about eight kilometres. The test drivers were told to perform two drives, one with the SPS, the other one with the CPS. Participants were instructed to drive as efficient as

possible by keeping to three advices: use the hydraulic brake as little as possible, sail as often as possible and try not to enter the highest “red area” of the power gauge when accelerating (i.e. >40 kW). After the first and the second ride participants were asked two questions answered by means of a 15 point category subdivision scale:

- What do you think, how successful have you been in driving energy efficiently? (not at all – very successful)
- How suitable is the pedal solution for driving energy efficiently? (not at all – very suitable)

At the end of the two drives participants were briefly interviewed. They had the possibility to answer how they liked the two pedal solutions, which pedal solution they would prefer and why.

### *2.4 Participants*

24 Participants were recruited from the WIVW test driver panel. All drivers had been trained for the simulator and had taken part in at least one driving simulator study before. There were 14 men and 10 women. Mean age was 35 (sd=10) years. Mean driving experience was 15 (sd=9) years. Mean kilometres driven per year were 16854 (sd=13700) kilometres.

## 3 Results

### *3.1 Pedal usage*

The pedal solution clearly influences the way how subjects use the two different braking modes. Driving with the CPS leads to hardly any usage of the hydraulic brake. 10 out of 24 subjects even managed to drive the total route without any hydraulic braking compared to none with SPS. In contrast, driving with the SPS resulted on average in 15.3 times of braking with the hydraulic brake ($t(23)=8.77$; $p<.001$; Figure 3 left). No effect could be found in the mean frequency of the electric braking usage considering the total route ($t(23)=-1.96$; $p<.062$; Figure 3 right). Having a look on the rural and urban area separately, the electric brake is used more frequently in urban areas in the CPS condition compared to the SPS condition ($t(23)=-3.36$; $p=.003$). This is presumably due to more frequent changes between sailing and electric braking during stopping manoeuvres.

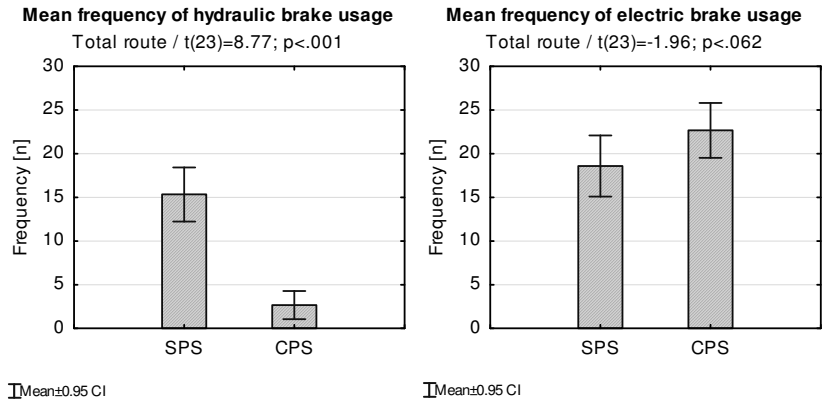


**Figure 3. Mean frequency of hydraulic (left) and electric (right) brake usage per pedal solution**

The pedal solution additionally affects the percentage of time in which hydraulic and electric brake were used. The share of braking time for both braking modes are larger in SPS condition (hydraulic brake: $t(23)=5.43$; $p<.001$; electric brake: t(23)=3.39; p=.003) compared to the CPS condition (Figure 4).

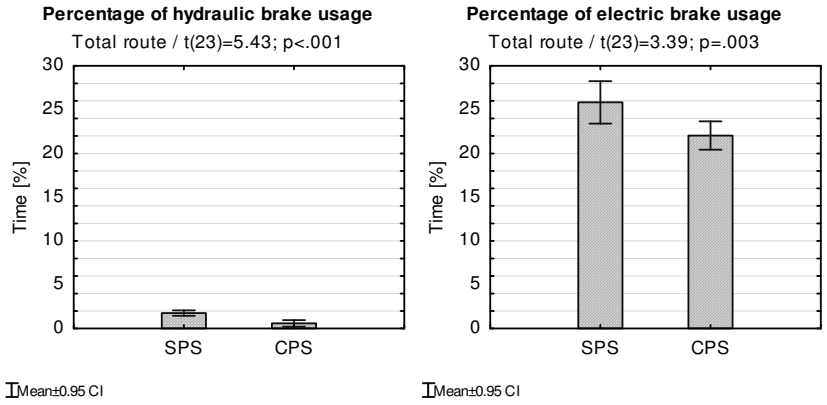


**Figure 4. Mean percentage of time in which the hydraulic (left) and electric (right) brake was used**

Sailing is most frequent when subjects drive in the SPS condition. This effect becomes significant only for the urban route (t(23)=2.90; p=.008). The fact that sailing is easier to perform in the SPS condition (no pedal has to be operated) is maybe the reason for the different percentage of sailing time.

## 3.2 Subjective ratings

There was a significant effect of pedal solution on the subjective rating on how efficient drivers were during the drive ($t(23)=6.59$; $p<.001$). Driving with the CPS made the drivers believe that they were driving more energy efficiently compared to the SPS condition (Figure 5 left).

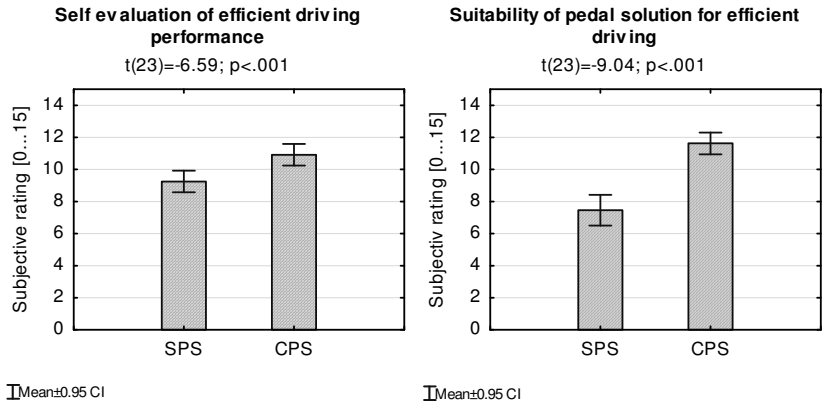


**Figure 5. Mean rating of own efficient driving performance (left) and of adequacy of pedal solution for efficient driving (right)**

Further, drivers rated the CPS as significantly more usable for driving energy efficiently than the SPS ($t(23)=9.04$; $p<.001$, Figure 5 right).

When asking which pedal solution drivers would prefer 23 out of 24 replied CPS. In the majority of cases the reasons were:

- CPS more comfortable, since no usage of brake pedal is needed anymore.
- Easier to regenerate energy, since the power gauge delivers exact information. The SPS lacks a gauge which delivers exact information whether the car brakes electric or hydraulic.

Points of criticism of the CPS were:

- Whilst driving with the SPS the area of sailing was much easier to find (i.e. neither stepping on the brake nor on the accelerator pedal)
- When driving with the CPS many glances to the gauge are needed in order to obtain information whether the car is sailing, accelerating, or regenerating energy.

## 3.3 Consumption measures

The subjective ratings were confirmed by the actual energy consumption. Considering mean energy consumption, analysis revealed a significant effect

of pedal solution (t(23)=6.84; p<.001). Using the CPS results in about six per cent less energy consumption compared to the SPS as depicted in Figure 6. A significant effect of pedal solution can be found in the rural as well as in the urban section.

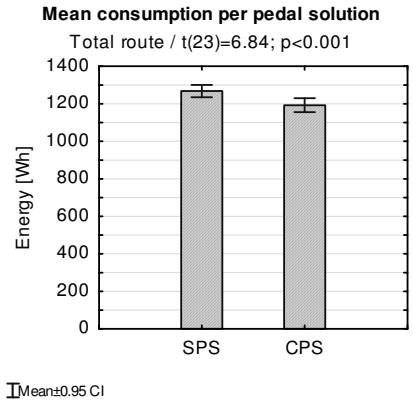


**Figure 6. Mean consumption (in sum) per pedal solution (total route)**

This effect of the pedal solution on the overall consumption is a consequence of significant more recuperation in the CPS condition (t(23)=7.34; p<.001). In average, more than 100 Wh more are recuperated during the CPS mode (Figure 7 right). This exceeds clearly the difference in the retrieved energy from the battery that is slightly higher in CPS condition (Figure 7 left).

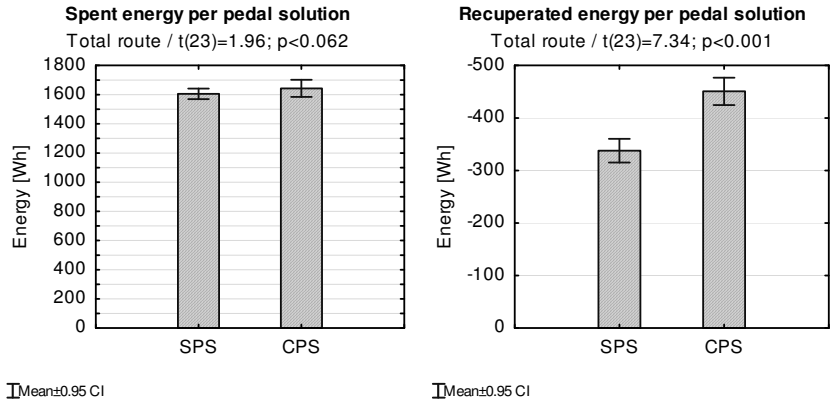


**Figure 7. Retrieved (left) and recuperated (right) energy (in sum) per pedal solution (total route)**

## 4 Discussion

The study compared the SPS with the CPS to obtain knowledge about acceptance, vehicle dynamics and consumption issues. Drivers clearly prefer the CPS over the SPS. Furthermore, drivers assume to drive more efficiently when using the CPS compared to the SPS. This confirms the impression that participants felt confident with the combined pedal solution and would even like to use the system frequently. Similar results were found in the UC Davis MINI E Consumer Study [5].

The CPS also changed drivers' behaviour. By using the hydraulic brake less often, less energy was needed. Accordingly, CPS led to a more efficient driving behaviour compared to the SPS. However, while using CPS drivers complained about the need to look quite often at the power gauge in order to know whether the vehicle is accelerating, decelerating or sailing. As an alternative feedback channel, an active accelerator pedal could be a supporting feature providing continuous feedback about the current pedal position.

Additional research should address the impact of the changed driving behaviour on surrounding traffic (e.g. following vehicles). Another issue to be investigated are long term effects of using the CPS as it has to be guaranteed that the driver could still use the hydraulic brake quickly and safely in non-routine (i.e. safety-critical) situations.

**Acknowledgment:** The study was conducted in the frame of the eFuture project [6] that is partially funded by the European Commission under FP7.

**References:**

[1] Meschtscherjakov, A., Wilfinger, D., Scherndl, T. & Tscheligi, M. Acceptance of future persuasive in-car interfaces towards a more economic driving behaviour. AutomotiveUI 2009, Essen, Germany, Sep 2009, pp. 81–88

[2] Walsh, C., Carroll, S., Eastlake, A. & Blythe, P. Electric Vehicle Driving Style and Duty Variation Performance Study, 2010, Available from: http://www.nichevehiclenetwork.co.uk/LinkClick.aspx?fileticket=WTmGSFXB8qA%3d&tabid=531, accessed April 2012

[3] Watanabe, T. N., Kishimoto, N., Hayafune, K. & Yamada, K. Development of an Intelligent Cruise Control System. Proceedings of the World Congress

on Intelligent Transport Systems, 1995, 3, pp. 1229-1235

[4] Hackenberg, U. & Heißing, B. Die fahrdynamischen Leistungen des Fahrer-Fahrzeug-Systems im Straßenverkehr. ATZ Automobiltechnische Zeitschrift, 1982, 84(7), pp. 341–344

[5] Turrentine, T., Garas, D., Lentz, A. & Woodjack, J. The UC Davis MINI E Consumer Study. Research report UCD-ITS-RR-11-05, 2011

[6] http://www.efuture-eu.org, accessed February 2012

*EVS27 Symposium*
*Barcelona, Spain, November 17-20, 2013*

# A safe Torque Vectoring function for an electric vehicle

Volker Scheuch, Gerd Kaiser, Matthias Korte, Peter Grabs, Fabian Kreft, Frédéric Holzmann

*Corresponding author: Volker Scheuch (volker.scheuch@intedis.com)*

*Intedis GmbH & Co.KG, Max-Mengeringhausen-Straße 5, D – 97084 Würzburg*

**Short Abstract**

A safe Torque Vectoring function is applied to an electric vehicle with a two front motors drivetrain concept. The function has been embedded in a lean and scalable functional architecture adaptable to various drivetrain concepts. The Torque Vectoring function comprises an LPV control algorithm with good performance even in extreme test cases. The controller can be parameterised for case specific performance. The implementation of functional safety requirements is presented for one safety goal.

## 1 Introduction

The application of an advanced Torque Vectoring System (TorVec, TVS) to a two front motor electric vehicle is presented. The choice of a two motor drivetrain is a reasonable compromise between a four wheel motor approach which is complex and expensive and a conventional single motor drive with no freedom of driving wheels individually. However, the advantages of an individual torque control on the wheels (i.e. torque vectoring) must exceed the disadvantages by the extra costs and the extra effort for the higher complexity (package space, weight, number of parts). This benefit for the driver first must be carefully developed and then clearly communicated as a unique selling point for the car manufacturer to enter the market with electric vehicles.

The results in this article will be presented for the two front motor drivetrain configuration but can be extended to arbitrary multi wheel drives. An alternative to use two motors can be one central motor combined with an active electric differential. This solution also suffers from extra costs and package and compared to the use of two individual motors the dynamic range is limited by the maximum differential ratio of torque transmission.

The advantages of a Torque Vectoring function are multiple. The first benefit arises by the mandatory need to have a differential function for a two motor drive to compensate for different wheel speeds in cornering situations. This principle can be used to support the steering request of the driver by a torque increase of the outer and a torque decrease of the inner wheel. This results in a lower steering force and is equivalent to the effect of a power steering system.

The option of automatic steering can also be used for supporting modern advanced driver assistances systems (ADAS) functions like Lane Keeping Assistance Systems (LKAS). After identifying the lane markings, these systems keep the vehicle in the track by controlling the yaw rate via an electric steering system. For small road curvatures, like on highways, this could also be achieved by the asymmetrical application of torque by a TVS.

Beside comfort applications like the above mentioned the largest benefit of TorVec is the safety aspect. In contrast to stabilising assistance systems like electronic stability control (ESC) or antilock braking systems (ABS) which are effective by braking individual wheels, TorVec is able to support this functionality by applying less positive or negative torque instead of using the hydraulic brakes. This benefit is experienced by the driver in situations where an increasing wheel slip could lead to an unstable condition. Before ESC

would be engaged, TorVec is able to smooth out the wheel slip by reducing or increasing the torque accordingly. Examples of these situations are laterally different friction coefficients (e.g. dry asphalt on the left and ice on the right; “μ-split”) or oversteer / understeer. Here, TorVec extends the capability of ESC to the very onset of these slip phenomena.

The different regimes of the assistance systems are shown in figure 1. The borders between the validity regions are drawn sharp but will smooth out in the future when one master dynamics controller is capable of stabilising the vehicle in both lateral and longitudinal direction. This controller must be able to drive the hydraulics brakes, the individual electric motors, and the steering system to have maximum flexibility and redundancy.

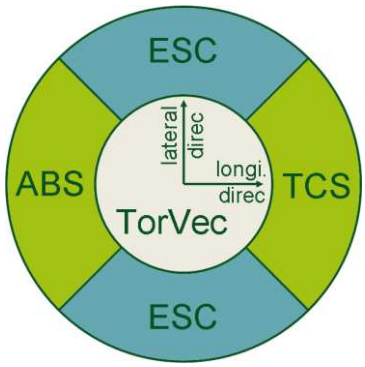


Figure 1: Regime of TorVec as the interfacing function between other stabilising functions. The borders could smooth out in the future by merging the functions to a master dynamics controller. ESC = electric stability control, ABS = antilock braking system, TCS = traction control system.

The TVS has been embedded into a new functional architecture as the link between the execution layer and the command layer [1, 2]. This architecture approach aims at a safe and efficient operation of the EV. The distinct separation of tasks is an important presumption for the scalability and flexibility of the concept. One major goal in the eFuture project was to support the Functional Safety requirements with a clearly arranged topology of the architecture and to ensure that all safety related functions – like TorVec – will have an easy and transparent dependency from other functions which are also easy controllable.

The paper demonstrates a technical deployment of a safe drivetrain architecture for an electrical vehicle. The implementation of the main safety requirements as prerequisites for the integration of dynamical stability functions is shown. The approach of a LPV controller for Torque Vectoring is described and examples for the performance of the assistance function are given.

The work is supported by the European Commission in the project eFuture [3] (grant no. 258133). The aim is to demonstrate innovative functions embedded in a flexible and lean architecture to support safe and efficient electric driving.

# 2 Functional architecture

The complexity of automotive architectures grew constantly through the last decades. The demand for safer cars, driver assistances, and car multimedia led to new components and functions requiring an increased number of interfaces, cables and control units with the corresponding software. This evolution, in turn, results in a confusing system of interconnected devices and functions which hampers the introduction of new features.

New vehicle generations offer the opportunity to think new ways for relieving this situation by modular approaches to account for different markets and vehicle types, and to ease the integration of future technology. The electro mobility age with its new use cases and new vehicle requirements enables the development of innovative architectures with reduced complexity and higher sustainability.

By defining a modular and flexible architecture for a full electric vehicle (FEV), the project eFuture translates this challenge into a demonstration car to examine the feasibility, the limits and the benefits of a “revolution” in E/E architecture. The top level picture of the approach basically consists of four layers and is shown in figure 2.

The perception layer collects all information of the vehicle's environment via exteroceptive sensors and the sensor fusion extracts the relevant information for the guiding ADAS function on the command layer. The driver with his senses is part of the perception layer but could also be attributed to the command layer as he performs the transition of perception to driving commands.

The human machine interface (HMI) is split into the two directions "driver to vehicle" and "vehicle to driver" which is advantageous for the modular implementation of new driver actuators (control buttons, pedals, etc.) and new driver feedback devices (displays, acoustic senders) and enables an easy adjustment of the driver's look-and-feel.

Both the HMI (driver-to-vehicle in this case) and the guiding ADAS (ACC, LKAS, EBS, etc.) are calculating motion requests consisting of the longitudinal acceleration and the steering angle. The requests are forwarded to a central control function, the Decision Unit 1 (DU1) which mitigates between the potentially conflicting motion requests [1, 2]. The DU1 also receives information on the energy status of the vehicle via the Energy Management function on the energy layer. According to the recommendation of the Energy Management, the DU1 can choose a limitation for acceleration and/or velocity avoiding an excessive current which could damage the high voltage battery.

The DU1 selects the best motion vector in terms of efficiency and safety and forwards this to the execution layer, responsible for choosing the best way to realise the motion vector by the actuators present in the vehicle (brakes, motors, active steering). The implementation of a Torque Vectoring function enables the dynamical split of torque required for the requested acceleration to the drive wheels. Together with the conventional stabilising ADAS (ESC, ABS, TCS), TorVec ensures safe and comfort driving in all situations. This will be addressed in section 3.

An important part of the execution layer for the perception of the dynamical vehicle status is the Vehicle Observer (VehObs). This function examines information of the various vehicle sensors (wheel speed sensors, yaw rate sensor, steering wheel sensor and acceleration sensor), improves their signal quality by the use of Extended Kalman filtering, and calculates immeasurable quantities out of the primary signals [4]. The VehObs is the source of information on dynamical vehicle stability and its limits for all functions in this architecture.

The concept of the decision unit has also been applied to the execution layer by implementing a central control function, the Decision Unit 2 (DU2), which decides, based on the inputs of the energy management (recuperation en-/disabled, current limitation) and the VehObs (dynamical limits), which actuator shall perform the requested action to achieve the requested trajectory. Here, the steering can be done by TorVec or Power Steering, and deceleration can be performed by recuperation or hydraulic braking.

The philosophy of the novel functional architecture is to decouple the core functions from the hardware (HW) and to create interfacing functions to the HW which can easily be adapted to different HW concepts (e.g. drivetrain architectures, ADAS equipment, degree of autonomous driving). This concept also avoids bypassing of functions by applying a hierarchic composition with the decision units being the final instance.

In chapter 4 the use of this modularity for the implementation of important safety requirements from the functional safety concept will be outlined. High ASIL ratings can be restricted to the core functions which only carry simple calculations and thus, can easily be secured by redundancies.

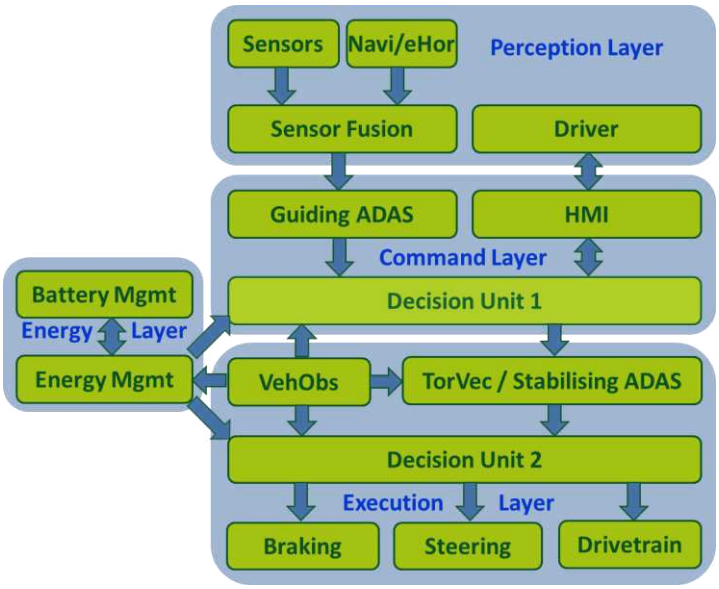


Figure 2: Top level schematics of the functional architecture used in the eFuture project

# 3 Control strategy and performance of Torque Vectoring

To use a Torque Vectoring System (TVS) a special vehicle configuration must be given. In the project eFuture the vehicle is equipped with two independent electric motors which drive the front wheels of a compact car – as shown in figure 3.

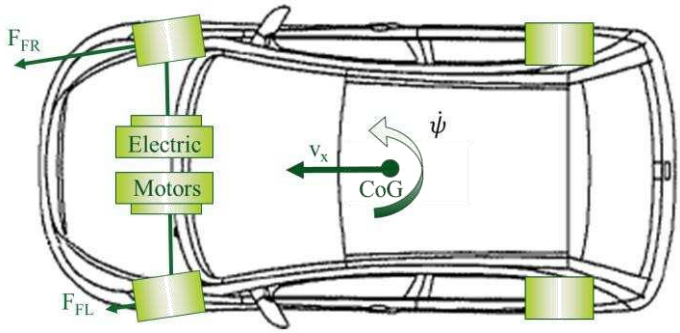


Figure 3: eFuture propulsion system

With the two electric motors, the lateral dynamics of the vehicle can be influenced and the control of the two motors is called torque vectoring. TVS is considered as a performance enhancement function which also improves the vehicle stability and thus, the safety of the vehicle. In normal, every-day driving conditions, the vehicle movement can be described with the nonlinear single track model [5]

$$\dot{v_x} = \frac{\sum F_x}{m} + \dot{\psi} v_y$$

$$\dot{v_y} = \left(\frac{-a_1 C_{\alpha f} + a_2 C_{\alpha r}}{m v_x} - v_x\right)\dot{\psi} - \frac{C_{\alpha f} + C_{\alpha r}}{m v_x} v_y + \frac{C_{\alpha f}}{m}\delta$$

$$\ddot{\psi} = -\frac{a_1^2 C_{\alpha f} + a_2^2 C_{\alpha r}}{I_z v_x}\dot{\psi} + \frac{a_2 C_{\alpha r} - a_1 C_{\alpha f}}{I_z v_x} v_y + \frac{a_1 C_{\alpha f}}{I_z}\delta + \frac{1}{I_z} M_z$$

Here the vehicle states are the longitudinal velocity $v_x$, the lateral velocity $v_y$ and the yaw rate $\dot{\psi}$. The system inputs are the total longitudinal force $\sum F_x$, the front wheel steering angle $\delta$ and the yaw moment $M_z$. Geometrical properties of the vehicle are included as distance $a_1$ which is the length between the front axle and the centre of gravity (CoG) and the variable $a_2$ which is the distance between the rear axle and the CoG. The vehicle mass is given as $m$ and the vertical moment of inertia is given as $I_z$. The parameters $C_{\alpha f}$ and $C_{\alpha r}$ represent the cornering stiffness of the front and rear axle, respectively.

In critical driving situations including icy road, vehicle spinning or wheel spin / blocking, the real vehicle behaviour is different from the nonlinear single track model. With unknown and unpredictable vehicle behaviour, most drivers are overstrained and cannot safely operate the vehicle. Torque Vectoring tries to keep the real driving behaviour as close as possible to the normal driving behaviour reflected by the above equations. Therefore the two electric motors at the front wheels are used to generate a total longitudinal force $\sum F_x$, which accelerates and brakes the vehicle. Additionally, the motors are used to generate the yaw moment $M_z$ which controls the lateral movement of the vehicle.

The control of the vehicle dynamics can be realised with different controller types [6, 7]. For the application in eFuture a linear parameter-varying (LPV) control design is chosen as Torque Vectoring controller. In LPV control linear time invariant (LTI) design concepts are applied to a certain class of non-linear systems [8]. The non-linear single track vehicle model fits perfectly the requirements of LPV control because the non-linearity of the system can be included into the controller design. With LPV control, it is possible to design a controller which guarantees stability over the complete operation range while maintaining the vehicle performance [9] – which can only be guaranteed for PID controllers with an unfavourable controller performance.

Besides the LPV controller, a torque and slip limiter (TSL) is included in the software which deals with the physical limitations of the actuators. TSL is composed of two elements.

1. An anti-windup configuration which deals with the physical limitations of the electric drivetrain. The power limitation introduced with the battery and the torque limitations related to the electric motor decrease the performance of the controller as soon as the physical limitations are reached. The anti-windup scheme [10] reduces the effects of the limitations and suppresses excessive overshoots and vehicle instability due to actor limitations.
2. The anti-windup scheme is enhanced to TSL because it also limits the tyre slip. Excessive slip values which represent spinning or blocking of the wheels have negative effects on the vehicle performance and safety. To suppress these events, TSL monitors the wheel slip and keeps it in the defined boundaries. In the actual configuration TSL does not perform any action until the tyre slip leaves the interval [-0.1 ; +0.1]. If the tyre slip exceeds these limits the driving torque is reduced towards zero to suppress spinning or blocking of the wheel.

The final control architecture is given in figure 4 with a desired value generator which uses the steering angle and acceleration request of the driver to calculate a velocity request and a yaw rate request. A similar scheme is used by [11] and shows satisfying results. The LPV controller controls the longitudinal velocity and the yaw rate with the two electric motors. The TSL is idle if moderate requests are performed. If the limits of the electric drivetrain or tyre slip are reached the TSL gets activated and reduces the torque requests of the controller in order to stabilize the control-loop and thus, the vehicle.

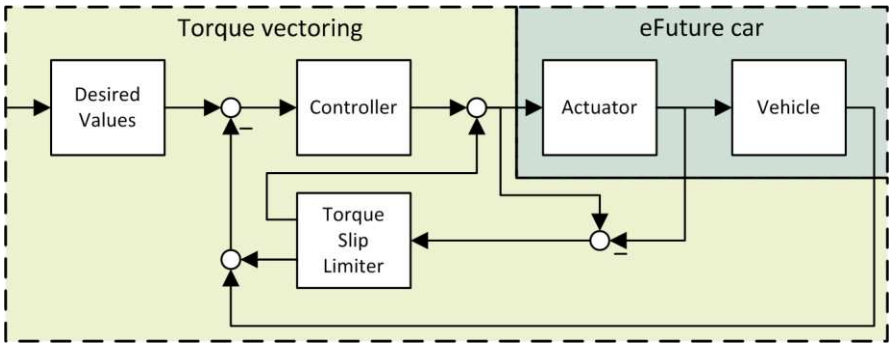


Figure 4: Torque Vectoring control architecture

In eFuture the vehicle movement is simulated with a 14 degree of freedom model, including a linear suspension model and a Pacejka tyre model [12]. This model is used to simulate the vehicle behaviour and to tune the TorVec control parameters. In order to validate the controller the following test cases are simulated:

- Straight line acceleration
- Straight line braking (ISO 21994)
- Constant radius turning (ISO 4138)
- Brake in bend (ISO 7975)

- Acceleration in a bend
- Step steer (ISO 7401)
- Lift off oversteer (ISO 9816)
- Sine with dwell (NHTSA [13], for ESC effectiveness)

In order to validate the lateral performance the National Highway Traffic Safety Administration (NHTSA) advises to use a sine-with-dwell manoeuvre [13]. This test should be used to evaluate the lateral performance of a vehicle and especially the functionality of an ESC system because an average vehicle gets unstable in this test. Here the same test is applied to test the lateral performance of Torque Vectoring. In the sine-with-dwell manoeuvre, the steering wheel is turned in a sinusoidal movement with a maximum angle of 120° at the steering wheel. At the second maximum the steering wheel is kept constant for 0.5 seconds. This manoeuvre is an open-loop manoeuvre which means that no real driver is necessary which makes the test repeatable. However, for a real vehicle test, this scenario might be too complicated because no suitable test track or steering robot is available. In this case a double lane change provides a similar test condition and should be used with a real driver and a real vehicle.

In this paper, simulation results for the sine-with-dwell test case are presented. Figure 5 shows the corresponding driver commands. The vehicle starts with 80 km/h, the road surface is in good condition and no cross-wind exists. At the beginning the virtual driver does not step onto any pedal, which means that the maximum recuperation torque for the specified velocity is requested. After 0.5 seconds the driver starts with the steering manoeuvre and steps to the accelerator pedal in order to request zero acceleration ('sailing' condition).

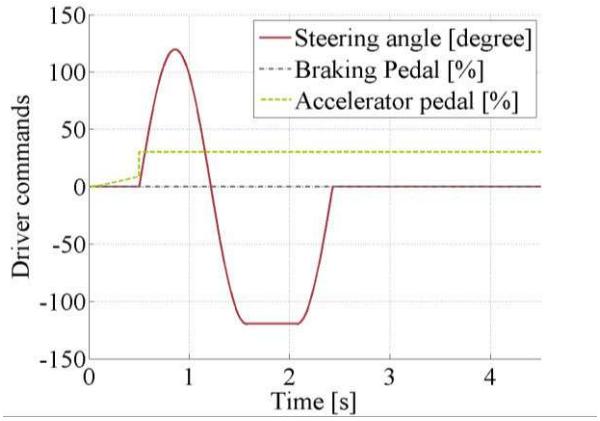


Figure 5: Driver commands for the sine-with-dwell test case (initial velocity = 80 km/h, friction coefficient 0.9)

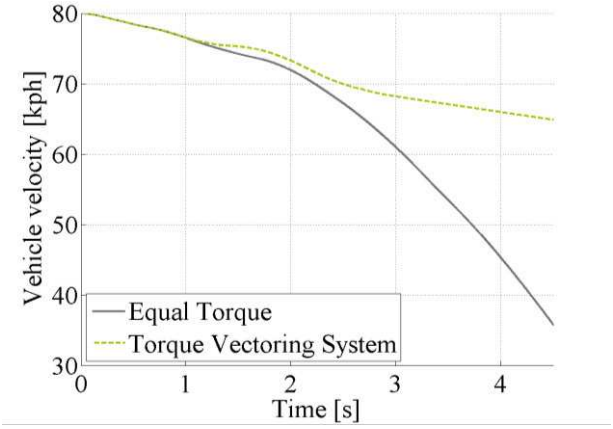


Figure 6: Vehicle velocity plot for the sine-with-dwell test case of figure 5

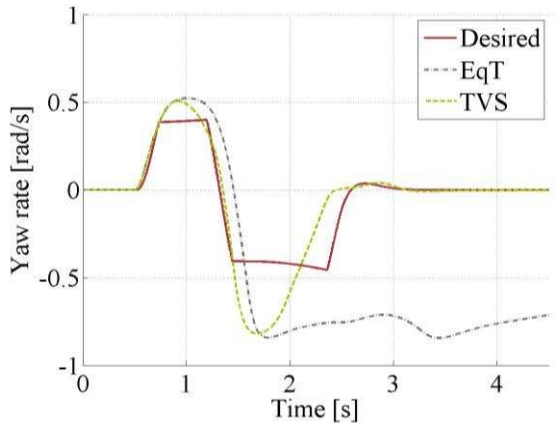


Figure 7: Vehicle yaw rate plot for the sine-with-dwell test case of figure 5.

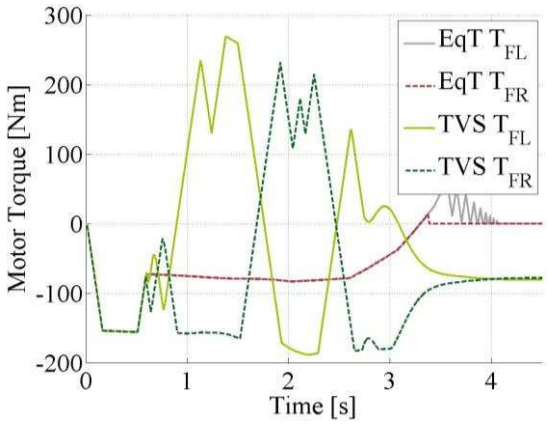


Figure 8: Electric motor torque plot for the sine-with-dwell test case of figure 5.

In the simulation two vehicles with the same properties are compared. The first vehicle (EqT) uses equal torques at both motors while the second vehicle uses the proposed Torque Vectoring System (TVS). Figure 6 shows the velocity of the two vehicles. At the end of the test, the EqT vehicle drives much slower than the vehicle with torque distribution. A low velocity is acceptable from a safety point of view but in terms of vehicle performance and efficiency it is favourable to keep the velocity and avoid unnecessary acceleration. This is accomplished by the TVS vehicle.

Figure 7 shows the major difference between the vehicles. The desired yaw rate (red solid curve) is calculated considering the steering angle and the velocity. The equal torque vehicle (blue dashed curve) has two overshoots and a slow response. Furthermore, the EqT vehicle is in an unstable condition and spins after this test, so it would fail the sine-with-dwell test. The TVS vehicle on the other hand responds faster to the yaw requests and is in a stable driving condition after the steering manoeuvre.

However, an undesired overshoot is still visible in figure 7 for the TVS performance. This overshoot can be explained with the limitations of the electric motor torques. Figure 8 shows the motor torques at the front left and front right wheel. Two major differences between left and right torque of the TVS vehicle can be observed. The first one (0.7 to 1.7 seconds) corresponds to the positive overshoot of the TVS vehicle yaw rate in fig. 7. The second major motor torque difference (1.7 to 2.6 s) is related to the second, negative yaw rate overshoot in fig.7. In both cases, the controller tries to compensate the overshoot and generates a yaw moment against the vehicle turning. However, the intrinsic slew rate limitation (1000 Nm/s) of the electric motor system suppresses a faster reaction to account for the changed vehicle movement. The overshoot is reduced but the motors need some time to reach the desired torque values.

The sine-with-dwell test shows that the Torque Vectoring controller improves the vehicle safety and keeps the vehicle stable in a very critical driving situation. So the major aspect of Torque Vectoring is fulfilled. However, this test shows that the slew rate limitation of the electric motors has a negative impact on the performance of the yaw rate controller and should be kept as small as possible – the faster the motors the better the control performance. Overshoots in the yaw rate response are visible but controllable even in this extreme driving test case.

The results will be validated by driving tests in the next few months and a comparison to the simulation results can be then be drawn.

# 4 Functional safety

The application of a multi motor drivetrain is connected with a high risk of accidents if an error occurs in the hardware or in one controlling function. Even for a vehicle without a TorVec system the failures by degradation of the HW (motors, inverters) have to be accounted for in the safety architecture. If the vehicle is equipped with an electronic differential or a TorVec function the risk of failures will even be increased by software functions distributing the torque unequally to the wheels. For both cases, possible hazard scenarios are unintended reverse, zero or persistent torque (one sided or two sided).

The safety analysis of the vehicle's drivetrain architecture led to the identification of four top hazards related to the drivetrain functions:

1. Unintended high acceleration
2. Unintended high deceleration
3. Unintended vehicle movement
4. Too high or unintended yaw rate

As the TorVec function is deemed to be contributing mainly to the fourth hazard, the corresponding safety requirements are deduced in this paper.

For determination of the Automotive Safety Integrity Level (ASIL) according to ISO 26262 the possible impacts of such a hazard are evaluated in a certain driving situation. This evaluation is done in three dimensions:

1. The exposure (E) representing the likelihood for experiencing the driving situation evaluated.
2. The controllability (C) assessing the capability of the driver or others to get him/themselves out of danger.
3. The severity (S) which is a measure for the degree of damage to the driver or other road users that is caused by the hazard in this particular driving situation.

Here we consider a drive on a country road with the typical speed of ~90 km/h. This is a very common scenario occurring very frequently for the average driver. Therefore the highest rating E = 4 is assigned. In this scenario an unintended yaw rate can lead to vehicle skidding and/or going off the lane. Most of the drivers will not be able to master such a situation by keeping track with counter steering. Hence the highest rating for the controllability C = 3 is chosen. By spontaneously applying an erroneous yaw rate it is very likely that the vehicle will leave the road or hit other cars of the opposing traffic. Considering the high speed of around 90 km/h life-threatening or fatal injuries have to be considered as very likely. This leads to the highest rating for the severity S = 3. Following the rating scheme given in ISO 26262, these ratings lead to an ASIL D overall rating for this hazard. This is the highest rating as per ISO 26262. The resulting safety goal derived from this top hazard is: "Avoid too high or unintended yaw rate!" (SG4). The safe state for this safety goal has been defined to "no torque application" because then the driver can keep control of the vehicle by steering and braking. For failures with a lower severity or a better controllability the system will turn in a degraded mode where both motors will receive equal torque requests (deactivation of TorVec). In the degraded mode, the vehicle has a limited driving capability but the driver can continue his trip.

The safety concept for the safety goal 4 has been derived using the results of a fault tree analysis. Safety requirements have been defined accordingly and attributed to the single vehicle functions. Here, the lean and modular architecture was beneficial for the decomposition of the requirements to the functions since the software blocks are small and well defined and the signal routes are simple, straight and non-branched.

The function chain contributing to the safety goal 4 ("Avoid too high or unintended yaw rate!") is shown in figure 9. The ADAS functions do not contribute here as they cover only longitudinal functions. The architecture allows for a clean separation between the different functional blocks. This makes it possible to derive the safety concepts for these blocks rather independently. The safety concept for the vehicle status acquisition in the Vehicle Observer relies on the model-based plausibility check of the observed values from the sensors (steering angle, wheel speeds, yaw rate), thus leading to lower safety requirements for the sensors. The TorVec function comprises several safety checks including

- Compare actual yaw rate with driver request and counteract in case of discrepancies (for SG4).
- Compare left and right torque request with overall acceleration request and limit torque request in case of discrepancies.
- Forward torque request if and only if the requests from the Decision Unit 1 are valid.

Finally, in the decision unit 2 (DU2) the proper application of the requested torques by the inverters / motors is monitored and the safe state is enforced if critical failures occur.

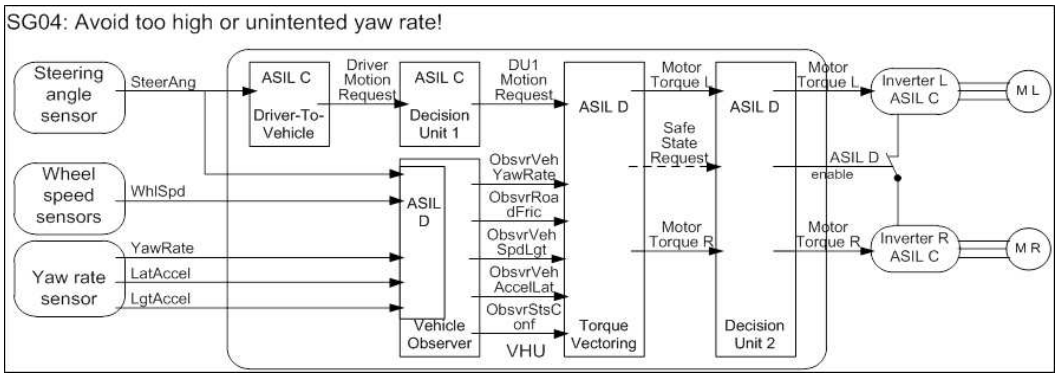


Figure 9: Functions contributing to the requirements of safety goal 4.

All safety requirements have been included in the functions code and proven for effectiveness in various tests. The same implementation strategy holds for the other safety goals, thus leading to a safe system following the ISO 26262 requirements.

# 5 Conclusion

The implementation and performance of a Torque Vectoring function to and in a two front motor electric drivetrain concept has been demonstrated. The TorVec function is part of a lean and scalable functional architecture applicable to any kind of vehicle architecture by clear separation of core functions and hardware interfaces and also allowing for an elegant consideration of functional safety. The safety requirements for avoiding an unintended yaw rate have been explained for the functional chain including

TorVec. The TorVec algorithm follows an LPV control approach with encouraging results of good vehicle stability for a sine-with-dwell test case. For fast controller performance the dynamics of the inverter-motor system must be optimised. The validation and parameter adjustment will be performed in forthcoming vehicle tests and will be presented in the conference talk.

## References


[1] V. Scheuch, G. Kaiser, F. Holzmann, S. Glaser: Simplified architecture by the use of decision units; in: Gereon Meyer (ed.): Advanced Microsystems for Automotive Applications 2012, Berlin, p. 121-130

[2] V. Scheuch, G. Kaiser, R. Straschill, F. Holzmann: A New Functional Architecture for the Improvement of eCar Efficiency and Safety; 21st Aachen Colloquium Automobile and Engine Technology 2012, p. 1567-1576

[3] www.efuture-eu.org

[4] M. Korte, F. Holzmann, V. Scheuch, and H. Roth: Development of an adaptive vehicle observer for an electric vehicle; 2011 European Electric Vehicle Congress, Brussels

[5] Reza N. Jazar: Vehicle Dynamics: Theory and Applications; in: Springer 2009

[6] L. Chu, M. Xu, Y. Zhang, Y. Ou, Y. Shi: Vehicle Dynamics Based on Optimal Sliding Mode Control Theory; in: International Conference on Computer, Mechatronics, Control and Electronic Engineering, 2010, p. 486 – 491

[7] M. Milehins, C. Cheng, T. Chu, R. Jones: Handling Behaviour of a TTR Hybrid Electric Vehicle with Independent Rear Wheel Torque Control; in: International Symposium on Advanced Vehicle Control 2010, p. 556 – 561

[8] J. Mohammadpour, C.W. Scherer: Control of Linear Parameter Varying Systems with Applications; Springer, 2012

[9] G. Kaiser, Q. Liu, C. Hoffmann, M. Korte, H. Werner: Torque vectoring for an electric vehicle using an LPV drive controller and a torque and slip limiter; Decision and Control (CDC), 2012 IEEE 51st Annual Conference on , vol., no., pp.5016,5021, 10-13 Dec. 2012

[10] S. Tarbouriech, M. Turner: Anti-windup design: an overview of some recent advances and open problems; in: IET Control Theory Appl., 2009, Vol. 3, No. 1, pp. 1–19

[11] C. Poussot-Vassal: Dissertation about “Commande Robuste LPV Multivariable de Châssis Automobile”; in: Grenoble Institut Polytechnique 2008

[12] H. Pacejka: Tyre and Vehicle Dynamics – Seccond Edition; in Elsevier 2006

[13] G. Forkenbrock, D. Elsasser, B. O’Harra: NHTSA’S Light Vehicle Handling and ESC Effectiveness Research Program, 2005


## Authors


Volker Scheuch
- Project leader for electro mobility at Intedis in Würzburg



Gerd Kaiser
- PhD student at Intedis in Würzburg

Matthias Korte
- PhD student at Intedis in Würzburg

Peter Grabs
- Functional Safety Manager at Intedis in Würzburg

Fabian Kreft
- System engineer at Intedis in Würzburg

Frédéric Holzmann
- Manager of the Functional Architecture team at Intedis in Würzburg